FUELS AND COMBUSTION IN ENGINEERING

FUELS, FIRE AND COMBUSTION IN ENGINEERING JOURNAL

Volume 4
2016

Editorial

As known, the world has been facing both environmental problems and petro-fuel restrictions. At the same time, recent standards aim to reduce fuel consumption and to lower emissions by using better mixture preparation and combustion control. Therefore, the scientists and engineers in the fields of fuels and combustion are working on the development of new technologies to lower fossil fuels consumption and to reduce their environmental impact. This requires understanding the fuel chemistry and its combustion in detail. The main purposes of these scientific meetings were to provide valuable opportunity for scientists and engineers to exchange up-to-date knowledge in the science and engineering of fuels and combustion. The following main topics were covered in oral presentation and poster sessions: Petroleum Fuels, Alcohol Fuels, Biofuels, Fuel Additives, Combustion Fundamentals, Practical Combustion Systems and Design, Air Pollution, Catalytic Combustion, Combustion Modeling and Reaction Kinetics, Reduction of Reaction Mechanisms, Emissions and Fuel Economy.

The papers in this issue were selected for publication by the scientific committee from the extended version of Authors' papers which were presented during the conference and the symposium. And then, they have been peer reviewed for publication by the several reviewers.

Editor
Prof.Dr.Hakan S. Soyhan
Department of Mechanical Engineering,
Sakarya University, Turkey

December, 2016

CONTENTS / İÇİNDEKİLER

Title of Manuscript/Makale Başlığı **Page Number/Sayfa No**

CI ENGINE MODELING AND EXPERIMENTAL STUDIES FOR LOWER EXHAUST EMISSIONS 4
Mehmet Zafer GUL, Mustafa YILMAZ, Hasan KÖTEN, Ismail Hakki SAVCI

INVESTIGATION OF HEAT RELEASE RATE OF BIODIESEL PILOT FUELLED NATURAL GAS ENGINE WITH STOCHASTIC REACTOR MODEL 14
Enes Fatih PEHLIVAN, İsmail ALTIN, Hakan Serhad SOYHAN

EXPERIMENTAL INVESTIGATION OF USING LNG IN VEHICLES 21
Nafiz KAHRAMAN, Mehmet Ali BEKTUR, Hayrettin ATAY

A NUMERICAL STUDY OF NO AND SOOT FORMATION IN AN AUTOMOTIVE DIESEL ENGINE FUELED WITH DIESEL-BIODIESEL BLENDS 27
Müjdat FIRAT, Şehmus ALTUN, Yasin VAROL

EVALUATING ENVIRONMENTAL EFFECTS OF BIOETHANOL-GASOLINE BLENDS IN USE A SI ENGINE 36
Ahmet Necati ÖZSEZEN

INVESTIGATION OF SMALL WIND TURBINE AIRFOILS FOR KAYSERI WEATHER CONDITIONS 42
Cevahir TARHAN, İlker YILMAZ

3D COLD FOLLOW SIMULATION INSIDE INTAKE MANIFOLD AND CYLINDER OF AN IC ENGINE 44
Bilge Albayrak ÇEPER, Melih YILDIZ, Vedat DEMIRTAS, Hakan Serhad SOYHAN, Nafiz KAHRAMAN

THERMAL PERFORMANCE ANALYSES OF WATER BASED CuO-TiO2 HYBRID NANOFLUID FLOW IN A HORIZONTAL TUBE 49
Toygun DAGDEVIR, Veysel OZCEYHAN

EFFECT ON EXHAUST EMMISSIONS OF ENGINE WITH TURBOCHARGED ON USE AS FUEL OF CAMELINA SATIVA ETHYL ESTER 55
Hasan AKAY, Hasan AYDOĞAN

THE PRODUCTION OF BIODIESEL CAMELINA SATIVA BIODIESEL AND EFFECT OF THE ON THE EMISSION OF AN ENGINE WITH A COMMON RAIL INJECTION SYSTEM 60
Rahman ŞİMŞEK, Hasan AYDOĞAN

TERMOELEKTRİK SİSTEMLİ YEMEK TAŞIMA MODÜLÜ TASARIMI VE ANALİZİ 65
Murat HACI, Zafer KAHRAMAN

TAŞIYICI-YÜKLEYİCİ BİR İŞ MAKİNESİ İÇİN DİFRANSİYEL DİŞLİ KUTUSU TASARIMI 72
Tuncay KAZAR, Cihan ASAL, Hakan Serhad SOYHAN, Vedat DEMIRTAS

CI ENGINE MODELING AND EXPERIMENTAL STUDIES FOR LOWER EXHAUST EMISSIONS

[1]Mehmet Zafer GUL, [2]Mustafa YILMAZ, [3]Hasan KÖTEN, [4]Ismail Hakki SAVCI
[1]Marmara University, zgul@marmara.edutr 02163375850
[2]Marmara University, mustafa.yilmaz@marmara.edu.tr, 02163480292
[3]Istanbul Medeniyet University, hasan.koten@medeniyet.edu.tr 02162803202
[4]FORD OTOSAN Company, isavci@ford.com 02165647100

ABSTRACT
In recent years, automotive companies and research centers have utilized different techniques to ensure tightened emission rules. These studies generally are divided into two main categories: in-cylinder and after-treatment applications. In the first stage, harmful exhaust emissions were decreased by optimizing engine parameters. After-treatment applications come into play after exhaust port for irreducible emissions. In the studies, done at Marmara University, three important works examined to get ultra-low emission for a single cylinder diesel engine. In the first study, engine parameters such as compression ratio (CR), intake and exhaust valve timings, mass flow rate were optimized for a range of engine speed. Then for the same engine injection parameters such as start of injection (SOI), injector cone angle, and split injection structures were examined to get optimum parameters for the diesel engine. In CR studies different combustion chambers were tested according to injector cone angles and fuel-wall interaction. In the second study, in addition to the above studies, dual fuel compressed biogas (CBG) and diesel combustion were analyzed under different engine loads both experimentally and computationally. Optimized single fuel diesel cases were compared with CBG + Diesel dual fuel cases which employed port injection for CBG fuel. In dual fuel engine applications, CBG fuel and air mixture is induced from intake port and this air-fuel mixture is ignited by pilot diesel fuel near top dead center (TDC). In dual fuel engine mode, exhaust emissions reduced considerably especially in NOx and particulate matter (PM) because of methane (CH4) rate and optimized engine parameters. The third study is focused on aftertreatment systems to minimize residual exhaust emissions. In this study, computational fluid dynamic (CFD) methodology was developed with conjugate heat transfer, spray, deposit and chemical reaction modeling then emission prediction tool was developed based on the CFD results with deposit prediction mechanism. CFD and deposit results were correlated with image processing tool in flow test bench.
Keywords: CFD, CI engine, emission, optimization, aftertreatment, SCR, NO_X

INTRODUCTION
In these investigations, three different works employed to get ultra-low emissions and high performance for a CI engine numerically and experimentally. Multidimensional simulations of the complete engine cycle of diesel engine for single and dual fuel cases are performed and presented here. Moreover, exhaust after-treatment emission modelling methodology are developed for NOx reduction system with experimental and numerical methods.

The intake and compression stroke analyses before the combustion has performed to verify the numerical results with more plausible turbulence model. Then spray and combustion modeling are performed with HCCI strategies in order to achieve clean combustion concept. Following the power stroke simulations emission are also calculated. Furthermore, emission treatment is analyzed in detail for a similar CI engine.

CFD studies for a single cylinder diesel engine were modeled using full engine geometry including intake-exhaust ports and valves. Selected cases were validated by experimental studies. As a result, both in-cylinder optimization studies and after-treatment application study were satisfied EURO6 emission criteria and increased combustion performance with new designed engine concept.

The emissions of the diesel engines consist of various harmful exhaust gases such as carbon monoxide (CO), particulate matter, unburned hydrocarbon (UHC), and nitrogen oxides. Several technologies have been developed to reduce diesel emissions especially NOx reduction systems in last decades [1-7]. The most promising NOx emission reduction technologies are exhaust gas recirculation (EGR) system to reduce peak cylinder temperature that reduces NOx formation caused by combustion and active selective catalyst reduction (SCR) system using reducing agent such as urea-water-solution for exhaust aftertreatment system [8-10].

Recent years many different emission reduction application strategies were developed. One of the challenging approaches is to remove the EGR from the engine, and design a high NOx conversion efficiency SCR with reducing agent system. Thus the comprehensive SCR modeling approach is required

to design compact aftertreatment systems that meet NOx emission legislation level [11-13].

NUMERICAL MODELING

In engine modeling study, optimum operating conditions in a diesel engine fueled with compressed biogas (CBG) and pilot diesel dual fuel were examined. One dimensional (1D), three dimensional (3D) computational fluid dynamics (CFD) code and multi-objective optimization code were employed to investigate the influence of CBG-diesel dual fuel combustion performance and exhaust emissions in a CI engine. In engine studies, 1D engine code and multi-objective optimization code were coupled and evaluated about 15000 cases to define the proper boundary conditions.

3D CFD codes were employed for single diesel fuel and dual fuel (CBG-diesel) cases. Detailed specifications of engine were given in Table 1. In this work, in-cylinder combustion pressure and rate of heat release (ROHR) were evaluated under different operating conditions, engine loads and analyzed the combustion characteristics of the CI engine for single-fuel (diesel) and dual-fuel (CBG-diesel) combustions [14]. Moreover, combustion pressure or indicated mean effective pressure (IMEP), exhaust gas temperature and also Soot, NOx, HC, CO and CO2 exhaust emissions were investigated under different engine operating conditions to investigate the engine performance and exhaust emission characteristics of single-fuel and dual-fuel modes.

Table 1 Engine specifications.

Bore [mm]	76.0
Stroke [mm]	80.5
Displacement volume [cc]	365,25
Number of Cylinders	1
Compression Ratio	17.6
Air intake	Turbo charged

The 3D engine code was used to define the piston movement, intake and exhaust valve lifts. It has been exploited to generate the grid to create the hexahedral cells for the engine model including cylinder head, intake and exhaust ports and piston bowl as shown in Fig 2. The number of cells changed from 500.000 cells in TDC and over 1,700,000 cells in BDC. For the mesh generation hexahedral cells have been accepted since they provided a better accuracy, stability and less computational time compared to tetrahedral cells.

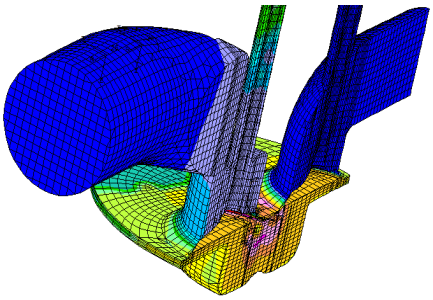

Figure 2 Sectional mesh view for full geometry.

The aftertreatment methodology was developed based on the selective catalyst reduction system after the engine outlet. The developed 3D numerical model accounts for all relevant physical effects. The multi modeling steps were correlated based literature data for each physics such as decomposition process, spray and reducing agent distribution. The influences of flow conditions exhaust system properties and spray parameters on the film formation were evaluated with the developed simple models.

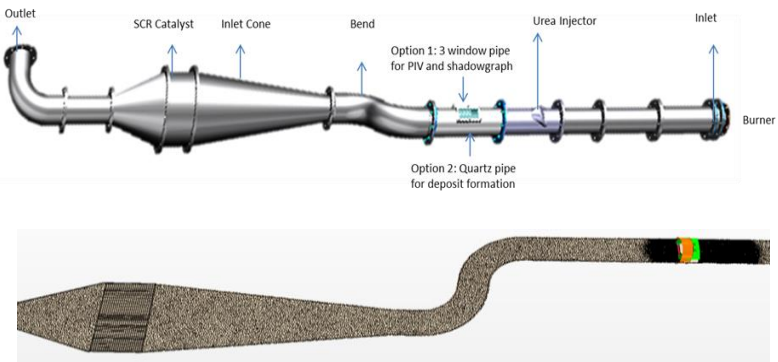

Figure 3. SCR Aftertreatment inline model and computational domain.

The mesh is created using Star-CCM with 2 million elements, including two prism layer around the mixer region to resolve the near wall conditions. The mixer wall and pipe wall are modeled as solid for conjugate heat transfer. Figure 3 shows the computational domain of inline exhaust aftertreatment system

NUMERICAL SIMULATION AND EXPERIMENTAL SETUP

The aim of engine modelling study is to develop engine modelling methodology in CFD. In addition, this methodology was provided proper injection parameters for the homogenous charge compression ignition (HCCI) combustion process for a heavy duty diesel engine. Three conventional type diesel engine cases and four homogenous charge compression ignition (HCCI) type diesel engine cases have been analyzed. The cases were prepared to study the effects of the parameters: start of injection, spray angle and spray profile. Two kinds of injection strategies, conventional diesel direct injection and two stage injection (split injection), were examined. The results confirmed that the split injection strategy is more effective in reducing NOx emissions than the direct injection (DI) diesel engine while maintaining high thermal efficiency. Also, it has been found that, the split injection strategy with narrow cone angle fuel injection has the potential for reducing CO emissions by optimizing both injection timings and piston bowl geometry.
Different injection parameters and their combinations were examined to understand how they effect on combustion process. Detailed investigations of cold flow, spray and combustion phenomenon for a heavy-duty CI engine were performed by Yilmaz [15,16]. In these cases, start of injection (SOI), spray angle and spray profile were changing. Table.2 and Table.3 shows the distinctive marks of the test engine and cases that are compared with each other.

Table 2 Some properties of the test engine

Engine parameters	Value
Type	1 Cylinder
Bore × Stroke	104×145 mm
Connecting rod length	231.2 mm
Compression ratio	19.75:1
Max. Lift (exhaust)	10,4 mm
Max. Lift (intake)	9,9 mm
Operating speed	1000 rpm

Three conventional cases which have cone angle of 149° CA and compression ratio of 19.75:1 are simulated in different SOI conditions. The proper case of these three conventional cases which has minimum NOx and CO is selected. Moreover, HCCI cases which have the same compression ratio and SOI of 120° CA TDC with two different cone angles of 80° and 60° CA were performed. Similarly, last two HCCI cases were performed in different compression ratios of 16.27:1 and same cone angles condition. In similar conditions cases were compared each other.

Table 3 Case studies

Type	Case #	Cone angle	SOI CA	Injection profile	Compression ratio
Conventional diesel	0	149°	-20	single	19.75
	1		-25		
	2		-15		
Narrow angle	3	80°	-120 -12 +6	Pre 30% Main 65% Post 5%	19.75
	4	60°	-120 -12 +6	Pre 30% Main 65% Post 5%	19.75
	5	80°	-120 -12 +6	Pre 30% Main 65% Post 5%	16.27
	6	60°	-120 -12 +6	Pre 30% Main 65% Post 5%	16.27

The conventional type diesel engine processes are shown in the first three cases. Other cases denote the Partially Premixed Compression Ignition (PPCI) type diesel engine. Effect of mass flow rate on the emissions and total heat release were examined in the first three cases. For both three cases total injected mass per cycle is same, but SOI and end of injection (EOI) are vary, so the mass flow rates are different.

The lower diesel fuel consumption (dodecane-2.14 kg/h) caused the reduction on the combustion performance as shown in figure 4 (a). When it came to the 60% load, shown in Fig. 4 (a), the diesel combustion showed slightly higher peak combustion pressure (Pmax = 8.4 MPa) and peak heat release compared to CBG-diesel case (Pmax = 8.3 MPa). Simultaneously, a greater indicated mean effective pressure (IMEP) was obtained for single fuel diesel injected fuel mass reached 5.3 kg/h. Figure 4(b) shows effects of dual fuels on the combustion characteristics with different engine loads.

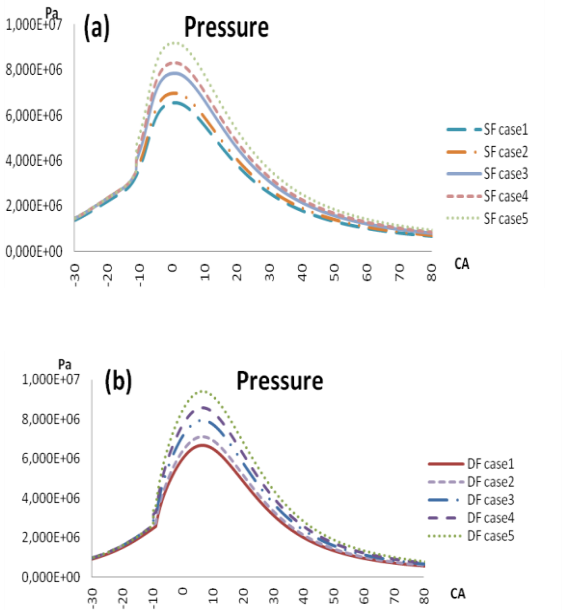

Figure 4 Combustion characteristics at different engine load. (a) Single fuel (dodecane) cases. (b) Dual fuel (CBG+dodecane) cases.

The concentrations of NOx emissions for the engine operated with single and dual-fuel combustion modes were shown in Fig. 5. In Fig. 5, when the engine load increased, NOx concentrations of all test cases increased steeply. Significantly lower NOx emissions were emitted within the dual-fuel operations compared to the single mode at all conducted test ranges. In Fig. 5, single fuel diesel combustion cases resulted in higher NOx emissions at all engine loads compared to dual fuel cases. The reason behind this trend could be explained by the faster injection and early ignition characteristics of diesel which are visible in previous outcomes of combustion characteristics.

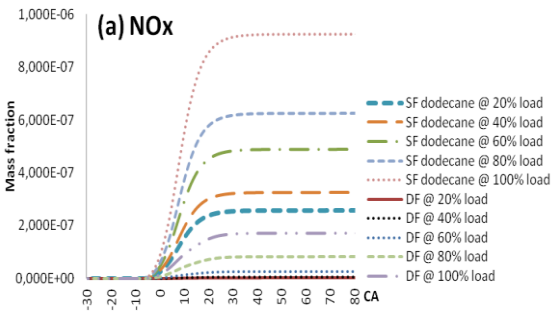

Figure 5. NOx for single and dual fuel cases versus CA.

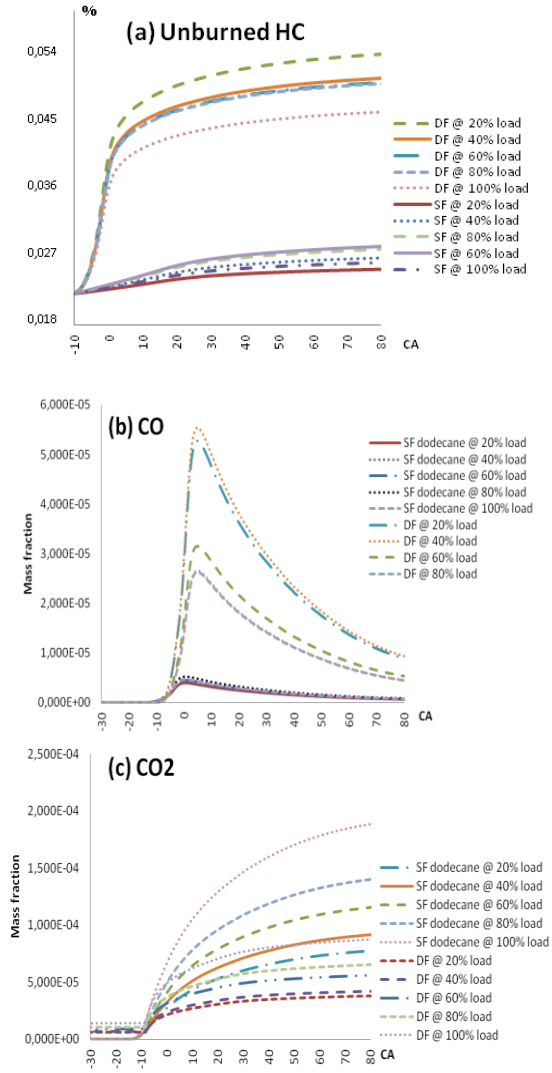

Figure 6 Exhaust emissions for single and dual fuel cases with different engine loads.

In fig. 6 (a), (b) and (c) for single and dual fuel cases at various engine loads, CO_2, HC and CO concentrations were shown. In dual fuel cases, gaseous fuel induced during the intake stroke, this air fuel mixture decreases the charge temperature and affects combustion performance and exhaust emissions. Ignition delay takes longer time in dual fuel cases because of decrease charge temperature and lower cetane number. For this reason, in dual fuel combustion cases concentrations of HC and CO emissions bigger than single fuel cases. In figure 6 (a) HC emissions decreased by increase of engine loads due to the increase of combustion temperature. Similarly, in figure 6 (b) CO concentrations decreased due to the increase of temperature inside the combustion chamber by engine loads. CO_2 content of CBG is ingested during the intake process clearly seen in figure 6 (c). For single fuel cases CO_2 emissions are higher than dual fuel cases when compared to CO_2 content of CBG-dodecane dual fuel cases. Carbon content of single fuel cases are

relatively higher than dual fuel cases, resulting significantly increase in CO_2 emissions. As shown in these figures, the concentrations of CO_2 emissions for dual fuel were obviously under those regarding single diesel combustion modes. Moreover, higher cetane number of diesel and the faster injection timing shortened the ignition delay and this reduction is related to a decrease in fuel-rich zone throughout the combustion process [3]. When single and dual-fuel combustions were compared, the concentrations of HC and CO emissions for the single-fuel mode were considerably lower than dual-fuel mode under all test conditions. CBG-air mixture needs to reach the specific temperature value to continue the flame propagation in the combustion region. CO emissions for single fuel combustion emitted somewhat lower and roughly constant amounts of soot in comparison to dual fuel combustion.

The last emission prediction work is aftertreatment modeling [17]. The aim of this work is to develop comprehensive approach to predict exhaust emission for selective catalyst reduction. The emission prediction is assessed by 1D modeling tools. The complex physics are modeling by 3D simulations of exhaust gas aftertreatment systems.

The CFD software calculates the conjugate heat transfer, flow field, spray modeling, species distribution and deposit modeling in the SCR systems. These results are calibrated by using the experimental data coming from the PIV, shadowgraph measurement in flow test bench and dyno test bench. Figure 7 shows the test bench for the exhaust aftertreatment modeling setup. PIV and shadowgraph was occurred to get velocity distribution and particle sizes.

The measurements are performed under a wide range of transient and steady state operating conditions. For this work flow test bench is built with compressor, burner and automation system.

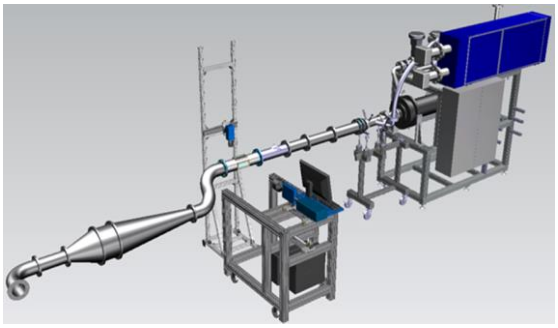

Figure 7. Schematic of Exhaust System Layout with Emission

Since deposit has complex phenomenological physics for 1D emission prediction tool is required whether the design meet the emission legislation target. This emission prediction tool should be fast and accurate method with 3D simulation and deposit effect on the SCR system. Before freezing the design of SCR system, emission level of design should be predictable whether further design optimizations or advanced SCR technologies are required. 1D emission tool can predict to different SCR catalyst sizing, chemical kinetic effect and different aftertreatment system layout on emission level.

RESULTS AND DISCUSSION

Figure 8 shows the example of the combustion characteristics of conventional diesel combustion attained by single injection [16]. In the case of conventional diesel, combustion starts by injection at 15°, 20°, 25° bTDC, as shown in Fig. 8. In these first three cases, the ignition delay was very short and ignition had begun during injection event. This led to significant in homogeneity during combustion. Corollary, high emission results such as NOx and soot could be expected as seen in Fig. 10. NOx emission decreases for conventional diesel engines when the distance between the start of the injection and TDC is larger. Because of the high temperature and heat release, NOx emission results higher and soot emission results lower than the other cases.

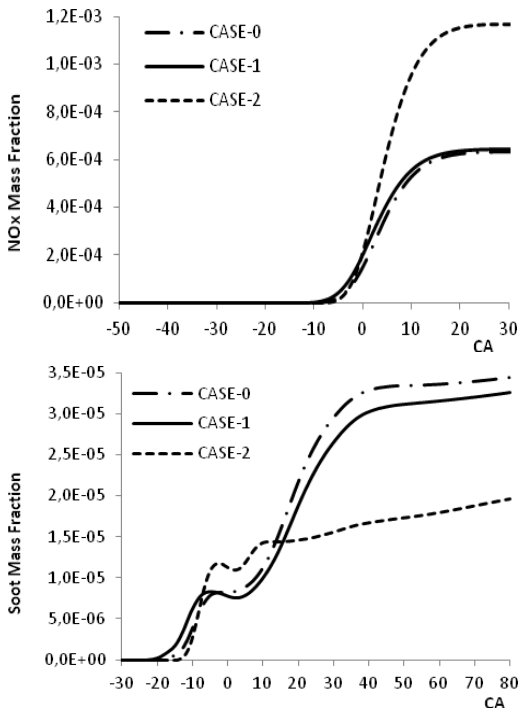

Figure 8 Injection rates and results for conventional cases.

NOx and soot emissions showed a strong dependence on the injection timing at a constant equivalence ratio. The peaks of the NOx emissions occurred between -10° and 20° which were slightly

advanced of the injection timing as typical of the operating conditions of a conventional diesel engine as shown in Figure 8.

Figure 9 shows the example of the combustion characteristics of PPCI diesel combustion attained by split injection. In this split injection strategy pre, main and post injections have 35%, 60%, 5% of fuel per stroke respectively with 80° and 60° narrow angle.

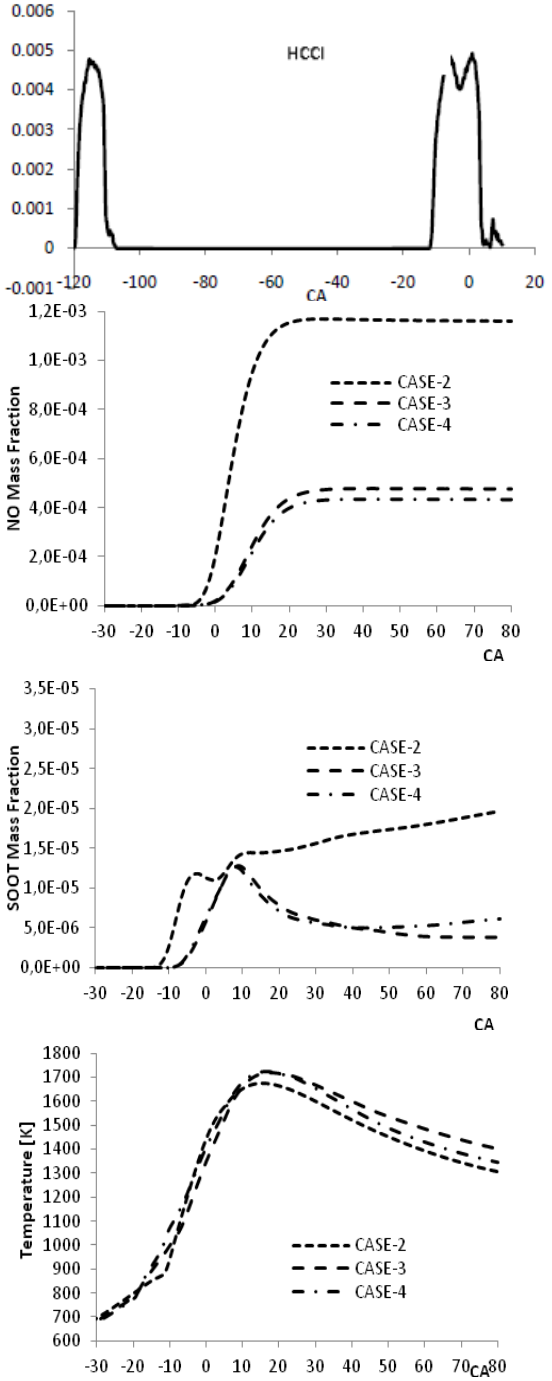

Figure 9 Comparison of the results for different the spray angles

In these cases, the ignition delay was very long and ignition had begun before main injection event close to TDC about 23° bTDC. This led to significant homogeneity during combustion. Corollary, low emission results such as NOx and soot could be expected.

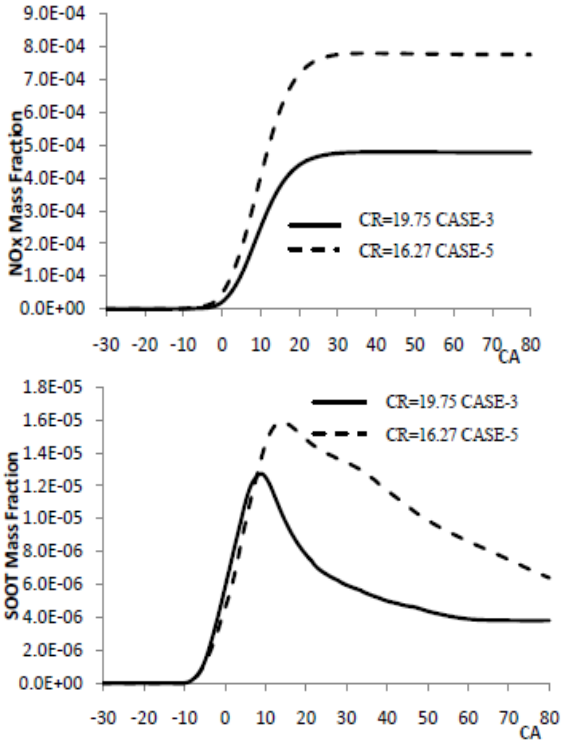

Figure 10 Comparison of the best PPCI cases according to emission performance for different compression ratio.

The results for PPCI cases shows that, case3 which is prepared with using 80° cone gives better emission performance for both soot and NOx emissions relative to case4 with 60° cone angle. PPCI cases were compared to obtain optimum case for NOx and soot emissions. Fig. 8 shows the results for these cases.

The injection profile has a consequential effect on the emissions as seen in the Fig. 11. The soot emission results show that partially-premixed type injection model reduces this emission. However, NOx emission fraction for case2 is much more than the other cases due to the single type injection of fuel and start of the injection. The pre-injection (%30 of total fuel per stroke) makes the average temperature in-cylinder higher than the other cases as seen in the Fig. 11. Locally high temperatures (~2700K) are formed especially at the regions close to the injection point. Same results occur in the case3, case4, case5, case6, which includes %30 pre-injection fuel mass. Case3 gives the best results for soot and NOx emissions. Fig. 11 shows that there is an improvement on emissions with narrow cone angles

and split injection strategy. The soot and NOx emissions decrease for PPCI cases which includes narrow spray angles although there is high in-cylinder temperature relative to conventional cases. PPCI results show that case3 in which the injector has 80° cone angle results in lowest emissions.

On engine geometry, compression ratio was reduced from 19.75:1 to 16.27:1 by decreasing maximum radius of the bowl and increasing the depth of the bowl to prevent the immoderately advanced ignition of the pre-mixture formed by early injection Table 3. Because of its effects on in-cylinder temperature and pressure during the compression phase, the engine compression ratio has an influence on the auto-ignition phase of the combustion: a reduction prolongs the air/fuel mixing process before combustion. Different works, performed on experimental single cylinder engines showed this significant advantage [16].

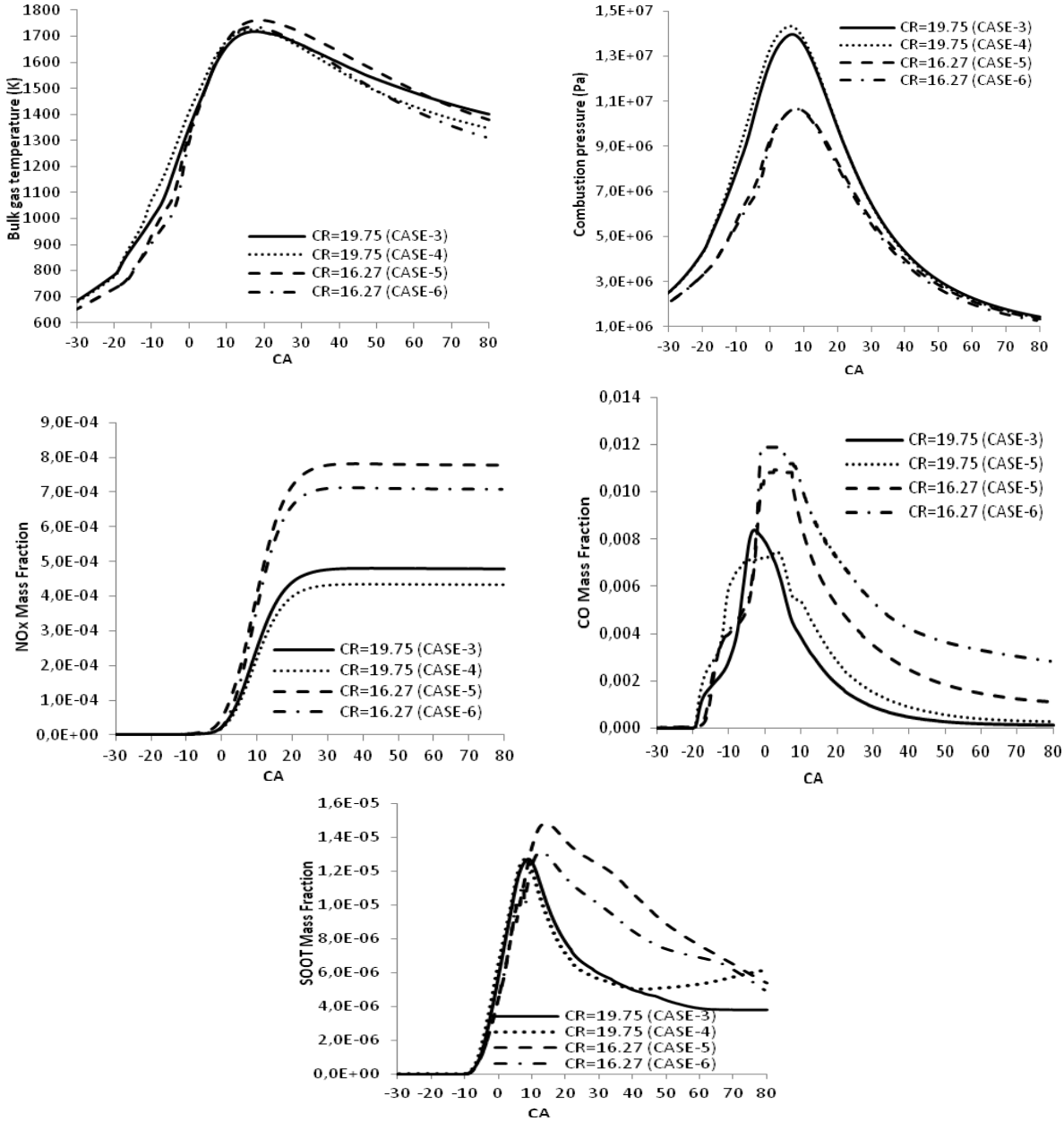

Figure 11 Effects of the compression ratio

According to soot emission results show to reduce the compression ratio increases emission values. Both of NOx and soot emission fractions for case5 is much more than for case3 due to compression ratio value. Reducing compression ratio should be made the average temperature and pressure in-cylinder higher than the other cases but not. Because of the high temperature and heat release, NOx and soot emission results are higher than other cases. Same results occur in the case6, which includes less

compression ratio value. Case3 gives the best results for soot and NOx emissions. Case3&5 which use 120 degree CA bTDC as a start of the injection time, has better emission values than the other two cases.
The results are shown in Fig.11 show that although there is a rise on the mass fraction of the soot, the NOx value for case4 which uses a narrow spray angle of with 60°, is better than case3. The peaks of the temperature occurred unexpectedly at cases have reduced compression ratio (16.27). Therefore, these two cases have indicated that the high temperature reaction (HTR) occurs at around 1000–1100 K. The calculated peak of the bulk gas temperature for reduced compression ratio as shown in Fig.13 was about 1800 K such as conventional diesel combustion, clearly lower than NOx formation temperature but higher than other PPCI cases.

As the compression ratio reduced, the peaks of heat release rate of HTR rapidly increased and the initiating timings of the reaction were also retarded. In these cases, the ignition delay was very long and ignition had begun before main injection event close to TDC about 20°-25° bTDC. This led to significant homogeneity and better combustion control during combustion. However, higher emissions such as NOx and CO could be unexpected. Only soot emissions consequently slightly decreased and kept reduction trend. Furthermore, it could be said that fuel is burned effectively with respect to other cases (Fig.11) especially for case4 has reduced compression ratio (case6).

The efficient design of selective catalyst reduction system is required to NOx reduction mechanism. This system design is crucial for emission legislation. In this study, comprehensive modeling approach has been developed to simulate active SCR system based on inline exhaust aftertreatment system from Flow Test Bench. By This method we can understand whether the design/design changes effect on emission. [10-13, 17, 18]

Three dimensional (3D) simulation of inline exhaust aftreatment system with spray injection of UWS, evaporation and thermal decomposition processes have been presented results in the present chapter using Star-CCM [17]. The deposit prediction of the CFD result was correlated with flow lab image processing. Then the deposit mass increased and ammonia mass flow rate are reduced based on the flow lab test results. The correlated values of ammonia are passes to emission prediction model. [18]

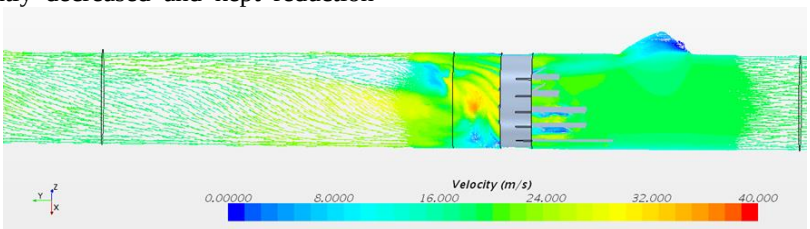

Figure 12. Velocity vector at the cone k-epsilon

The velocity fields are investigated in details. The turbulence model of the RSM predict in good agreement of the flow recirculation at the upstream of the catalyst. k-ε turbulence model cannot predict the swirl region upstream of the mixer in Figure 12.

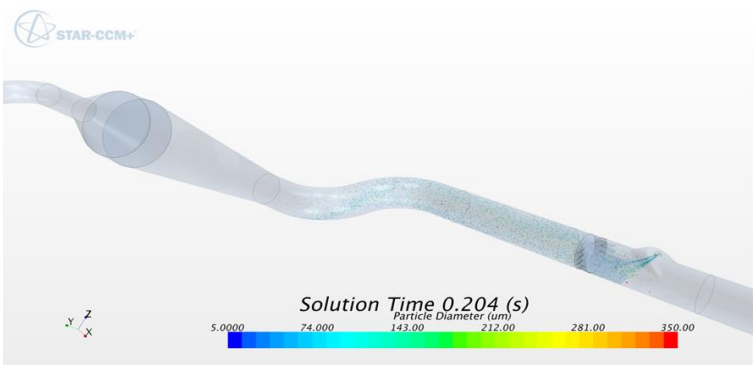

Figure 13. Droplet Distribution across the system at 0.1325 **s**

The mixers are installed at the downstream of the injector of the inner pipe. They are enhanced droplet evaporation, breakup and distribution of the spray. [19] The mixer has significant effect on the break-

up process. Figure 13.shows the application of mixer. [20]

Emission results of the inline exhaust aftertreatment system shows high temperature operating point NOx conversions are %98.

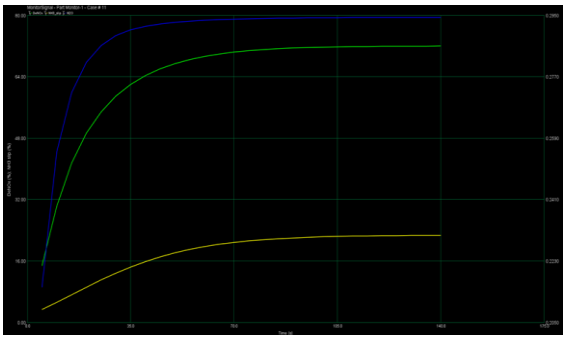

Figure 14. WHSC point for NH3 distribution from CFD

Figure 14.shows emission result of the inline exhaust aftertreatment system. For high temperature operating point NOx conversions are %98.

CONCLUSION

In this work, three main studies; effects of engine parameters on the diesel engine performance, effects of dual fuels on the diesel engine performance and aftertreatment system investigations were studied and presented. Various configurations of compression ratio, injection timing, cone angle and bowl geometry are compared to get the best performance of the engine. Obtained CFD results are found qualitatively in agreement with the previous experimental and computational studies in the literature.

In the present study new combustion model (ECFM-3Z) is used successfully. Moreover, on an engine configuration with compression, spray injection and combustion in a DI Diesel engine are satisfactorily modeled. Effect of combustion chamber design and injection parameters for single and dual fuels in a DI diesel engine are investigated and presented. Simulations how the injection parameters affect emissions, show that the emission results under some PPCI circumstances may be highly affected by a relatively small change of injection rates. Multicomponent UWS injection modelling and multi reaction modeling as thermolysis and hydrolysis have been implemented into inline exhaust aftertreatment system and validated with literature work and flow test bench capabilities as pressure, temperature NOx and FTIR information. The PIV gives reasonable result to correlate this complex SCR system.

The developed numerical simulations for droplet and species show the dependency of the SCR system to the injection characteristics and flow field parameters. The good agreement is shown in terms of injection and flow field between numerical model and flow test bench.
The simulation of active SCR system has been performed in spray-wall interaction framework as well. The multi component Bai impingement model has been adopted into numerical simulation to predict deposit location but mass of deposit cannot predict well.

These comprehensive 1D emission models are used to predict emission level in WHSC cycle and compared the dyno test results. These results are comparable well. Considering the results of this work, following conclusions can be drawn:

The present work revealed that Reynolds stress turbulence model is sufficient to model. PIV measurement and RSM simulations may be employed to directly validate turbulent exhaust flow field and spray simulation.
The heat transfer correlation work of inline exhaust aftertreatment system shows conjugate heat transfer is required.

In addition to serving their primary purpose of enhancing mixing between exhaust gas and spray, mixers are quite effective in reducing deposits. Heat transfer via spraying onto a mixer's hot surfaces results in enhanced boiling and convective heat flux. Mixers with large surface area are promising in enhancing particularly conjugate heat transfer despite the fact that mixers often reduce spray particle transport length. System design has a significant impact on the system performance and formation of the deposit.

The pipe surface temperature is a critical factor due to the deposits that form on the inner pipe walls of the system. Below a certain critical temperature, wall wetting and ensuing deposit formation are built.

1D emission prediction models with species, velocity and temperature data from 3D CFD at the SCR inlet and deposit mapping from image processing tool shows the good validation according to engine dyno data.

NOMENCLATURE

1D : One-Dimensional
3D : Three-Dimensional
aBDC : After bottom dead center
aTDC : After top dead center
BDC : Bottom dead center
Bsfc : Brake specific fuel consumption (g/kWh)
CA : Crank Angle
CAD : Crank angle degree

CFD :Computational Fluid Dynamics
CI : Compression ignition
CO : Carbon monoxide
CO :Carbon Monoxide
EC :European Commission
EGR :Exhaust Gas Recirculation
NOx :Nitrogen Oxides
PM :Particulate Matter
SCR :Selective Catalytic Reduction

ACKNOWLEDGMENTS

These works have been supported by Marmara University BAPKO institution and FORD-OTOSAN Company. This work has been supported by Marmara University BAPKO Institution entitled of FEN-D-091116-0505.The authors would like to thank the BAPKO institution for supporting this research project.

REFERENCES

[1] Albrecht, A., Grondin, O., Le Berr, F. and Le Solliec, G., 'Towards a stronger simulation support for engine control design: a methodological point of view', Les Rencontres Scientifiques de l'IFP – New Trends in Engine Control, Simulation and Modelling; 2006.
[2] Chauvin, J., Corde , G., Petit, N. and Rouchon, P., 'Experimental air path control of a Diesel engine', Les Rencontres Scientifiques de l'IFP – New Trends in Engine Control, Simulation and Modelling, 2006.
[3]M.Y. Kim, S.H. Yoon, C.S. Lee, "Impact of split injection strategy on the exhaust emissions and soot particulates from a compression ignition engine fueled with neat biodiesel" Energy and Fuels 22, 1260–1265, 2008.
[4] R.L. McCormic, C.J. Tennant, R.R. Hayes, S. Black, Sharp, "Regulated Emissions from Biodiesel Tested in Heavy Duty Engines Meeting 2004 Emission Standards", SAE 2005-01- 2200, 2005.
[5] M.Y. Kim, S.H. Yoon, J.W. Hwang, C.S. Lee, "Characteristics of particulate emissions of compression ignition engine fueled with biodiesel derived from soybean", Journal of Engineering for Gas Turbine and Power 130 (5) 052805-1–052805-7, 2008.
[6] N.N. Mustafi, R.R. Raine, "A study of the emissions of a dual fuel engine operating with alternative gaseous fuels", SAE 2008-01-1394, 2008.
[7] Gatellier, B., Ranini, A. and Castagné, M., 'New development of the NADITM Concept to improve operating range, exhaust emissions and noise. Combustion'. Oil and Gas Science and Technology, Vol. 61 , No 1, pp. 7–23, 2006.
[8]F. Birkhold, U. Meingast and P. Wassermann, "Analysis of the Injection of Urea-water-solution for automotive SCR DeNOx-Systems: Modeling of Two-phase Flow and Spray/Wall-Interaction," SAE, 2006-01-0643, 2006.
[9] A. A. Mckinely T.L., "Urea Decomposition Modeling Framework for SCR," SAE Int.J.Fuels Lubr, pp. 612-626, 2009.
[10] A. Munnannur and Z. Liu, "Development and Validation of a Predictive Model for DEF Injection and Urea Decomposition in Mobile SCR DeNOx Systems," SAE International, no. 2010-01-0889, 2010.
[11] H. Ström, A. Lundström and B. Andersson, "Choice of urea-spray models in CFD simulations of urea-SCR systems," Chemical Engineering Journal, no. 150, 2009.
[12] P. P. S. G. K. A. Zheng G., "Mixer Development for Urea SCR application," SAE, no. 01-2879, 2009.
[13] L. S. K. W. L. C. Jeong S., "Simulation on the optimum shape and location of urea injector for urea SCR system of HDDE to prevent NH3 slip," SAE, no. 01-3886, 2005.
[14] Koten H., "Experimental Investigation and Multidimensional Modeling Of Biogas Effects On The Diesel Engine Combustion Characteristics" Phd Thesis, Marmara University, 2014.
[15] Yilmaz M, Köten H, Gul M. Z,. Effects of the injection parameters and compression ratio on the emissions of a heavy-duty diesel engine. International Journal of Vehicle Design. v59, 147-162, 2012.
[16] Yilmaz, M., "Effect of CDC Concept on the Design Parameters of a Heavy Duty PPCI Engine by Use of Multidimensional Modeling", PhD Thesis, University of Marmara 2009.
[17] Savci I., "An Integrated Modeling Approach to Investigate Performance of Selective Catalyst Reduction" PhD Thesis, University of Marmara 2015.
[18] E. Aburamadan, K. Saha and X. Li, "Modeling the Depleting Mechanism of Urea-Water-Solution Droplet for Automotive Selective Catalytic Reduction Systems," AIChE J., no. DOI 10.1002/aic.12523, 2011.
[19] Birkhold, Selektive katalytische Reduktion von Stickoxiden in Kraftfahrzeugen, Stuttgart: PhD Thesis, 2007.
[20] F. Birkhold, U. Meingast, P. Wasserman and O. Deutschmann, "Analysis of the Injection of Urea-Water-Solution for Automotive SCR DeNOx-Systems: Modeling of Two-Phase Flow and Spray/Wall-Interaction," SAE Paper,no. 2006-01-0643, 2006.

Sayı 4, Aralık 2016 Volume 4, December 2016

INVESTIGATION OF HEAT RELEASE RATE OF BIODIESEL PILOT FUELLED NATURAL GAS ENGINE WITH STOCHASTIC REACTOR MODEL

Enes Fatih PEHLIVAN[1], Ismail ALTIN[2]*, Hakan Serhad SOYHAN[3]
[1]Ordu University, Fatsa Faculty of Marine Sciences, Department of Naval Architecture and Marine Engineering, Ordu, TURKEY
[2]Karadeniz Technical University, Surmene Faculty of Marine Sciences, Department of Naval Architecture and Marine Engineering, Trabzon, TURKEY
[3]Sakarya University, Faculty of Engineering, Department of Mechanical Engineering, Esentepe Campus, Sakarya, TURKEY

Abstract
In this study, heat release rate (HRR) characteristics of natural-gas (NG) dual-fuel (DF) engine using biodiesel pilot fuel were investigated by stochastic reactor model (SRM). SRM Engine Suite software having solution method in zero-dimensional was used to apply stochastic reactor model into the DF engine. Results of the study were validated by the experimental data obtained from biodiesel pilot fuelled NG engine. Biodiesel surrogate fuel was considered as a mixture of methyl decanoate (25 v%), methyl-9-decenoate (25 v%) and n-heptane (50 v%) and its skeletal kinetic mechanism includes 71 species and 217 reactions. In addition, it is shown that biodiesel surrogate fuel chemical kinetic mechanism could represent soy biodiesel fuel. Case studies were realized under 50, 100, 150 and 200 stochastic particles with 120 MPa pilot fuel injection pressure and 17°BTDC pilot fuel injection timing conditions in the simulations. It was observed that SRM method is a good tool to investigate HRR of biodiesel pilot fuelled DF engine.

Keywords: Dual fuel engine, Biodiesel pilot fuelled natural gas engine, Stochastic Reactor Model, Monte Carlo stochastic particle method, Probability Density Function

1. Introduction

Effects of air pollution and climate change on life quality of people have been inclusively discussed by the authorities, scientists and researchers during the last decades. One of the most significant sources of this deterioration is exhaust emissions stemmed mainly from road vehicles', marine-, and jet engines. Exhaust emissions from these engines are caused by combustion of hydrocarbon fuels and composed of Carbon monoxide (CO), Nitrous oxides (NO_x), unburned hydrocarbon (UHC), Sulphur oxides (SO_x), and Carbon dioxide (CO_2) in general [1]. There are various legislations and regulations to control and to mitigate harmful exhaust emissions. European Emission Standards (i.e. Euro VI) [2] and International Maritime Organization (IMO) MARPOL Annex VI [3] are fundamental standards for road vehicles and maritime field, respectively.

The 'dual fuel' engine concept is developed to enhance engine emissions. Two different fuels (i.e. LPG, biogas, natural gas as the main fuel and diesel, DME, etc. as the pilot fuel) are simultaneously admitted into combustion chamber [4] in DF engines. They are either originally produced by factory or converted from available compression ignition (CI) engines. They can be operated on either conventional liquid fuels or gaseous fuel (NG) [5,6].

Diesel fuel is conventionally used as a pilot fuel in DF engines since it does not require major modifications in the engine fuel system. Recently, biodiesel has also been commonly used as a pilot fuel in DF engines since its properties are similar to diesel fuel. Furthermore, biodiesel has higher cetane number than conventional diesel fuel. It decreases ignition delay and is an environmentally friendly fuel with low smoke emissions as it contains 10% oxygen [7,8,9].

Nowadays, NG is conventionally used as a main fuel in DF engines. Natural gas has lower carbon-to-hydrogen ratio and higher auto-ignition temperature according to other hydrocarbon fuels. Therefore, using NG in DF engines lowers the CO_2 emissions. In addition, when NG amount entered into the combustion chamber is increased, oxygen ratio in the combustion chamber decreases. Hence, biodiesel pilot fuel can be considered for starting ignition to increase oxygen ratio.

It was investigated impacts of pilot injection pressure on engine performance and exhaust emissions characteristics in a single cylinder diesel engine and also aimed to obtain a simultaneously reduction of PM and NO_x emissions [7]. It was found by author that biodiesel pilot fuel injection at high pressure had lower indicated mean effective pressure (IMEP) than diesel fuel injection. As pilot fuel injection pressure of biodiesel was increased, smoke and NOx emissions are decreased and increased, respectively. It was investigated effects of pilot injection timing on combustion and exhaust

emissions with a biodiesel-CNG dual fuel combustion system in a single cylinder diesel engine [8]. It was found that performance could be optimized for biodiesel-CNG dual fuel combustion by adjusting the pilot injection timing at low loads and retard injection timing at high loads. Smoke was reduced and NO_x was increased by advanced pilot injection timing in biodiesel-CNG dual fuel combustion. It was performed an experimental investigation about the use of Jojoba Methyl Ester as a pilot fuel and natural gas or LPG as a primary fuel under dual fuel mode in Ricardo E6 variable compression diesel engine [10]. They found that Jojoba Methyl Ester fuel revealed improved dual fuel engine performance, reduced the combustion noise, extended knocking limits and reduced the cyclic variability of the combustion. It was extensively tested natural gas combustion to obtain performance and emissions maps in a direct injection CI engine [11]. Diesel and Rapeseed Methyl Ester (RME) were used as a pilot fuel. It was found that thermal efficiency of dual fuel mode was lower except from highest powers than that of single diesel fuel operation and specific NO_x contours of diesel and RME based single fueling were significantly different when these fuels were used to pilot natural gas combustion. Also, it was found that RME piloted specific NO_x at the highest speeds were the only exception to this trend and higher specific UHC and lower specific CO_2 emissions were observed in case of natural gas based dual fueling. An experimental investigation is carried out to compare engine performance and emissions in natural gas dual fuel engine being originally CI engine. In their study, Pongamia pinnata methyl ester (PPME) and Diesel were used as a pilot fuel. It was found that PPME-CNG dual fuel operation was more effective than Diesel-NG dual fuel operation in terms of engine performance and emission characteristics and also PPME-CNG operations slightly increased NOx when compared to Diesel-CNG operation [12].

It is carried out an experimental study to investigate effect of eucalyptus biodiesel on engine performance and exhaust emission of NG dual fuel engine. They found that biodiesel as pilot fuel shows similar pressure–time history, with highest peak, as diesel fuel in conventional and dual fuel modes and also the use of eucalyptus biodiesel as pilot fuel decreased the high emission levels of UHC, CO and CO_2 particularly at high engine loads. NO_x emissions increased since eucalyptus biodiesel has lower heating value and the oxygen presence in the molecules [13].

There are a several studies on biodiesel pilot fuelled DF engines being NG as a main fuel, but it could be not found any stochastic based theoretical study on NG-DF engines with biodiesel pilot fuel in available literature. Thus, in this study, a theoretical model is developed and HRR of DF engine, having biodiesel being a pilot fuel and NG being a main fuel is investigated by using a SRM.

2. Model Description

Stochastic reactor model, its algorithm and numerical method for engine simulation are introduced in this section.

2.1. Stochastic Reactor Model for dual fuel engine

For general dual fuel engines simulated, it must be chosen Dual Fuel-SRM mode. The SRM is a spatially zero dimensional model of the contents of the combustion chamber based on Probability Density Function (PDF) transport methods. SRM in ICEs is realized by dividing the mass within the cylinder into an arbitrary number of virtual packages called particles. Each of these particles has a chemical composition, a temperature and a mass and can mix with other particles and exchange heat with the cylinder walls [14, 15, 16, 17, 18, 19].

The contents of the cylinder are subjected to pressure and volume changes, etc.. All quantities of interest are space independent and calculated from these processes. Solutions were obtained for SRM equations by Monte Carlo particle method. [14].

The global quantities in the SRM model are the total mass, volume, mean density and mean pressure. They are assumed not to vary spatially in the combustion chamber. These quantities are calculated based on known engine geometry, density and pressure [16,19].

Scalars, temperature and mass fractions for each species are local quantities. They are considered as random variables. These variables are expressed by MDF [16].

The fuel injection model includes fuel mass, which was injected, and the injection rate profile. The injected fuel is assumed to be vaporized at the moment of injection and introduces new fuel particles into the ensemble. This changes the total mass inside the cylinder and causes a change in the mass fractions and temperatures of the current set of particles [16, 19].

2.2. Main Equation

SRM Model calculates the evolution of the N_S chemical species' mass fractions, $Y_1, \ldots, Y_{Ns}$, and the temperature, T, as a function of time.

The N_S+1 random scalar variables are put together into the vector

$$\psi = \left(\psi_1, \ldots, \psi_{N_S}, \psi_{N_S+1}\right) = \left(Y_1, \ldots, Y_{N_S}, T\right)$$

whose distribution is given by the PDF, f. Mean quantities may be calculated using the PDF by:

$$\left\langle \psi_j(t) \right\rangle = \int \psi_j f(\psi;t)\, d\psi \tag{1}$$

In engine context, the in-cylinder density varies during an engine cycle, so it is more convenient to use the Mass Density Function rather than the PDF. The MDF is associated with the PDF by:

$$\mathrm{F}(\psi;t) = \rho(\psi) f(\psi;t) \tag{2}$$

where ρ is the mass density. The time evolution of the MDF in the SRM is described by the following PDF transport equation:

$$\begin{aligned}\frac{\partial}{\partial t}\mathrm{F}(\psi;t) = &\underbrace{-\sum_{j=1}^{N_S+1}\frac{\partial}{\partial \psi_j}\left[G_j(\psi)\mathrm{F}(\psi;t)\right]}_{chemical\ reaction} + \underbrace{\sum_{j=1}^{N_S+1}\frac{\partial}{\partial \psi_j}\left[A_j(\psi)\mathrm{F}(\psi;t)\right]}_{turbulent\ mixing} \\ &\underbrace{-\frac{1}{V}\frac{dV}{dt}\mathrm{F}(\psi;t)}_{piston\ movement} \underbrace{-\frac{\partial}{\partial \psi_{N_S+1}}\left[U(\psi_{N_S+1})\mathrm{F}(\psi;t)\right]}_{convective\ heat\ transfer} \\ &\underbrace{+\frac{\mathrm{F}_C(\psi;t)}{\tau_{crev}} - \frac{\mathrm{F}(\psi;t)}{\tau_{cyl}}}_{crevice\ flow} \underbrace{+\frac{\mathrm{F}_f(\psi;t)}{\tau_f}}_{fuel\ injection}\end{aligned} \tag{3}$$

with the initial conditions:

$$\mathrm{F}(\psi;0) = \mathrm{F}_0(\psi) \tag{4}$$

The right hand side of Equation (3) introduces the physical in-cylinder processes of chemistry, turbulent mixing, heat transfer, piston movement, crevice flow and fuel injection [16].

2.3. Solution Method

Equation (3) is solved using a Monte Carlo stochastic particle method [14, 16]. An ensemble of N_{par} stochastic particles make up a statistical representation of the PDF, which is approximated by:

$$f(\psi;t) \approx \frac{1}{N_{par}} \sum_{i=1}^{N_{par}} \delta\left(\psi - \psi^{(i)}(t)\right) \tag{5}$$

where superscripts attribute individual particles. Equations (1) and (5) combine to give an approximation of the mean quantities:

$$\left\langle \psi_j(t) \right\rangle \approx \frac{1}{N_{par}} \sum_{i=1}^{N_{par}} \psi_j^{(i)}(t) \tag{6}$$

To solve Equation (3), an operator splitting technique is employed so that each term can be treated separately [14, 20]. The operator splitting loop is described below:

1. Initialized t=0, Δt, CAD=IVC. Determine temperature, composition, mass, volume and pressure of particle ensemble.
2. Progress in time $t \rightarrow t+\Delta t$. If CAD≥EVO or $t \geq t_{stop}$ then save the detailed exhaust composition as input EGR and stop.
3. Perform volume change due to piston movement.
4. Perform gas exchange between bulk and crevice volumes.
5. Perform the first half of the turbulent mixing splitting step.
6. Perform stochastic heat transfer splitting step.
7. Perform the pressure equilibration step.
8. Perform the chemistry step.
9. Perform the pressure equilibration step.
10. Perform the second half of the turbulent mixing splitting step.
11. Perform the direct injection splitting step.
12. Go to step (2).

3. Results and Discussions

3.1. Biodiesel Chemical Kinetic Mechanism Feasibility

Chemical kinetic mechanisms for each biodiesel have not been developed yet. Hence, biodiesel surrogate fuel chemical kinetic mechanisms were used available studies. Firstly, these mechanisms were developed as detailed chemical kinetic mechanism, but use of this mechanism in CFD or SRM Software is very time-consuming. Therefore, reduced chemical mechanisms using some reduction methods were used instead of detailed chemical mechanisms. Thanks to reduced chemical kinetic mechanisms, simulations with CFD or SRM software has been very fast in terms of time. Surrogate fuel mixture considered for biodiesel in this study is composed of 25% of methyl-decanoate (MD), 25% of methyl-9-decenoate (MD9D), and 50% of n-heptane [21]. Reduced chemical kinetic mechanism, given by [22], for aforementioned fuel mixture was used during simulations. It was made a comparison between soy methyl ester lower heating value and the biodiesel surrogate fuel chemical kinetic mechanism lower heating value to show representability of soy biodiesel. While defined lower heating value for soy biodiesel, given by [7, 8], is 40.001 MJ/kg, defined lower heating value for biodiesel surrogate fuel chemical kinetic mechanism is 37.7 MJ/kg [22]. As mentioned above, it was demonstrated that biodiesel surrogate fuel chemical kinetic mechanism could represent soy biodiesel fuel.

3.2. Energy Audit for natural gas and biodiesel surrogate fuel

In this section, it was calculated as 36.443 MJ/m^3 thermal energy of natural gas used in SRM Engine Suite software and also calculated for

different conditions thermal energy of biodiesel surrogate fuel used in SRM Engine Suite software. Table 1 shows these results. Finally, calculated the energy audit for natural gas and biodiesel surrogate fuel is shown in Table 2. As seen in Table 2, biodiesel energy share has low values in terms of percentage and these values are allowable level.

Table 1. Released thermal energy amounts for injected pilot fuel cases

Thermal energy amounts for different pilot injection timings		
Pilot injection timings	Injected amounts of pilot fuel [kg]	Thermal energy for biodiesel pilot fuel [MJ]
11^0 BTDC	3.8127E-5	0.001437388
14^0 BTDC	3.85151E-5	0.001452018
17^0 BTDC	3.92305E-5	0.001478991
20^0 BTDC	3.88978E-5	0.001466448
23^0 BTDC	3.94592E-5	0.001487611

Thermal energy amounts for different pilot injection pressures		
Pilot injection pressures	Injected amounts of pilot fuel [kg]	Thermal energy for biodiesel pilot fuel [MJ]
30 MPa	2.75624E-5	0.001039102
60 MPa	3.18815E-5	0.001201932
90 MPa	3.50035E-5	0.001319634
120 MPa	3.92728E-5	0.001480586
150 MPa	4.1864E-5	0.001578274

Table 2. Calculated thermal energy values for dual fuel engines

Thermal energy for different pilot injection timings		
Pilot injection timings	Total thermal energy [MJ]	Biodiesel energy share [%]
11^0 BTDC	36.44443739	0.003944052
14^0 BTDC	36.44445202	0.003984196
17^0 BTDC	36.44447899	0.004058204
20^0 BTDC	36.44446645	0.004023789
23^0 BTDC	36.44448761	0.004081855

Thermal energy for different pilot injection pressures		
Pilot injection pressures	Total thermal energy [MJ]	Biodiesel energy share [%]
30 MPa	36.4440391	0.002851227
60 MPa	36.44420193	0.003298005
90 MPa	36.44431963	0.003620958
120 MPa	36.44448059	0.00406258
150 MPa	36.44457827	0.004330615

3.3. Heat Release Rate Characteristics

The number of particles governs the precision of predictions. Normally, 100 particles are sufficient in many applications according to previous study [23]. However, simulations were carried out for 50, 100, 150 and 200 stochastic particles to see the effect of different stochastic particles on solution. Firstly, Figure 1 and 2 show the history of heat release rate (HRR) vs. crank angle for 14°BTDC pilot injection timing and 17°BTDC pilot injection timing, respectively. The simulation results were obtained in 100 stochastic particles. Secondly, Figure 3 and 4 show the history of heat release rate (HRR) vs. crank angle for 90 MPa pilot injection pressure and 120 MPa pilot injection pressure, respectively. The simulation results were obtained in 100 stochastic particles. Finally, Figure 5 and 6 show the history of heat release rate (HRR) vs. crank angle for 120 MPa pilot injection pressure and 17°BTDC pilot injection timing, respectively. The simulation results were obtained in 50, 100, 150 and 200 stochastic particles. Simulation results are in good agreement with experimental data. However, deviations of model results from experimental data can be rooted in lacking of fully chemical kinetic mechanisms of biodiesel fuel and some unknown operating parameters of engine requested by this software. In addition, these skippings are due to stochastic jump process into the solution algorithm [24]. Characteristics of HRR of the Figures between 1 and 6 also resembles to the results given in [25, 26, 27, 28]. Thus, it was observed that the SRM method is a good tool to investigate HRR of biodiesel pilot fuelled dual fuel engine.

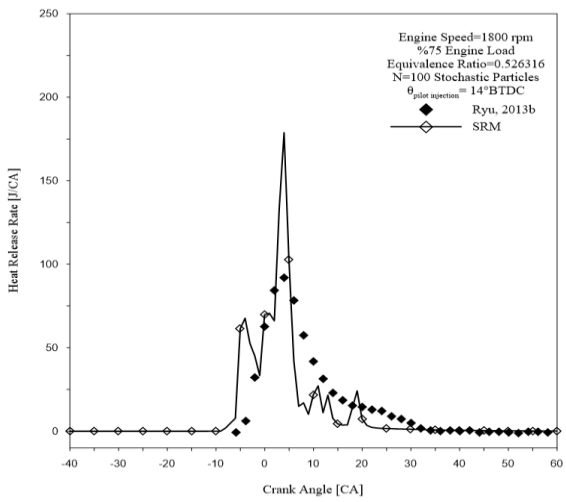

Fig. 1. HRR vs. Crank Angle for the 14°BTDC pilot injection timing

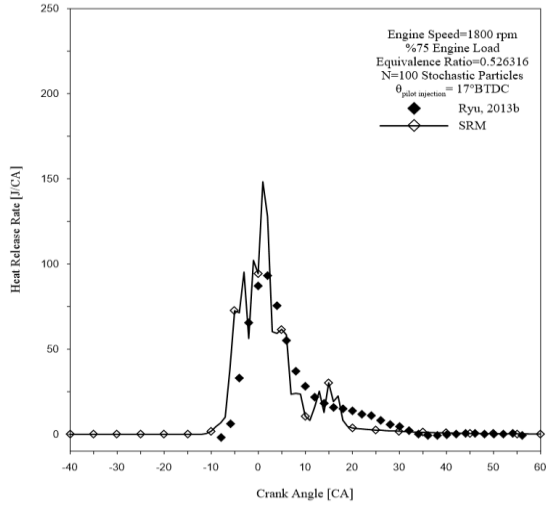

Fig. 2. HRR vs. Crank Angle for the 17°BTDC pilot injection timing

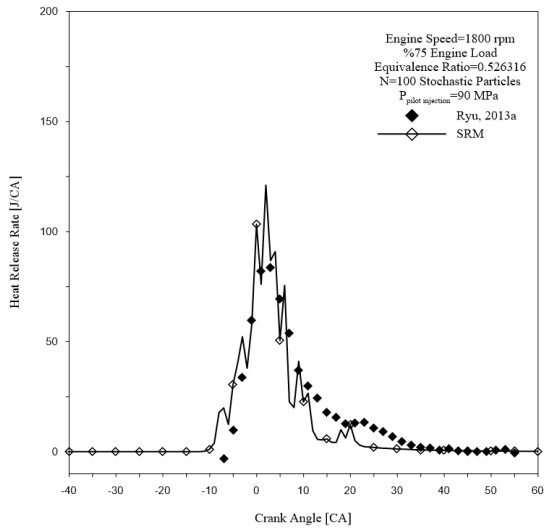

Fig. 3. HRR vs. Crank Angle for the 90 MPa pilot injection pressure

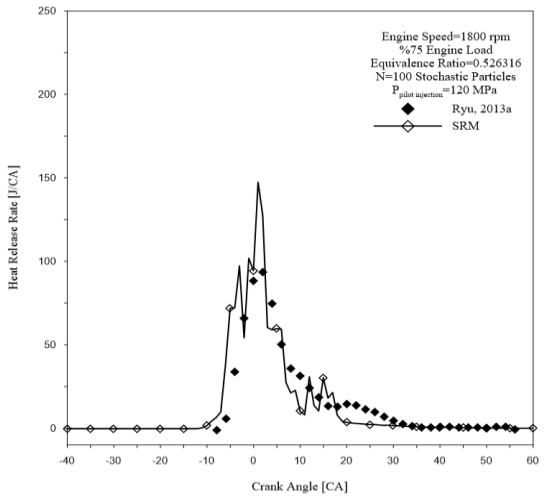

Fig. 4. HRR vs. Crank Angle for the 120 MPa pilot injection pressure

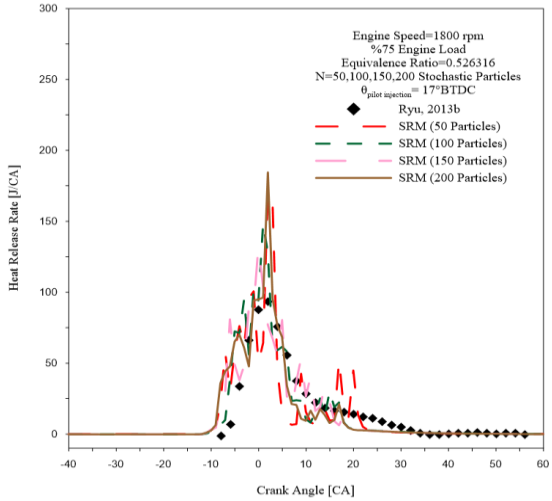

Fig. 5. HRR vs. Crank Angle for the 17°BTDC pilot injection timing for different stochastic particles

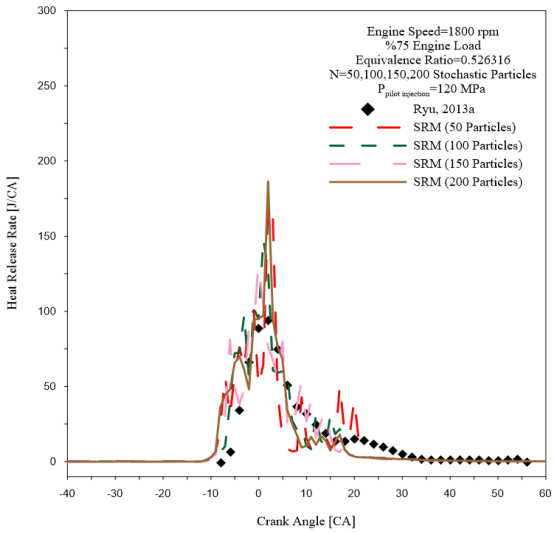

Fig. 6. HRR vs. Crank Angle for the 120 MPa pilot injection pressure for different stochastic particles

4. Conclusions and Future Work

It was firstly used a novel dual fuel-SRM model based on the probability density function (PDF) approach to simulate biodiesel pilot fuelled natural gas engines. This approach was performed with 'kinetics & srm engine suite v8.2.9' software. In this software, due to the fact that some parameters (inlet temperature, inlet manifold pressure, piston head, cylinder head, cylinder liner temperatures) are not absolutely specified, it was approximately predicted using 'trial-and-error' method. Furthermore, crevice volume (%) parameter which affected 'maximum pressure location' was nearly calculated by benefitting engine geometry.

The simulation results showed in good agreement with experimental data. However, deviations of model results from experimental data

can be rooted in lacking of fully chemical kinetic mechanisms of biodiesel fuel and some unknown operating parameters of engine requested by this software. SRM method (SRM Engine Suite Software) is a good tool to investigate HRR of biodiesel pilot fuelled dual fuel engine. When detailed chemical kinetic mechanisms for each biodiesel (soy bean, canola, rapeseed methyl esters) is developed, maybe we will gained more better agreement in experimental data.

Acknowledgements

This study was funded by Scientific Research Projects Unit of Karadeniz Technical University (Project ID: FHD-2015-5292). Also thank you so much to Prof. Dr. Hakan Serhad Soyhan and his research team due to their valuable contributions.

Nomenclature and Units

BTDC	: Before Top Dead Center [°CAD]
CAD	: Crank Angle Degrees
CFD	: Computational Fluid Dynamics
EVO	: Exhaust Valve Opening [°CAD]
HRR	: Heat Release Rate [J/°CAD]
IVC	: Intake Valve Closing [°CAD]
MD	: Methyl decanoate
MD9D	: Methyl-9-decenoate
MDF (F)	: Mass Density Function
N_{par}	: Stochastic particle numbers
PDF	: Probability Density Function
RPM	: Revolution per minute
SRM	: Stochastic Reactor Model
t_{stop}	: Iteration stop time
°	: Degree
(i)	: Individual particle
ρ	: Mass Density [kg/m^3]
ψ	: Chemical species

References

[1] J.B. Heywood, Internal Combustion Engines Fundamentals, McGraw-Hill Book Co., Singapore, 1988.
[2]http://www.smmt.co.uk/industry-topics/environment/intro/european-engine-emission-standards/, accessed on Jan 5, 2016.
[3]http://www.imo.org/en/OurWork/Environment/PollutionPrevention/AirPollution/Pages/Air-Pollution.aspx, accessed on Jan 5, 2016.
[4] M. Ikeda, M. Mikami, N. Kojima, Exhaust emission characteristics of DME/diesel fuel engine, SAE Technical Paper No. 2000-01-2006 (2000).
[5] http://www.wartsila.com/, accessed on Jan 5, 2016.
[6] http://cumminsengines.com/dual-fuel, accessed on Jan 5, 2016.
[7] K. Ryu, Effects of pilot injection pressure on the combustion and emissions characteristics in a diesel engine using biodiesel-CNG dual fuel, Energy Conversion and Management 76 (2013) 506-516.
[8] K. Ryu, Effects of pilot injection timing on the combustion and emissions characteristics in a diesel engine using biodiesel–CNG dual fuel, Applied Energy 111 (2013) 721-730.
[9] F. Ma, M.A. Hanna, Biodiesel production: a review, Bioresource technology 70:1 (1999) 1-15.
[10] M.Y. Selim, M.S. Radwan, H.E. Saleh, On the use of jojoba methyl ester as pilot fuel for dual fuel engine running on gaseous fuels, SAE Technical Paper No. 2007-24-0121 (2007).
[11] S. Imran, D.R. Emberson, A. Diez, D.S. Wen, R.J. Crookes, T. Korakianitis, Natural gas fueled compression ignition engine performance and emissions maps with diesel and RME pilot fuels, Applied Energy 124 (2014) 354-365.
[12] A. Paul, R.S. Panua, D. Debroy, P.K. Bose, Effect of compressed natural gas dual fuel operation with diesel and Pongamia pinnata methyl ester (PPME) as pilot fuels on performance and emission characteristics of a CI (compression ignition) engine, Energy 68 (2014) 495-509.
[13] L. Tarabet, K. Loubar, M.S. Lounici, K. Khiari, T. Belmrabet, M. Tazerout, Experimental investigation of DI diesel engine operating with eucalyptus biodiesel/natural gas under dual fuel mode, Fuel 133 (2014) 129-138.
[14] S.B. Pope, PDF methods for turbulent reactive flows, Progress in Energy and Combustion Science 11 (1985) 119–192.
[15] U. Demir, N. Yilmaz, G. Coskun, H.S. Soyhan, Evaluation of zero dimensional codes in simulating IC engines using primary reference fuel, Applied Thermal Engineering 76 (2015) 18-24.
[16] Version 8.2 User Manual, SRM Engine Suite, CMCL Innovations, United Kingdom, 2015.
[17] B. Wang, S. Mosbach, S. Schmutzhard, S. Shuai, Y. Huang, M. Kraft, Modelling soot formation from wall films in a gasoline direct injection engine using a detailed population balance model, Applied Energy 163 (2016) 154-166.
[18] M. Tuner, Stochastic Reactor Model for engine simulations, Doctoral Thesis, Lund University, Sweden, 2008.
[19] A. Ahmedi, S.S. Ahmed, G.T. Kalghatgi, Simulating combustion in a PCI (premixed compression ignition) engine using DI-SRM and 3 components surrogate model, Combustion and Flame 162:10 (2015) 3728-3739.
[20] G. Strang, On the construction and comparison of difference schemes, SIAM Journal on Numerical Analysis 5:3 (1968) 506-517.
[21] J. Brakora, R.D. Reitz, A comprehensive combustion model for biodiesel-fueled engine simulations, SAE Technical Paper No. 2013-01-1099 (2013).

[22] J.L. Brakora, 2012. A Comprehensive Combustion Model for Biodiesel-Fueled Engine Simulations, Doctor of Philosphy, University of Wisconsin-Madison, Mechanical Engineering, Wisconsin.
[23] S. Mosbach, M.S. Celnik, A. Raj, M. Kraft, H.R. Zhang, S. Kubo, K.O Kim, Towards a detailed soot model for internal combustion engines, Combustion and Flame 156:6 (2009) 1156-1165.
[24] A. Bhave, M. Balthasar, M. Kraft, F. Mauss, Analysis of a natural gas fuelled homogeneous charge compression ignition engine with exhaust gas recirculation using a stochastic reactor model, International Journal of Engine Research 5:1 (2004) 93-104.
[25] L. Cao, H. Su, S. Mosbach, M. Kraft, A. Bhave, S. Kook, C. Bae, Studying the Influence of Direct Injection on PCCI Combustion and Emissions at Engine Idle Condition Using Two Dimensional CFD and Stochastic Reactor Model, SAE Technical Paper No. 2008-01-0021 (2008) 1-13.
[26] W.E. Holly, T. Lauer, H.A. Schuemie, S. Murakami, Prediction of the knocking combustion and NOx formation for fuel gases with different methane numbers, International Journal of Engine Research 17:1 (2016) 35-43.
[27] M. Pasternak, F. Mauss, C. Perlman, H. Lehtiniemi, Aspects of 0D and 3D Modeling of Soot Formation for Diesel Engines, Combustion Science and Technology 186: 10-11 (2014) 1517-1535.
[28] A. Smallbone, A. Bhave, M. Hillman, A. Saville, R. McDavid, Virtual Performance and Emissions Mapping for Diesel Engine Design Optimization, SAE Paper No. 2013-01-0308 (2013) 1-23.

EXPERIMENTAL INVESTIGATION OF USING LNG IN VEHICLES

Nafiz KAHRAMAN[1], Mehmet Ali BEKTUR[2], Hayrettin ATAY[1]

[1.] Erciyes University, Faculty of Engineering, Department of Mechanical Engineering, 38039 Kayseri/Turkey
e-mail: nafiz@erciyes.edu.tr (Corresponding Author)
[2.] Aşık Veysel Bulvarı, Erciyes Teknopark-Tekno 2 Binası No:23 38039 Kayseri/Turkey
e-mail: malibektur@doğa-can.com

ABSTRACT

Nowadays fossil rooted fuels used in the internal combustion engines being exhausted and taking form harmful exhausted gases conclusion of burning these fuels soiling environment have cause to increase investigations about alternative fuels used in the internal combustion engines. If a fuel use in an internal engine, that can be easily evaporate, easily mixed with air, get high energy, easily burn, easily obtain. Liquid hydrocarbon fuels which obtained in fossil (petrol), includes nearly all these properties. Because of this, diesel and gasoline which are the famous petrol products raise the first line. By this time, petrol reserves limited and not separated on regularly. And by the extremely usage of these, that causes various local air currents, air pollution and potential climatic currents. Lots of various alternative fuels were attempted since diesel and gasoline become a fuel in internal engines. Lots of these alternative fuels get low emissions than diesel and gasoline. But that can not found market place because of these limited reserves and higher prices. Nowadays, few of alternative fuels use as a commercial mark. It is necessary using alternative fuel in vehicles because of high petrol price and air pollution is a result of using fossil fuels in vehicles. Although natural gas (NG) is fossil fuel but in gas form is cleaner than petrol and diesel, and has large reserve than petrol. Because of these reasons NG becomes an important alternative fuel. Unfortunately, storing the NG as Compressed Natural Gas (CNG) form brings many problems. The most important problem is especially in small vehicle like cars; 200 bar resistant tanks are heavy and big volume. As a result of this, the vehicle's distance of range using CNG is different according to tank volume that is about 150 km. However, storing the NG as Liquid Natural Gas (LNG) form in the same tank volume, the tank's weight becomes lower, by the same time distance of range approaches the petrol using vehicles. In this study, we work at the properties of natural gas (LNG) and the usage of NG in internal engines. Experiments were studied at Erciyes University Mechanical Engineering's Engines Laboratory. Ford brand, 105 Hp, 1800 cc motor was used in experiment. Exhaust emissions was measured in SUN MGA 1500 gas analyser.

Keywords: LNG, Alternative Fuel, Storing of Natural Gas, Vacuum Insulation

1.Introduction

As alternative fuel, natural gas provides a low CO_2 emission rate and holds a dominant position with widely distributed resources in the world compared with the other fuels for vehicles. Natural gas should be widely used in liquid phase (LNG) specially in automobile use because of its energy density [1]. LNG requires large insulated tanks to keep the liquefied gas at a very low temperature and is therefore seen as more suitable for long-haul trucks [2]. Liquefied Natural Gas (LNG) offers the possibility of using this fuel for heavy-duty road transport applications due to its higher energy density. It should be taken into account that a temperature of -162°C [3] is required (at atmospheric pressure) to maintain the fuel in liquid state, therefore the main issue of this technology lies on the cryogenic tank installed on board with a thermal behaviour control system and the board vaporizer required to feed the internal combustion engine.

The scientific literature concerns LNG with its various implementations. In one of studies, it has been seen that the components of LNG system (LNG tank, vaporizer, LNG control valve and gas injector) were developed. In addition, the LNG tank and the LNG control valves also were insulated to prevent gas boil off. In this way, the LNG engine system provided a high compression ratio, manifold gas injection, and spark ignition for the effective use of natural gas. Tests were carried out for exhaust gas emissions, vehicle dynamics and driveability and as a consequence, the exhaust gas emissions were seen lower Japan 10 and 11 mode regulations [1].

A life cycle assessment has been carried out to quantify the energy saving and environmental emission of a remanufactured LNG engine and newly manufactured diesel engine. As to result of tests, compared with diesel engine, LNG remanufacturing could reduce 42.62% of primary energy demand (PED); the environmental impacts reduction of acidification potential (AP) and nutrient enrichment potential (EP) could reach to 69.61% and 71.34%, which are most distinct; global warming potential (GWP) and photochemical ozone formation potential

(POCP) could be reduced by 46.42% and 43.90% respectively [4].

In another study was focused on improving performance of LNG. For this aim, a set of intake air supply device was designed and coupled to a LNG engine and the performance of LNG engine with intake air supply was compared with the original engine. The results indicate that engine torque could be improved obviously at low-speed, while the specific gas consumption (SGC) was almost unchanged with intake air supply. At 1000 r/min, the torque could be increased by 31%, and the SGC was decreased by 1.64%. Based on the test results, the optimal injection pressure of supplied air at various speeds was determined. Finally, the vehicle test of intake air supply was also conducted under road conditions. Compared with the original natural gas vehicle, the acceleration time was decreased by 14.7–30% through intake air supply, and the higher gear ratio contributed to the better acceleration performance. [5]

It was seen that liquefaction of natural gas provided a safer and economical alternative for transportation and also increased its storage capabilities in another study. LNG transported in cryogenic vessels offers several advantages [6] over pipeline transport of natural gas especially when the gas consuming areas are far away from the gas producing areas. In the study, it was also investigated about characteristics of LNG compared with the other fuels (diesel, gasoline and LPG).

A study from Austria has showed that there are severe barriers which impede the application of LNG in the landlocked areas of Europe. The objective of the present work is to build a basement for launching LNG in this region. This carried out in two stages: First by deliberately examining the potential demand for LNG and second by identifying the stakeholders which have to be taken into account to successfully accomplish this process. LNG application have been categorized and prioritized using Maslow's hierarchy of needs. The results revealed that interest for LNG exists and the potential for introducing LNG in landlocked Europe is given [7].

For refrigerated vehicles, it has been conducted in the other study, an additional advantage is that recovering of the LNG cold energy during vaporization will provide the refrigerating effect and therefore reduce the engine power used to drive the conventional vapor–compression system (VCS). Analysis of the feasibility of a self-refrigerated vehicle by recovering the cold energy of LNG fuel. A prototype of a self-refrigerating system was constructed and its refrigeration performance has been investigated experimentally. The interrelations of the refrigerating temperature, the cooling capacity and the consumption rate of LNG fuel were studied.

The experiment results showed that the refrigerating temperature of the compartment could be kept lower −20 °C when the LNG consumption rate is larger than 5.607 kg/h. This value of LNG consumption rate could be achieved when the power output of the engine for the LNG-fueled refrigerated vehicle is more than one third of its maximum output power (75 kW) [8] under the full-load operating condition.

There were performed to compare the life cycle, in terms of greenhouse gas (GHG) emissions, of diesel and liquefied natural gas (LNG) used as fuels for heavy-duty vehicles in the European market (EU-15). Two possible LNG procurement strategies were considered. These were purchasing it directly from the regasification terminal (LNG-TER) or producing LNG locally (at the service station) with small-scale plants (LNG-SSL). The use of LNG-TER enables a 10% [9] reduction in GHG emissions by comparison with diesel, while the emissions resulting from the LNG-SSL solution are comparable with those of diesel.

In another study, it has been seen that if LNG is used in a direct-injection engine having the same efficiency as a diesel engine, the “well-to-wheel” lifecycle greenhouse gas(GHG) emissions were typically around 19% lower than conventional diesel, or around 17% lower than diesel containing 7% FAME (B7). As a consequence, different sources of LNG might have higher or lower savings, depending on the efficiency of liquefaction and the shipping distance. In the best cases, the Well to Wheel reduction might be as high as 25% [10].

Potential of LNG as vehicle fuel was shown positive and negative aspects related to its introduction and comparing the different supply options. The analysis has pointed out that purchasing LNG at the regasification terminal is convenient up to a terminal distance of 2000 km from the refuelling station. The liquefaction on site, instead, asks for liquefaction efficiency higher than 70% [11] and low natural gas price.

It was investigated effects of compression ratio on performance and emissions of a modified diesel engine fuelled by HCNG in another study. They investigated the effects of compression ratio (CR) have been investigated engine performance and emissions characteristics of a modified diesel engine fuelled by HCNG (hydrogen enriched compression natural gas) blends (100% CNG, 95% CNG +5% H-2, 90% CNG + 10% H-2 and 80% CNG + 20% H-2). The experiments have been carried out using a modified Isuzu 3.9 L diesel engine having 9.6, 12.5

and 15 different compression ratios at 1500 rpm under full load conditions [12]. Engine brake torque, brake specific fuel consumption, combustion analysis and emissions parameters (CO, THC and NOX) have been realized at 10 CA BTDC ignition timing and different excess air ratios. As seen above, NG uses in vehicle have become increasingly very important in the past decades and will be more in the near future. Hence, this paper presents investigation of using LNG in vehicle at various scenarios.

2.Material and methods

2.1. Experimental set up:

There is a saturated liquid-gas mixture in pressure tank. When the LNG tank which is initially in 0.5 bar gauge pressure receives 1258.55 kJ heat from environment, relief valve opening pressure reaches 4.9 bar gauge pressure. If it still receives more heat, depending on this heat, the relief valve will be open and discharge this overpressure. It is determined initial gauge pressure as 0.5 bar and relief valve set gauge pressure as 4.9 bar in the calculations.

Table 2.1 shows that as evaporation loss ratio of tank increase, relief valves' opening time is shortened. For the same loss ratio, as amount of fluid carrying in the tank increases, relief valve opening time is shortened again. Testing of relief valve and design of tank at higher pressure will extend relief valves' opening time.

Table 2.1. Tank's distribution of pressure, temperature and level received heat from external environment

P [bar]	T [K]	mg [g]	mf [g]	Vg [l]	Vf [l]	x	U [kj/kg]	FR [%]
1.5	117	12.31	15.877	4.603	38.297	0.00077	-267.75	89.27
2.5	124	15.14	15.875	3.59	39.31	0.00095	-242.94	91.62
5.9	139	9.58	15.880	0.992	41.91	0.00060	-188.54	97.67

P: Absolute pressure [bar] **Vf:** Volume of fluid [l]
T: Temperature [K] **x:** Dryness fraction
mg: Mass of gas [g] **U:** Internal energy [kj/kg]
mf: Mass of fluid [g] **FR:** Fluid ratio [%]
Vg: Volume of gas [l]

2.2. Production of LNG Autogas Tank

On-board fuel storage is considerably different between diesel and LNG. Standard diesel tanks are single-wall aluminum containers and cost in the hundreds of dollars, depending on size.

Tanks for cryogenic LNG require double-wall construction from stainless steel with super insulation and vacuum inter-tank space. (Fig. 2.1). Typical tank pressures are between 138 kPa to 1040 kPa, but the design must withstand more than two times that amount to compensate for heat gain when not in use. LNG fuel storage systems are significantly more complicated to design and manufacture and their cost is an order of magnitude greater than that of a diesel tank.

The weight of LNG is approximately 3.5 lb/gal, compared to diesel at 7.6lb/gal. Unfortunately, the more complex LNG fuel tank is substantially heavier. In total, given the difference in tank design and fuel density, LNG-powered tractors have suffered a weight penalty.

Figure 2.1. The cryogenic LNG tank

External tank body has also been made taking into account the dimensions of the project. Fig. 2.2 shows that inner tank and external tank are nested with minimizing of heat bridges. After preparing vacuum filters, they are mounted between two walls.

Figure 2.2. Nested Inner and external tanks

Figure 2.3. LNG Autogas filled with LNG and mounted to experiment set

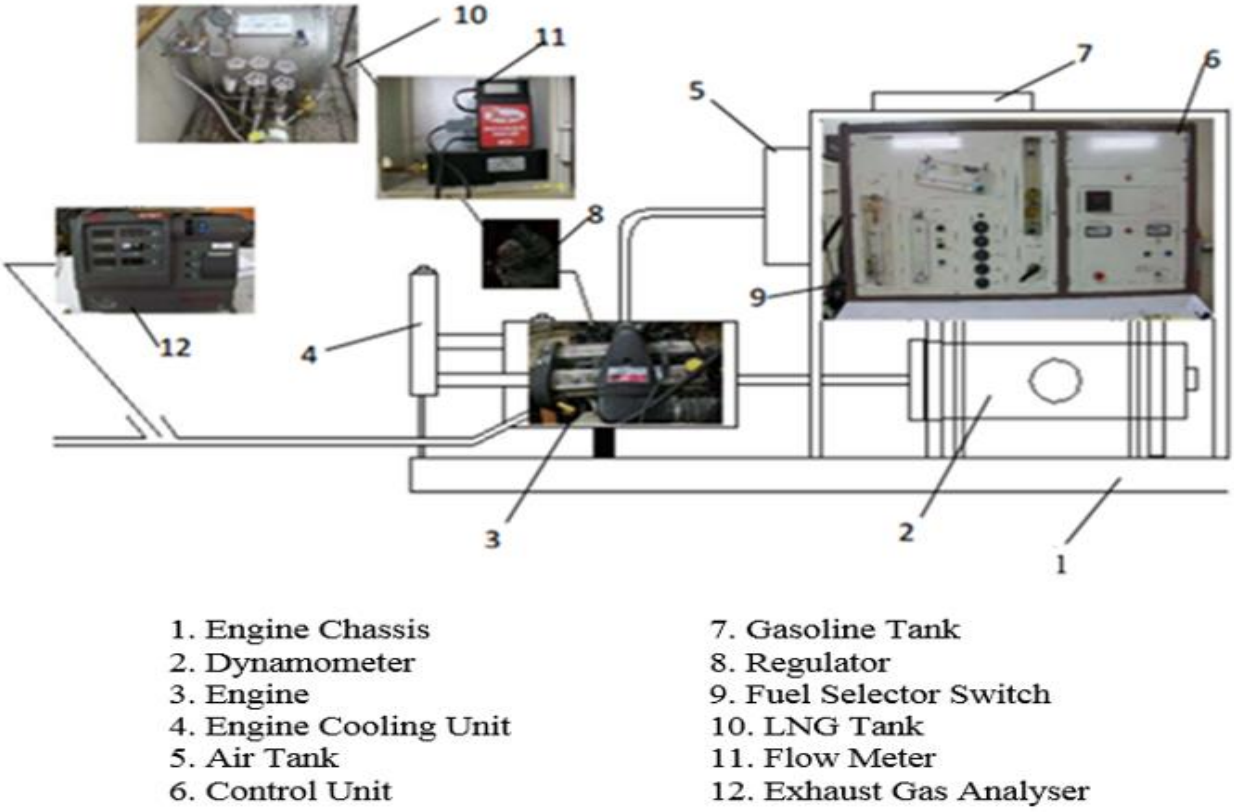

Figure 2.4 Experimental setup

Completed assembly is seen Fig. 2.3 and its cold test has been conducted with liquid nitrogen. Firstly, the inner tanks' indoor temperature has been reduced gradually with purging tank by three times with nitrogen gas phase. Afterwards, the tank has been filled with a small amount of liquid nitrogen and it has been expected to evaporate it. After being discharged of vaporized nitrogen, the tank has been filled with liquid nitrogen until LNG filling. The cold test has carried out with nitrogen liquefying at -192 °C and atmospheric pressure.

Experiments has been carried out using LNG for different engine speeds (1500, 2000, 2500 rev/min.) and excess air coefficient values. The experimental set up is shown in the Fig. 2. 4.

3.Results and discussion

Fig. 3.1 indicates that full combustion is seen to better between the values of the excess air coefficient 1-1.3 depending on the engine speeds. In addition, while the engine speed is 2000 rev/min and excess air coefficient is 1.14, %CO_2 is seen to be maximum level.

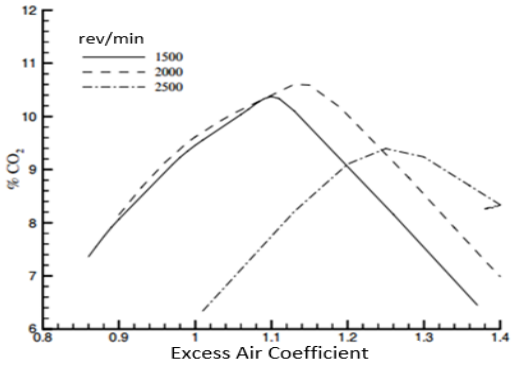

Figure 3.1. Changes of % CO_2 depending on excess air coefficient

Fig. 3.2 shows that, when the values of excess air coefficient is bigger than 1.1, it is seen to be fall in the values of %CO. It is also seen that while the engine speed is 2000 rev/min., %CO is seen to be minimum level.

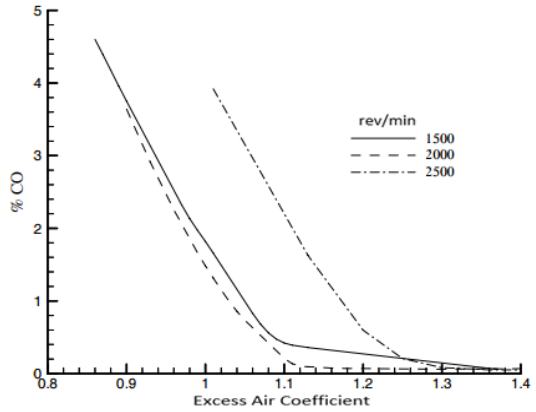

Figure 3.2. Changes of % CO depending on excess air coefficient

Fig. 3.3 indicates that, amount of the unburned fuel is seen to be least between the values of the excess air coefficient 1-1.3. As excess air coefficients move off from range of 1-1.3, it is seen to be rise in the amount of the unburned fuel. Also, while the engine speed is 2000 rev/min., the amount of HC is seen to be less than the other speeds.

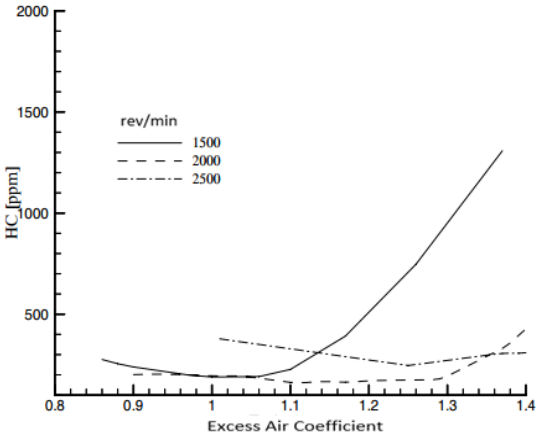

Figure 3.3. Changes of % HC depending on excess air coefficient

As seen Fig. 3.4 that torque is increased due to the increase in engine speed. Methane is stored in two phases, liquid and gas phase in the LNG fuel tank. When the tank pressure falls, gas flow from tank is reduced. After the engine speed exceeds 2000 rev/min, the amount of gas coming from tank is not been adequate. Actually, pressurisation circuit was applied for being increased pressure when the tank pressure falls. But methane was thrown the external environment, because relief valves were opened at 5 and 8 bar (false relief valve is fitted by the manufacturer). Hence, to avoid the increase of tank pressure, pressurisation circuit was been closed. In case of fixing the relief valves, torque will also increase with increasing number of speeds. This case will be also after occurring a fall in gas pressure following not end of the liquid in the tank. Thus, not using LNG alone as fuel, but it will be more accurate to use as alternative fuel such as LPG. It is seen parallels between torque and brake power.

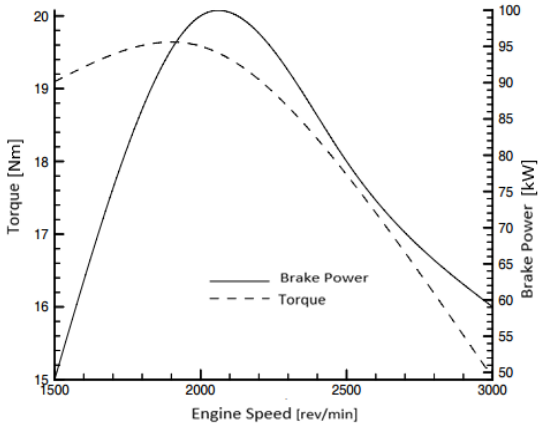

Figure 3.4. Changes of torque and brake power depending on engine speed

According to Fig. 3.5, due to the increase in engine speed the amount of specific fuel is increased. Brake efficiency is reduced due to the increase in engine speed, too. The decrease in brake efficiency and increase in specific fuel consumption is become more pronounced in case of exceeding of engine speed 2000 rev/min.

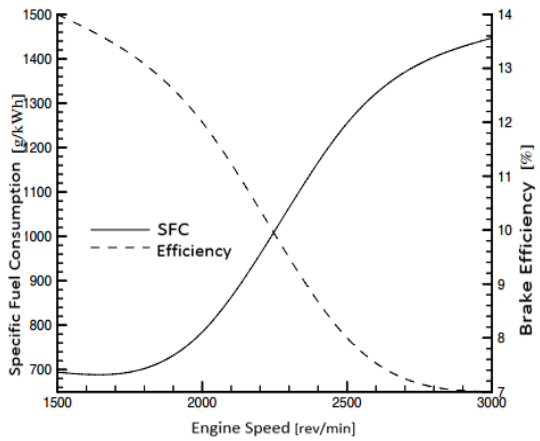

Figure 3.5. Changes of SFC and brake efficiency depending on engine speed

As to Fig. 3.6, it is observed an increase in pressure values depending on the angle the crankshaft. The increase in engine speeds lead to an increase in the cylinder pressure. It is seen to be fall at pressure due to increasing at excess air coefficient comparing with at the different excess air coefficients and the same speeds.

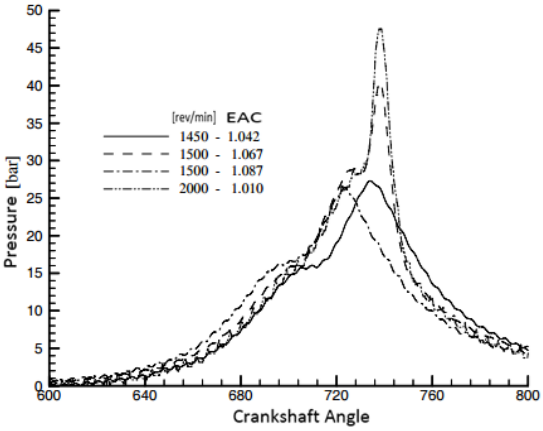

Figure 3.6. Changes of depending on crankshaft angle

LNG in the tank internal volume 42.9 liter has bigger 2.3 times equivalent energy than CNG which has 50 liter volume and 200 bar pressure. Vehicles using LNG as fuel has approximately 2.3 times greater range than vehicles using CNG.

Though currently the supply shortage of LNG, it is seen as an alternative fuel to be used widely in internal combustion engines in the future due to the low exhaust emissions that cause air pollution and having economic advantages comparing with conventional fuels. What is more, this also means more fresh air to be inhaled, a greener environment for us and extend the life of our old world.

REFERENCES

[1] Y. Ko, K. Kurihara, T. Sakai, R. Osuga, et al., Research and Development of LNG Vehicle for Practical Use, SAE Technical Paper(1992) 920594, doi: 10.4271/920594.

[2] B. Canis, R. Pirog, B. D. Yacobucci, Natural gas for cars and trucks: Options and challenges, https://www.fas.org/sgp/crs/misc/R43791.pdf Last Accessing Date: 28/11/2016.

[3] A. Bassi, Liquefied Natural Gas (LNG) as Fuel for Road Heavy Duty Vehicles Technologies and Standardization, SAE Technical Paper(2011) 2011-24-0122, doi: 10.4271/2011-24-0122.

[4] J. Shia, T.Z. Liua, H. Zhanga, S. Penga, Q. Jiang, J. Yin, Life Cycle Environmental Impact Evaluation of Newly Manufactured Diesel Engine and Remanufactured LNG Engine, The 22nd CIRP conference on Life Cycle Engineering, Procedia CIRP 29 (2015), 402– 407.

[5] Q. Tang, J. Fua, J. Liub, F. Zhoub, Z. Yuana, Z. Xub, Performance improvement of liquefied natural gas (LNG) engine through intake air supply, Applied Thermal Engineering (2016), Volume 103, Pages 1351–1361.

[6] S. Kumar, H-T. Kwon, K-H. Choib, W. Lima, J.H. Choa, K. Taka, I. Moona, LNG: An eco-friendly cryogenic fuel for sustainable development, Applied Energy (2011), Volume 88, Issue 12, Pages 4264–4273.

[7] S. Pfoser, G. Aschauer, L. Simmer, O. Schauer, Facilitating the implementation of LNG as an alternative fuel technology in landlocked Europe: A study from Austria, Research in Transportation Business & Management (2016), Volume 18, Pages 77–84.

[8] H. Tan, Y. Li, H. Tuo, Theoretical and experimental study on a self-refrigerating system for LNG-fueled refrigerated vehicles, Journal of Natural Gas Science and Engineering (2014), Volume 20, Pages 192–199.

[9] A. Arteconi, C. Brandoni, D. Evangelista, F. Polonara, Life-cycle greenhouse gas analysis of LNG as a heavy vehicle fuel in Europe, Applied Energy, Energy Policy (2010), Volume 87, Issue 6, Pages 2005–2013.

[10] M. Kofod, T. Stephenson, Well-to Wheel Greenhouse Gas Emissions of LNG Used as a Fuel for Long Haul Trucks in a European Scenario, SAE Technical Paper(2013) 2013-24-0110, doi: 10.4271/2013-24-0110.

[11] A. Arteconi, F. Polonara, LNG as Vehicle Fuel and the Problem of Supply: The Italian Case Study, Energy Policy (2013), Volume 62, Pages 503–512.

[12] S. Tangoz, et all., Effects of compression ratio on performance and emissions of a modified diesel engine fueled by HCNG, International Journal of Hydrogen Energy (2015), Volume: 40 Issue: 44 Pages: 15374-15380 Special Issue: SI, DOI: 10.1016/j.ijhydene.2015.02.058.

Sayı 4, Aralık 2016 Volume 4, December 2016

A NUMERICAL STUDY OF NO AND SOOT FORMATION IN AN AUTOMOTIVE DIESEL ENGINE FUELED WITH DIESEL-BİODIESEL BLENDS

Müjdat FIRAT[1], Şehmus ALTUN[2], Yasin VAROL[3]
[1]Firat University, Technical Education Faculty, Department of Mechanical Education, 23119, Elazig, Turkey
[2]Batman University, Technology Faculty, Department of Automotive Engineering, 72100, Batman, Turkey
[3]Firat University, Technology Faculty, Department of Automotive Engineering, 23119, Elazig, Turkey

Abstract
In this paper, engine simulation results are presented to give information on the effect of diesel-biodiesel blends on combustion and emission characteristics of a multiple injection automotive diesel engine. Numerical Study was performed in Computational Fluid Dynamics (CFD) simulation software AVL-FIRE coupled to AVL-ESE Diesel. An improved version of the ECFM-3Z combustion model has been applied coupled with advanced Zeldovich and Kinetic models for NO and soot formation, respectively. The simulation results were validated against the experimental results by comparing the in-cylinder pressure and heat release rate for diesel-biodiesel blends at 2000 rpm under 100% load, and a maximum variation of 5% deviation on the peak cylinder pressure and 4% for heat release rate was found. Simulation results revealed that with the increase of biodiesel amount in the fuel, CO and soot emissions were reduced while NO increased at the simulated operating conditions. In addition, in-cylinder NO and Soot mass fractions were found to be high at 20 and 10 CA ATDC, respectively.
Keywords: Diesel Combustion, Biodiesel, NO and Soot Formation

1. Introduction

Biodiesel is a notable alternative to petroleum diesel, which should conform to international standards such as ASTM D6751 and EN 14214 specifications for use in diesel engines when it is produced from vegetable oils and animal fats by transesterification. The European Commission set the target to replace 10% of the energy used in transportation with biofuels by 2020 **[1]**, and a large portion of biofuel use is expected to be biodiesel. Accordingly, its production and use probably increases in the next years. Previous researches with biodiesel fuels from vegetable oils **[2]** and with some others made using unconventional feedstocks **[3][4],** have demonstrated advantages on diesel emissions such as hydrocarbon (HC), carbon monoxide (CO), and PM but generating higher NO_x emissions **[5][6]** when combusted in diesel engines. In addition, it is a renewable, biodegradable, non-toxic and engine-friendly (due to its excellent lubricity) alternative fuel. Although numerous experimental studies have been conducted on biodiesel use in diesel engines, in recent years, researchers have turned their interest on numerical simulations using CFD tools **[7]**, as experimental testing is usually costly and time-consuming **[8]**. In addition, numerical simulations allow a better understanding of the in-cylinder phenomena. **An et al. [9]** studied the impacts of biodiesel blend ratio on the emission formation processes of a diesel engine using 3-D CFD simulation software KIVA4 coupled with CHEMKIN II. **Yuan et al. [10]** developed a detailed numerical spray atomization, ignition, and combustion model using KIVA3V code for investigating NO_x emissions. The effect of the fuel temperature on the combustion and emissions characteristics is investigated numerically by **Ren and Li [11]**. The effect of different injection strategies on the pollutant formation were studied by **Meloni and Naso [12]** and **Wang et al. [13]** while **Som and Longman [14]** investigated the influence of fuel properties on the combustion and emission characteristics of the compression ignition engine focusing on the spray behavior.

In this study, the combustion and emission characteristics of an multiple injection automotive diesel engine fueled with diesel-biodiesel blends was simulated by using a computational fluid dynamics (CFD) software AVL-FIRE, and the results were validated against the experimental results acquired on an engine test-bed. A diesel fuel (B0) and the blends of diesel with biodiesel (soybean oil based) in percentages of 10% (v/v) (B10), 20% (v/v) (B20) and 30% (v/v) (B30) were employed as test fuels at a constant speed of 2000 rpm under full load condition.

2. Numerical Study

Numerical study was conducted using 3D CFD software AVL-Fire, which is thermo-fluid dynamics software, and it uses a pressure based segregated solution algorithm. AVL-ESE Diesel, which is a part of the AVL-Fire package, was used to set up, simulate, analyze and optimize aerodynamics, fuel injection, and combustion and emission formation in Diesel engines **[15]**. The engine specifications, initial and boundary conditions and sub-models employed are given in **Tables 1, 2** and **3**, respectively.

Table 1 Engine Specifications

maximum power	75 kW @ 4000 rpm
maximum torque	280 Nm @ 2000 rpm
cylinder arrangement	four cylinders, in-line
bore (mm)	82
stroke (mm)	90.4
compression ratio	18:1
displacement (L)	1.9
fuel injection	common rail, with pilot
number of nozzle holes	6
spray angle	140°
nozzle hole diameter	0.145mm

Table 2. Initial and boundary conditions

Engine speed	2000 rpm
Intake air temperature	293.15 K
Intake air pressure	1.4 bar
Fuel injection temperature	320.15 K
Cylinder head temperature	550.15 K
Piston top temperature	550.15 K
Cylinder wall temperature	470.15 K
1. Start and end of injection	-20/-10 CA
2. Start and end of injection	5 / 15 CA
Fuel consumption rate	5.8

Table 3. AVL-FIRE Sub-Models

Spray Model	WAVE
Spray Wall Interaction Model	Walljet
Droplet Evaporation Model	Dukowicz
Combustion model	ECFM-3Z
Turbulence model	k-zeta-f
Ignition model	Auto-Ignition
NO formation	Extended Zeldovich Mechanism
Soot formation	Kinetic

A three-dimensional mesh of engine combustion chamber was built based on the basis of the engine piston geometry (**Figure 1**). Computations are performed on 60^0 sector meshes with approximately 100000 cells near at TDC.

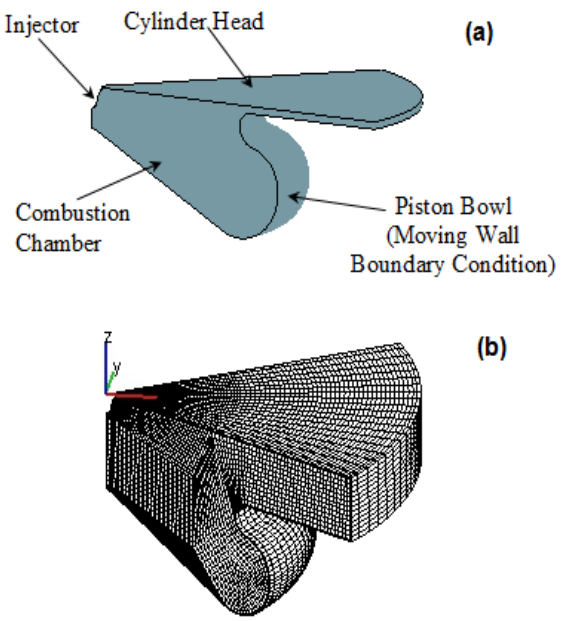

Figure 1 Computational domain

The experimental tests were carried out in a four-cylinder, four-stroke, turbocharged, direct-injection, 1.9 L Fiat diesel engine coupled to a hydraulic brake. Engine tests were carried out at 1000, 2000 and 3000 rpm under full throttle position. The cylinder pressure signal was determined by averaging 200 pressure cycles obtained with a fiber optic pressure sensor Optrand D33288-GPA (with a sensibility of 1.35mV/psi). A zero-dimensional thermodynamic model was used to determine the main parameters of the combustion process, such as the heat release rate (HRR).

3. Model validation

The simulation results were compared with those obtained from experimental testing in **Figure 2**, which was carried out at 2000 rpm. Validation was made by comparing the in-cylinder pressure and heat release rate for B0, B10, B20 and B30 fuels. The first peak cylinder pressure of 7.31 MPa, 7.33 MPa, 7.23 MPa and 7.17 MPa for B0, B10, B20 and B30, respectively, was obtained from experimental testing while in the case of simulation they were 7.46 MPa, 7.39 MPa, 7.36 MPa and 7.25 MPa. On the other hand, the experimental second peak pressure is lower than those obtained from simulation. The maximum deviation in the peak cylinder pressure was found to be less than 5%. For HRR, a similar trend is seen from the figure, the difference does not exceed 4%. Simulated HRR values are in advance compared with experimental ones especially in case where first injection occurred except for B30 **[16].**

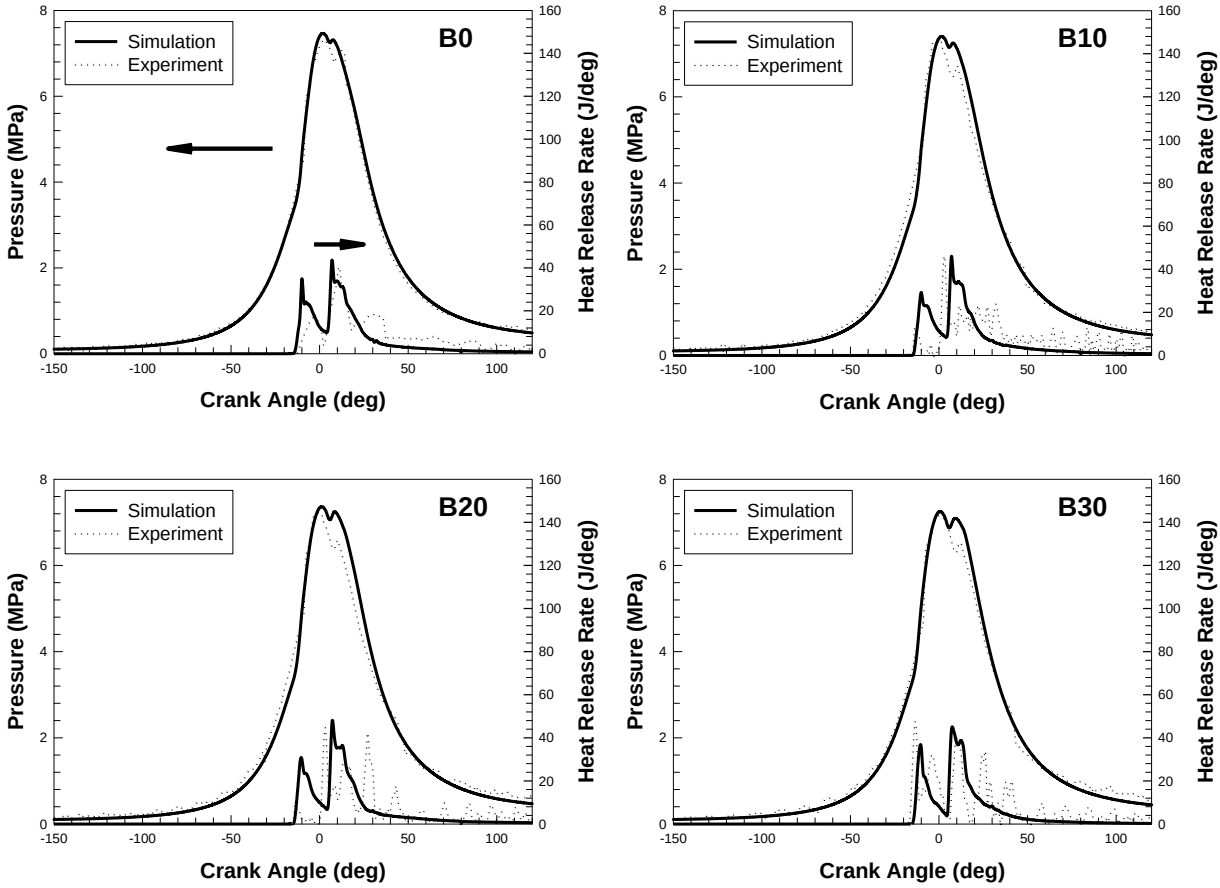

Figure 2 Experimental and calculated in-cylinder pressure and heat release rates with respect to mixing ratios of biodiesel

5. Results and discussions

5.1. Combustion characteristics

The change in cylinder pressure and heat release rate for diesel-biodiesel blends is shown in **Fig. 3**. The cylinder peak pressure is highest with diesel followed by B10, B20, B30, and these differences are respectively of 0.0418 MPa, 0.0817 MPa and 0.2076 MPa according to the corresponding biodiesel amount in the fuel. In case of the first injection, the maximum pressure for all fuels occurs within the range of 0-5 CA ATDC while for second it is within 7-12 CA ATDC. In HRR graph, two curves are seen; the first one corresponds to the pre-injection while the second (the larger one) is the main injection, and they have very similar trend for all of the fuels. However, at around the TDC, a lower HR is appeared for blended fuels. The combustion advance reported in the literature **[16]** for biodiesel fuels is not high enough for present study. **Lapuerta et al. [17]** reported that in multiple injection common-rail engines, the cetane number is the main property responsible for differences in combustion timing whereas this effect is negligible as biodiesel content in the fuel is relatively low.

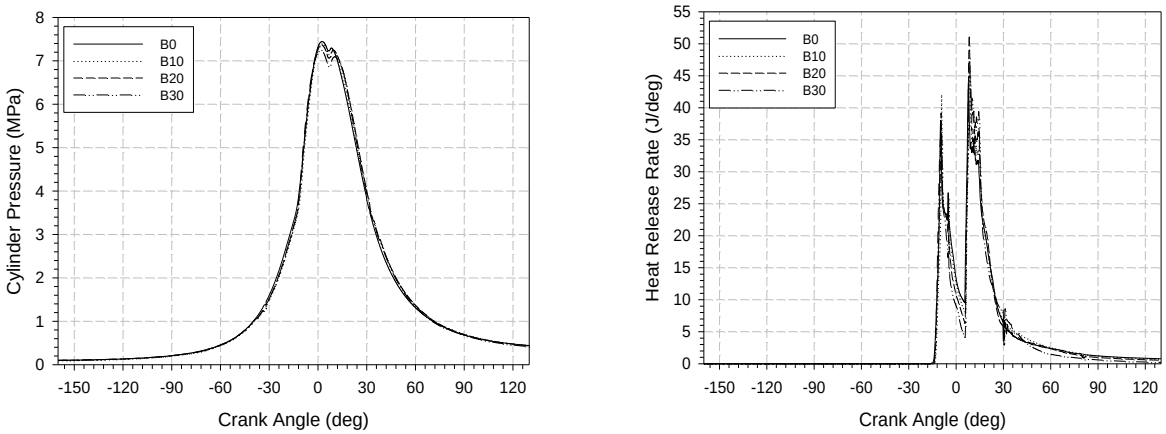

Figure 3 Comparison of (a) the in-cylinder pressure, and (b) the heat release rate (HRR) for diesel-biodiesel blends

Figure 4 shows in-cylinder average combustion temperature against crank angle diagrams for the fuels. The average combustion temperature starts to increase rapidly after the pilot injection where the ignition is started, and reaches to its first peak value for a slightly higher than 1600 K for each fuels, as shown in **Fig. 4**. The second peak, the highest one, was occurred after 21 CA ATDC, and in this case the temperatures above 2000 K were obtained with biodiesel blended fuels while it was 1990 K for diesel case. The highest NO formation was also observed in these conditions for blended fuels. It can already be seen that the regions with higher NO concentrations matched very well with higher temperature zones (this will be discussed later). On the other hand, the pilot injection reduces the ignition delay and therefore the amount of premixed combustion, leading to lower temperatures.

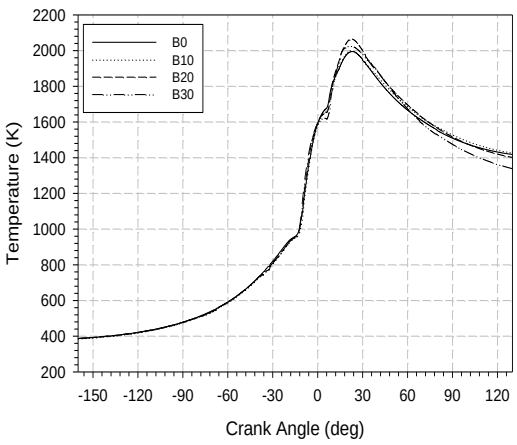

Figure 4 In-cylinder average combustion temperature for fuels

5.2. Emission characteristics

The temporal development of the CO for tested fuels is shown in **Fig. 5**. The CO starts to form before TDC when the pilot injection was occurred, and then CO formation was increased as the main injection was made at ATDC. On the other hand, the peak in-cylinder CO concentration was found to be the greatest for diesel fuel, and it was reduced with the increase of biodiesel ratio in the fuel, which is attributed to the oxygen content in the biodiesel contributing to more complete combustion **[17]**.

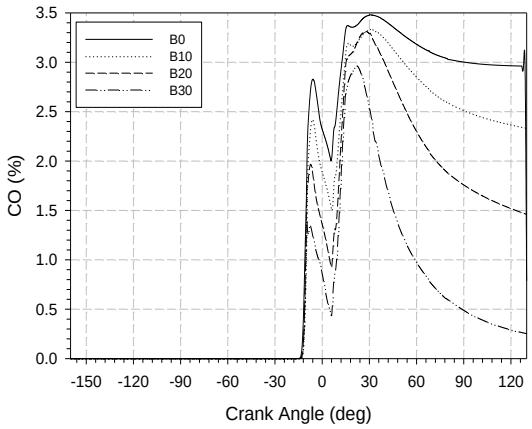

Figure 5 In-cylinder CO emission histories with respect to crank angle for diesel-biodiesel blends

Increase in the emission of NO was observed in comparison with diesel for all biodiesel blends, and the magnitude of this increase depended upon the biodiesel content in the fuel blends, as shown in **Fig. 6-a** where NO is seen as higher at ATDC when the main injection was made for all fuels. It is likely that higher in-cylinder temperature for biodiesel blends than diesel operation, which can be seen in **Fig. 4**, is responsible for NO increase. The soot emissions for the blends are significantly lower than those obtained with the diesel, as shown in **Fig. 6-b**. This reflects the potential of biodiesel blends to reduce soot emissions with respect to the diesel, as it is reported by other authors, and this is mainly due to the oxygen content of the biodiesel fuel molecules.

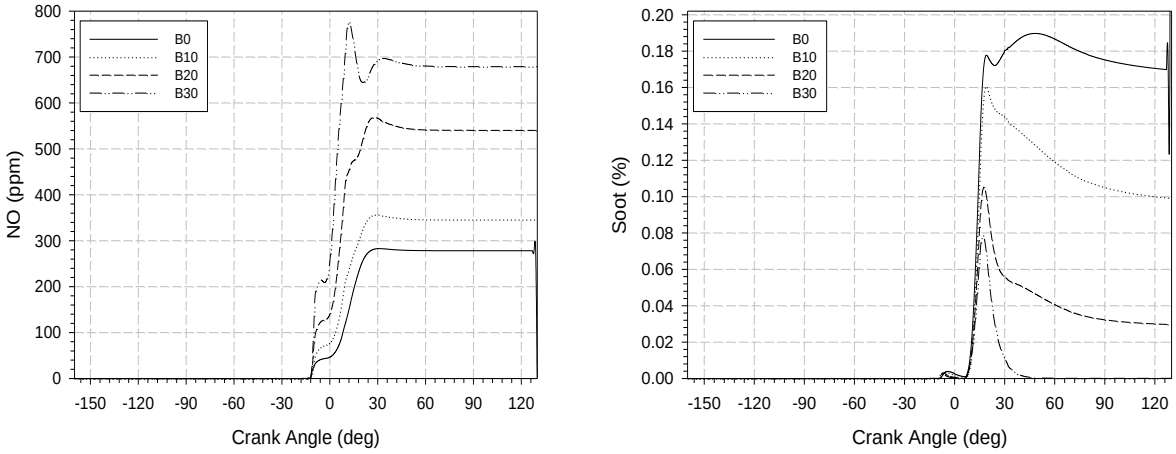

Figure 6 In-cylinder emission histories with respect to crank angle (a) NO emissions, and (b) Soot emissions for diesel-biodiesel blends

Local temperature, NO and soot emissions with various biodiesel ratios are shown in **Fig. 7-8.** Obviously, higher biodiesel ratio leads to higher burned gas temperature, which cause a slightly rise in NO emissions for all three cases. NO may increase due to higher oxygen content of biodiesel blends. The main cause is that biodiesel have higher viscosity hence the droplet size after start of injection is estimated to be larger than that of diesel fuel. These fuel droplets have all combustion process and important heat release rate during the late combustion process. The soot emissions are another important parameter used to appraise the combustion characteristics of test fuels. Soot is usually formed in the overly fuel rich regions in cylinder. Indeed, the high soot concentration areas move in the direction to the piston bowl wall in biodiesel blends as the flame propagation. **Fig. 7-8 (right)** shows the variation of local soot mass fraction of diesel and biodiesel blend fuels with depend on crank angle. It is observed that the use of biodiesel blends improve the combustion process and reduces the soot emissions. Therefore these results confirm the combustion and temperature data.

Conclusion

In this study, the authors have investigated the performance, combustion and emission characteristics of diesel fuel and biodiesel blends in a direct injection diesel engine at multiple injection case. Model validation was performed for the AVL-FIRE model in terms of heat release rate and combustion pressure against measurements in the test engine. The conclusions from the results are summarized as the following:

i. Multi-component combustion model was used of simulation biodiesel combustion for diesel-biodiesel blends and better performance of the results compared to the experimental data.
ii. Biodiesel blends were presented different combustion characteristics at different engine speed. The peak cylinder pressure and heat release rate were larger at high engine speed.
iii. Biodiesel blends increased CO_2 and NO emissions at all crank angle while its decreasing CO and soot emission at all crank angle, compared with diesel fuel.
iv. The combustion and flame temperature increases with the biodiesel blend ratio as slightly.

Acknowledgments

Author thanks to AVL company for their valuable software support and Firat University Scientific and Research Fund for their financial support with projects number TEKF.12.06 and TEKF.12.07.

	Spray formation and temperature contour	local NO fraction	local Soot fraction
B0	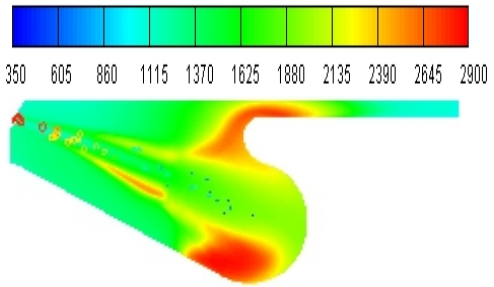	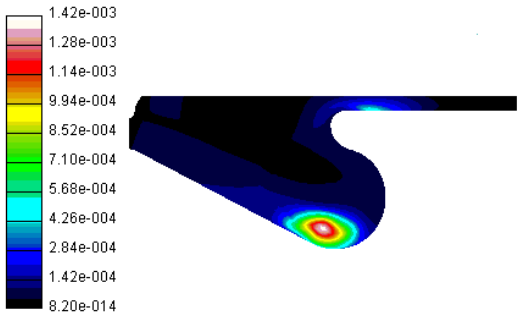	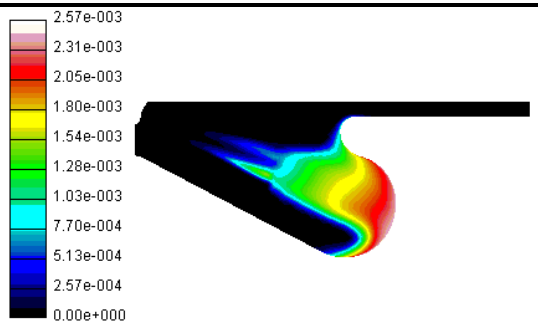
B10	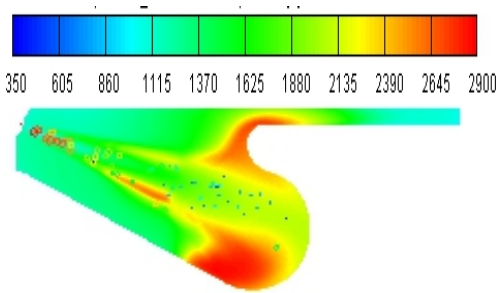	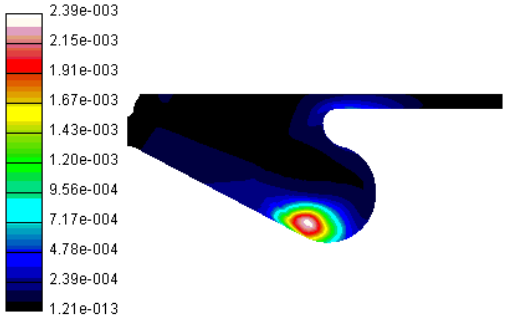	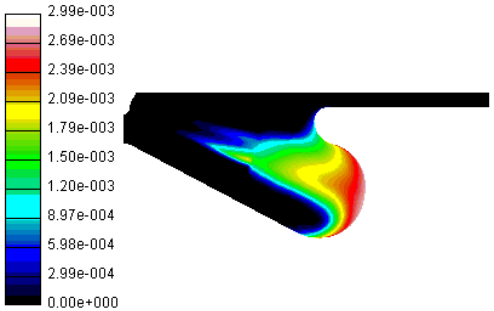
B20	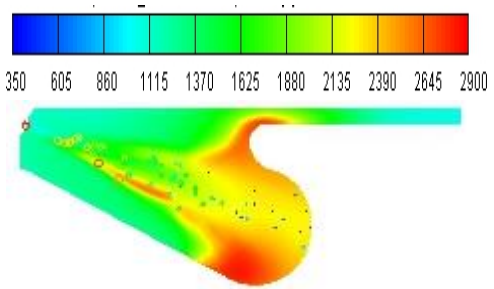	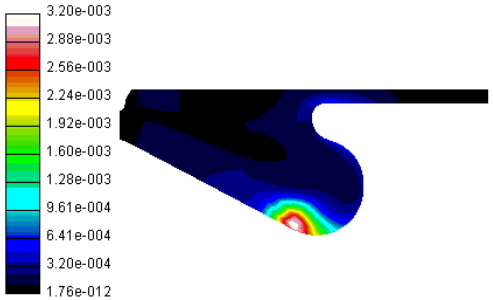	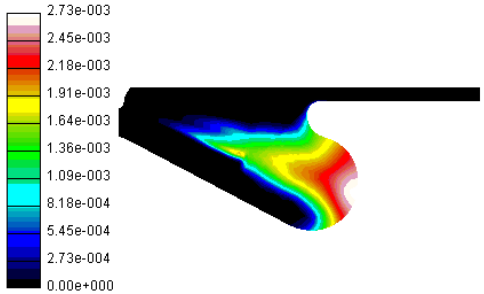

B30

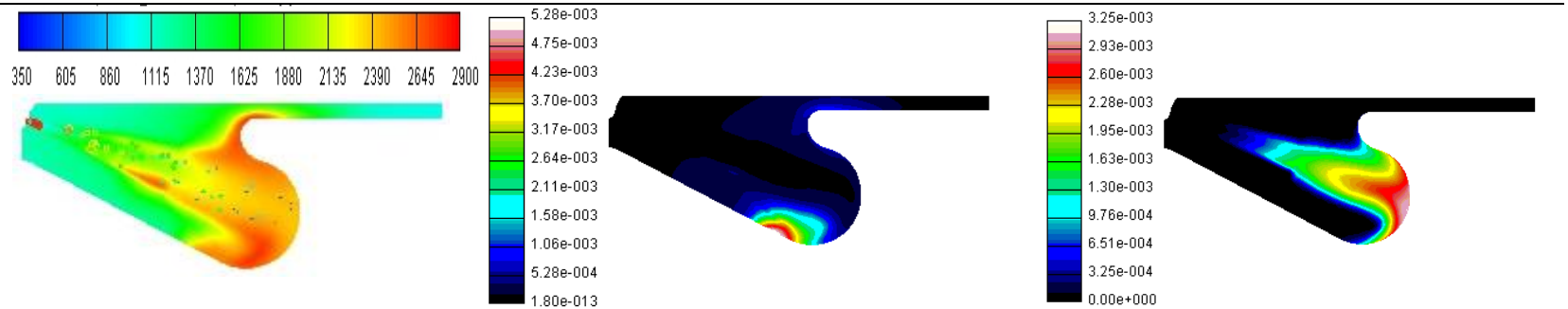

Figure 7 Variation of tempretures, NO and Soot fraction at 10 CA

	Spray formation and temperature contour	local NO fraction	local Soot fraction
B0	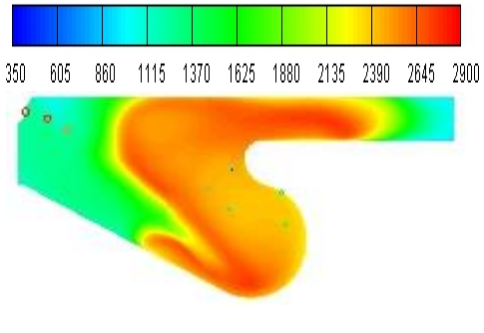	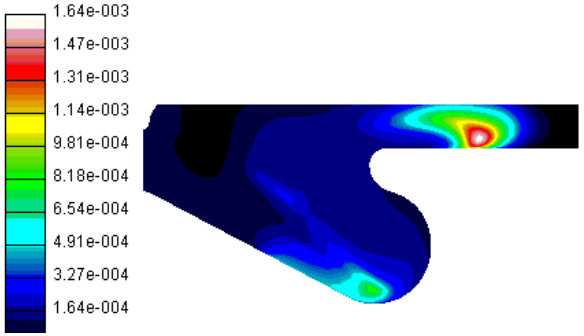	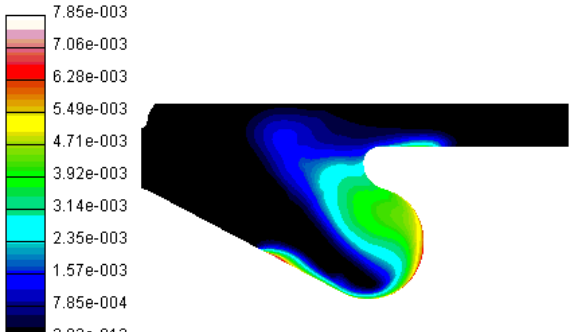
B10	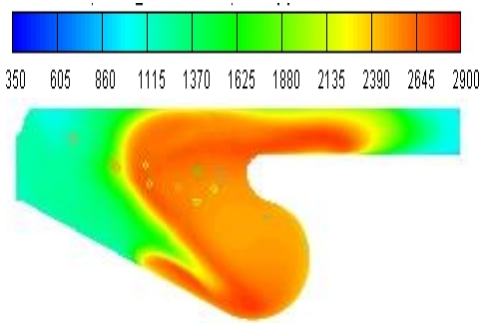	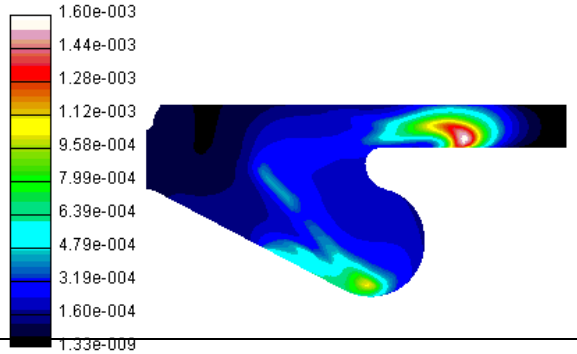	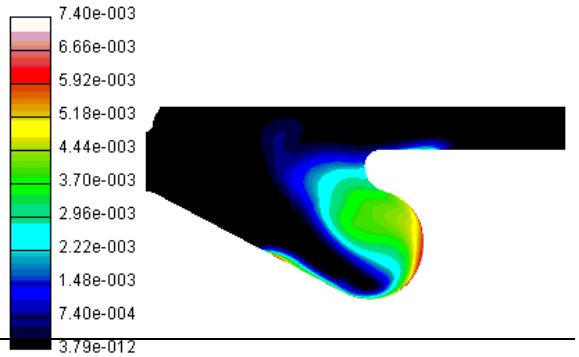

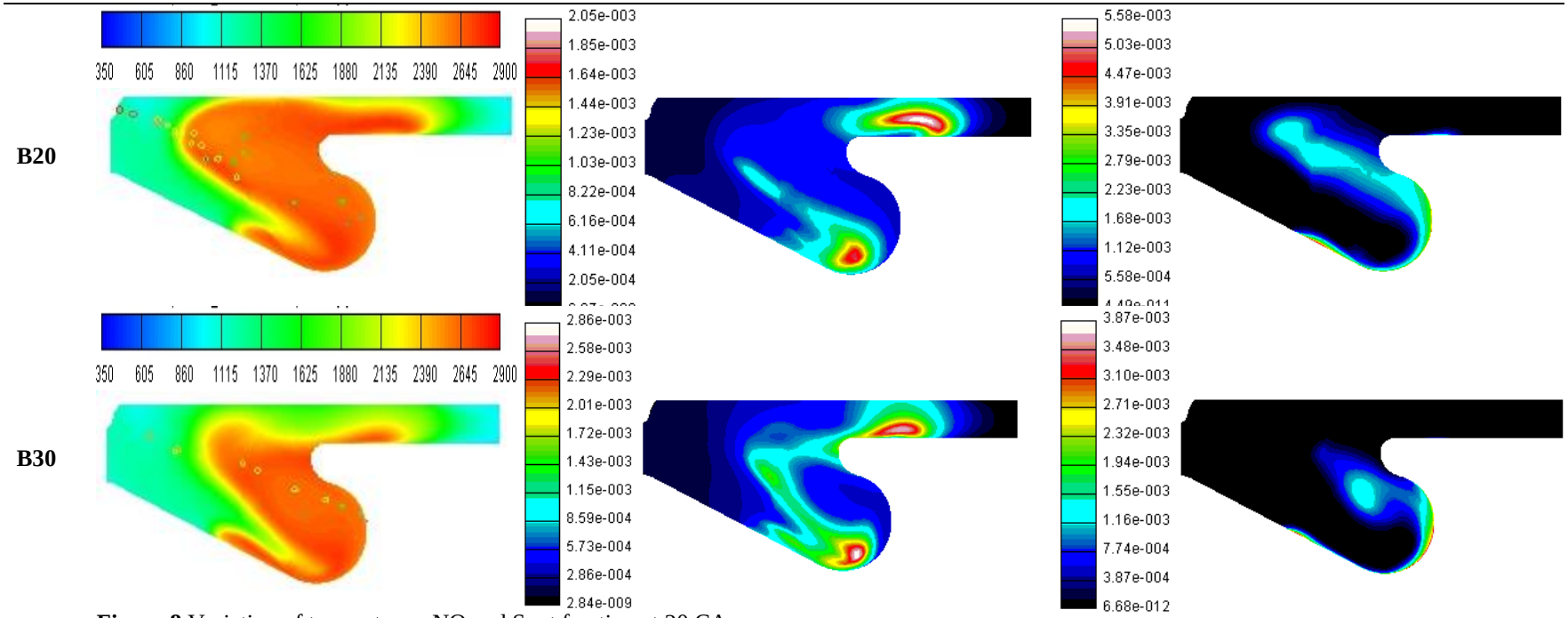

Figure 8 Variation of tempretures, NO and Soot fraction at 20 CA

References

[1] Directive 28/2009/CE of the European Parliament and the Council on the Promotion of the Use of Energy from Renewable Sources, 2009.

[2] Krahl J. et al. Comparison of exhaust emissions and their mutagenicity from the combustion of biodiesel, vegetable oil, gas-to-liquid and petrodiesel fuels. Fuel 88 (2009) 1064–1069.

[3] Behçet R, Performance and emission study of waste anchovy fish biodiesel in a diesel engine. Fuel Processing Technology 2011;92(6):1187–94.

[4] Altun S. Effect of the degree of unsaturation of biodiesel fuels on the exhaust emissions of a diesel power generator. Fuel 117 (2014) 450–457.

[5] Graboski MS, McCormick RL. Combustion of fat and vegetable oil derived fuels in diesel engine. Progress in Energy and Combustion Science 1998;24:125-64.

[6] Lapuerta M, Armas O, Rodríguez-Fernández J. Effects of biodiesel fuels on diesel engine emissions. Progress in Energy and Combustion Science 2008;34:198-223.

[7] Harun Mohamed Ismail, Hoon Kiat Ng, Suyin Gan, Tommaso Lucchini. Computational study of biodiesel–diesel fuel blends on emission characteristics for a light-duty diesel engine using OpenFOAM. Applied Energy 111 (2013) 827–841.

[8] Luka Lešnik, Jurij Iljazˇ, Aleš Hribernik, Breda Kegl. Numerical and experimental study of combustion, performance and emission characteristics of a heavy-duty DI diesel engine running on diesel, biodiesel and their blends. Energy Conversion and Management 81 (2014) 534–546.

[9] An H, Yang W, Li J, Maghbouli A, Chua K-J, Chou S-K. A numerical modeling on the emission characteristics of a diesel engine fueled by diesel and biodiesel blend fuels. Applied Energy 130 (2014) 458–465.

[10] Yuan W, Hansen A. C, Tat M. E, Van Gerpen J. H, Tan Z. Spray, Ignition, And Combustion Modeling Of Biodiesel Fuels For Investigating NOx Emissions. Transactions of the ASAE 48(3), 2005, 933−939.

[11] Yi REN, Ehab ABU-RAMADAN, Xianguo LI Numerical simulation of biodiesel fuel combustion and emission characteristics in a direct injection diesel engine. Front. Energy Power Eng. China 2010, 4(2): 252–261.

[12] Roberto Meloni, and Vincenzo Naso. An Insight into the Effect of Advanced Injection Strategies on Pollutant Emissions of a Heavy-Duty Diesel Engine. Energies 2013, 6, 4331-4351.

[13] D. Wang, C. Zhang, Y. Wang. A Numerical Study of Multiple Fuel Injection Strategies for NOx Reduction from DI Diesel Engines. International Journal of Green Energy, 4:4, 2007, 453-470.

[14] S. Som and D. E. Longman. Numerical Study Comparing the Combustion and Emission Characteristics of Biodiesel to Petrodiesel. Energy Fuels 2011, 25, 1373–1386.

[15] AVL-FIRE User Guides, 2013.

[16] Firat M. Investigation of spray dynamics and combustion on different combustion chambers and spray models in internal combustion engines. PhD Thesis, Firat University, Inst. Science Graduate School Natural Applied Sciences, 2014

[17] Magin Lapuerta, Jose´ Rodrı´guez-Ferna´ndez, Fermı´n Oliva, and Laureano Canoira. Biodiesel from Low-Grade Animal Fats: Diesel Engine Performance and Emissions. Energy & Fuels 2009, 23, 121–129

[18] Lapuerta M, Armas O, Rodríguez-Fernández J. Effects of biodiesel fuels on diesel engine emissions. Prog. Energy Combust. Sci. 2008;34:198-223.

EVALUATING ENVIRONMENTAL EFFECTS OF BIOETHANOL-GASOLINE BLENDS IN USE A SI ENGINE

Ahmet Necati ÖZSEZEN
Department of Automotive Engineering, Kocaeli University, 41380, Izmit-Turkey
Alternative Fuels R&D Center, Kocaeli University, 41275, Izmit-Turkey

Abstract
Bioethanol produced from sugarcane is anticipated to make a major input on transportation fuel markets. In this paper, the environmental effects of bioethanol-gasoline blends were evaluated in use a spark ignition (SI) engine. The bioethanol used in this study was produced by a sugar refinery in Turkey. To determine the exhaust emissions of bioethanol and gasoline blends, SI engine operated at different engine test conditions, and also the test results of bioethanol-gasoline blends compared with those of pure gasoline. The experimental results showed that when the test engine was fueled with bioethanol-gasoline blends, CO and unburned HC emissions decreased, but CO_2 and NO_x emissions increased. At the same time, the results indicated that the air-fuel equivalence ratio increased with the increase of bioethanol percentages in fuel blends.
Keywords: Bioethanol, spark ignition engine, performance, emission.

1. Introduction

Energy security and environment friendly technologies necessitate the use of biological fuels in gasoline or diesel engines, to substitute gasoline and diesel. So, recent years there has been increasing interest in the use of biofuels in internal combustion engine. The latest European regulations force the utilization of biofuels by at least 10% as energy source in transport by 2020 to reduce the pollutant emissions. One of these biofuels is Bioethanol (C_2H_5OH) which is a renewable fuel, and it can be produced from agricultural feedstocks such as sugarcane, wood wastes and agricultural residues. It also contains an oxygen atom, which can be viewed as partially oxidized hydrocarbon. The addition of ethanol to gasoline results in the enhancement of the octane number of blended fuels increases engine knock resistance and reducing the engine emissions (Ozsezen and Canakci, 2011; Stein et al., 2013).

Indeed, the idea of ethanol use as a vehicle fuel dates back to the initial development of the automobile one century ago. When Henry Ford designed his first automobile (Model T), it was built to run on both gasoline and pure ethanol (Sward, 1948). At the present time, it's a well-known fact that bioethanol can be used in blends with petroleum based engine fuels. The smaller the bioethanol addition, the easier typical blending problems (phase separation, corrosion, changed vapor pressure, changed air requirement etc.) can be solved (Pischinger, 1983). Bioethanol has high octane number; consequently their addition to gasoline enhances the octane number of the fuel, therefore reducing the knock problem in the engine (Menrad et. al., 1982). Bioethanol have nearly the same anti-knock effect (Popuri and Bata, 1993). However, increasing bioethanol content of the fuel blend results in decreasing the power, and increasing fuel consumption caused by its lower energy content (Raveendran and Ganesh, 1996). Palmer (1986) stated that the addition of ethanol to unleaded gasoline resulted in an increase in the research octane number by 5 units for each 10% addition. He also found that 10% ethanol addition to gasoline improved the engine power by 5%.

In literature, some researchers (Topgül et. al., 2003; Canakci et. al., 2012; Costagliola et al., 2013; Masum et. al., 2013) showed depending upon air-fuel mixture ratio that the bioethanol-gasoline blends reduce exhaust emissions levels compared to gasoline fueled engine. Generally in these studies, the reductions in the exhaust emissions have been presented depending upon the oxygen content in bio-ethanol. Some researchers (Costa and Sodre, 2010; Li et. al., 2003) have obviously shown reductions in CO and HC emissions, it could be appeared an increasing in NO_x emission. They also explained with faster flame speed of ethanol which increases the high peak pressure inside combustion chamber; this situation produces peak temperature in the combustion chamber. In this study, the effect of bioethanol-gasoline (E5, E10) blends on the SI engine performance and emissions has been discussed. And also, the objective of this study is to provide the information about an SI engine operated with bioethanol-gasoline blends.

2. Material and Method

For this study, bioethanol provided from a commercial company in Turkey. Since the bioethanol production utilizes organic sugar beets contributing to the environment by producing oxygen, and also the produced bioethanol has a purity of 96%. The bioethanol and regular grade gasoline's properties are shown in Table 1.

For the experimental work used a single cylinder spark ignition (Honda GX 390) with 8:1 compression ratio. The engine bore and stroke are 88 and 64 mm,

respectively, 9.75 kW power with rated speed of 3600 rpm, giving a displacement of 389 cm^3. A hydraulic dynamometer is used to be kept at 5 kW of engine load. The experiments were performed at variable speeds of 1000, 1500, 2000, and 2500 rpm (±25) with constant engine output. In the experiments, the values of CO, CO_2, unburned HC, and NO_x for stable running modes in the exhaust gases were monitored by the Bosch BEA-250 exhaust analyzer with pre-calibration. Air mass flow was determined with use of a sharp edged orifice plate and digital differential manometers. The relative humidity and ambient temperature were monitored by a hygrometer. Six different digital thermocouples monitored the temperatures of the intake air, fuel, engine oil, exhaust gas, coolant inlet and outlet.

Table 1. The properties of pure bioethanol and regular grade gasoline

Fuel Property	Unit	Gasoline	Bioethanol
Formula		~ C_7H_{17}	C_2H_5OH
Molar C/H ratio		0.44	0.33
Molecular weight	kg/kmol	98.18	46.07
Net heating value	MJ/kg	44	26.9
Stoichiometric air-to-fuel ratio		14.7	9
Auto ignition temperature	°C	257	425
Heat of vaporization	kJ/kg	305	840
Research octane number		88–100	108.6
Freezing point	°C	-40	-114
Boiling point	°C	27–225	78
Density	kg/m^3	765	785

The engine was sufficiently warmed up for each test and exhaust gas temperature until it was maintained at certain level. During the tests, the engine did not show any starting difficulties when it was fueled with bioethanol-gasoline blends, and it ran satisfactorily throughout the entire tests at room temperature. The brake thermal efficiency and *bsfc* were corrected depending upon the atmospheric conditions as defined in Society of Automotive Engineers (SAE) standard (2001), since the engine tests had been carried out in different days.

3. Result and Discussion

3.1. Performance Results

Fig.1 show that bioethanol addition to the fuel blend results to an increase in brake specific fuel consumption (*bsfc*). As seen Table 1, the energy content of bioethanol is approximately 39% less than that of pure gasoline on a mass basis. Based on this fact, Fig.1 indicates that the engine need much more fuel amount when it is fueled with bioethanol blends to produce the same power output as a gasoline-fueled engine. Thus, the utilization of bioethanol-gasoline fuel blends led to a slightly increasing fuel consumption compared to the use of pure gasoline. This penalty can be absorbed by improved brake thermal efficiency, but thermal efficiency does not improved with use of bioethanol-gasoline blends.

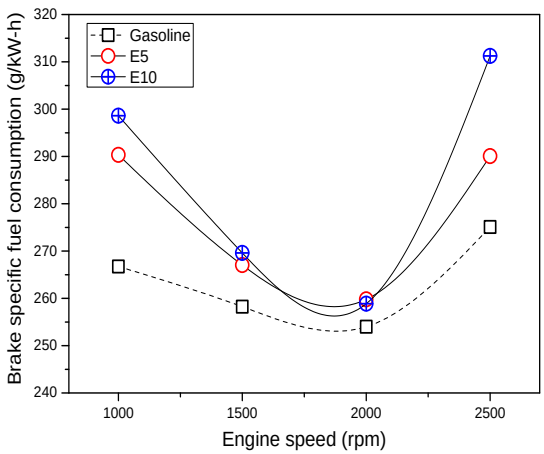

Fig.1. The *bsfc* values for test fuels

As seen Fig.1, for all test fuels, the minimum *bsfc* values were obtained at 2000 rpm of engine speed which are possibly maximum thermal efficiency of the test engine. The minimum *bsfc* for pure gasoline, E5, and E10 was measured as 254 g/kWh, 260 g/kWh, and 259 g/kWh at 2000 rpm, respectively.

For all test fuel blends at 1000 and 2500 rpm of engine speeds, the *bsfc* increased in proportion with the bioethanol content in the fuel blend. However, this case may be explained with the higher octane value of ethanol. In literature, some research (He et al., 2003; Ozsezen and Canakci, 2011) stated same expressions for explaining this fact.

Two important efficiency expressions are used to show the combustion and energy conversion quality in an internal combustion engine; brake thermal and combustion efficiency. The fuel's chemical energy is not entirely converted to the mechanical energy due to the losses in the combustion process. Thus, the completeness of combustion must be defined (Heywood, 1998). In this study, the combustion efficiency was calculated from the exhaust emission values using the following formula;

$$\eta_C = \frac{H_R(T_0) - H_P(T_0)}{\dot{m}_f Q_{LHV}} \quad (1)$$

where; η_c is combustion efficiency (%); H_R is the enthalpy of reactants (fuel and air) at ambient temperature (T_o); H_P is the enthalpy of products (exhaust gases) at ambient temperature; Q_{LHV} is the lower heating value of the fuel (kJ/kg). And then, the thermal efficiency (η_{th}) was calculated as seen in eq.2 depending on the combustion efficiency, engine brake power ($\dot{W}_b$), fuel consumption per second ($\dot{m}_f$), and lower heating value. Fig.2 shows the calculated combustion and thermal efficiencies versus fuel type.

$$\eta_{th} = \frac{\dot{W}_b}{\dot{m}_f Q_{LHV} \eta_C} \quad (2)$$

Fig. 2 shows that the combustion efficiency slightly increased with the use of the bioethanol-gasoline blends. The combustion efficiency enhanced with increasing ethanol content in the fuel blend at 1000 and 1500 rpm, but similar trend was not seen at 2000 and 2500 rpm. The maximum combustion efficiency for pure gasoline, E5, and E10 was calculated as 98.37%, 98.58% and 98.65%, respectively, at 2500 rpm of engine speed. These results are as expected, because bioethanol have 10-20% higher oxygen than their stoichiometric condition. The slight rich of oxygen provide complete combustion of the fuel carbon and hydrogen, and the combustion efficiency appeared at maximum level. It is noted that combustion efficiency is little affected by other engine operating and design variables, provided the engine combustion process remains stable.

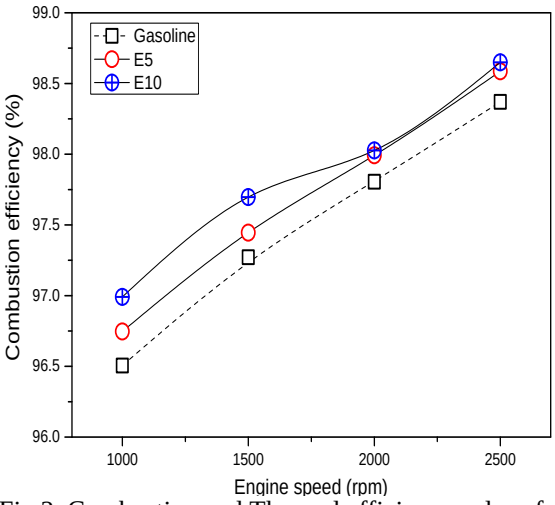

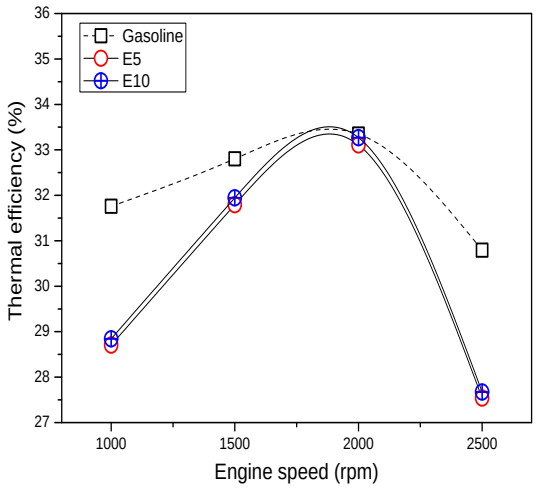

Fig.2. Combustion and Thermal efficiency values for test fuels

As seen in the Fig. 2, the maximum brake thermal efficiency values for pure gasoline, E5, and E10 were calculated as 33.35%, 33.11%, and 32.27% at 2000 rpm, respectively. The brake thermal efficiency is simply the inverse of the product of the specific fuel consumption and the lower heating value of the fuel; thus, the maximum brake thermal efficiency values were obtained in the minimum fuel consumption region. And also, it was seen that the brake thermal efficiency decreased with the increasing amount of bioethanol in the fuel blend. This means that the increase of *bsfc* for the bioethanol-gasoline fuel blends is lower than the corresponding decrease of the lower heating values of the blends.

Additionally, the complete combustion reaction formulas of pure gasoline and bioethanol with atmospheric air are shown below in eq. 3-4. For the same concentration air, the ethanol is higher energy release than pure gasoline. As a result of this situation, the brake thermal efficiency improved. In a similar study (Yanju et. al., 2008), the low content alcohol-gasoline blends were seen to be improving in brake thermal efficiency.

Gasoline:

$$C_7H_{14} + 10.5(O_2 + 3.76N_2) \rightarrow 7CO_2 + 7H_2O + 39.5N2 + 4.568\ MJ \quad (3)$$

Bioethanol:

$$4.66C_2H_5OH + 10.5(O_2 + 3.76N_2) \rightarrow 9.32CO_2 + 11.65H_2O + 39.5N_2 + 6763\ MJ \quad (4)$$

3.2. Emission Results

One of the key parameters which affect CO and unburned HC emission formations is the air-fuel ratio (Abdel-Rahman, 1998). Fig.3 show that air/fuel ratios for test fuels on the engine operating conditions.

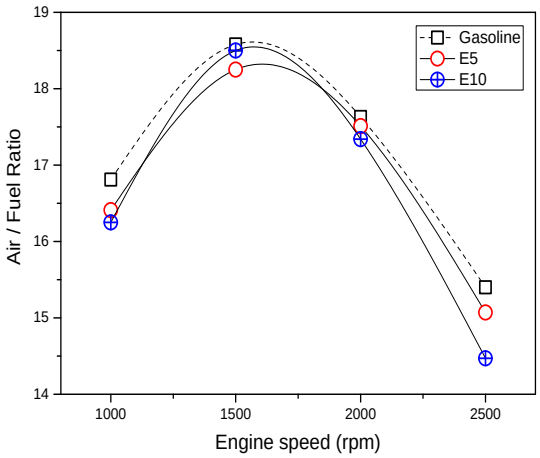

Fig.3. Air/fuel ratios for test fuels

Especially, if the engine is running in rich conditions, CO emission concentrations will increase because there is not enough oxygen to convert all carbon atoms of fuel into CO_2 (Wu et al., 2004). Fig.4 shows CO and unburned HC emissions values for test fuels. Emission test results indicate that when bioethanol is added to gasoline, the combustion of the engine becomes better and therefore CO emission is reduced. The mean average of CO emission decreases to 0.3%, 6%, 3.6% and 2% with E5, and 3.5%, 8%, 13% and 13.7% with E10, respectively, at 1000, 1500, 2000 and 2500 rpm of engine speeds. One of the most important properties of bioethanol is having oxygenated atoms in their molecular compounds which provide significant reduction in the CO and HC emissions. In the past, some researches (Zervas et. al., 1999; Hsieh et. al., 2002) explained that the decrease of CO emissions is due not only to dilution of the fuel but is also because addition of oxygenated compounds promotes the combustion of CO in the cylinder. The inclination of CO emission increased when the engine speed increased from 1000 to 2500 rpm.

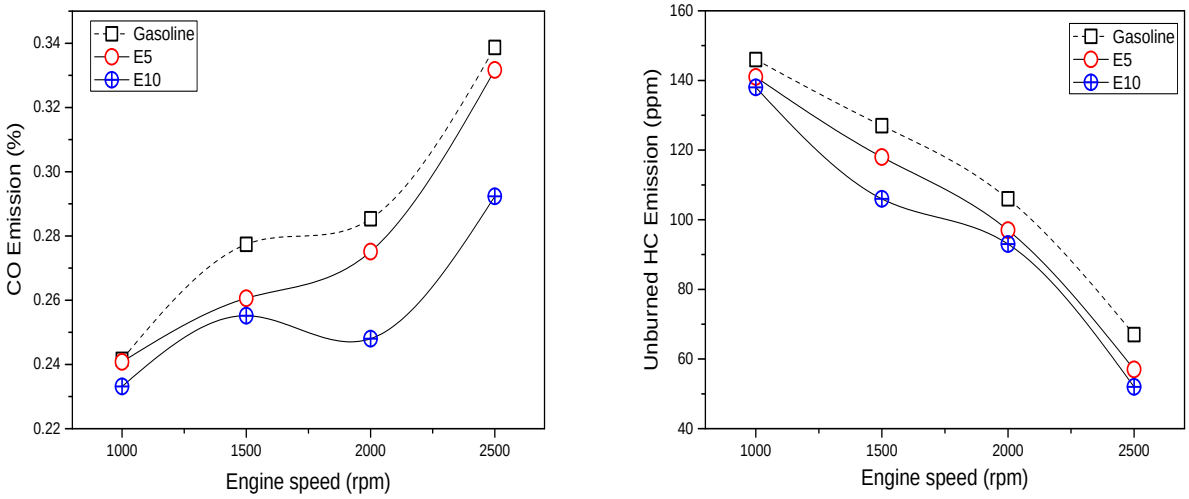

Fig.4. The effect of test fuels on CO and unburned HC emissions

The mean average of unburned HC emissions decreased 3.4%, 7.1%, 8.5% and 14.9% by E5, and 5.5%, 16.5%, 12.3% and 22.4% by E10, respectively, at 1000, 1500, 2000 and 2500 rpm of engine speeds. The explanation is that increasing engine speed leads to an increase in the combustion temperature, which combined with the high level of excess oxygen at these loads results in lower unburned HC emissions when compared with pure gasoline.

Other significant emissions are CO_2 and NO_x which contribute to serious air pollution and public health problems. In this study, the humidity correction factor for the NO_x was calculated as assured in the reference, Society of Automotive Engineers (SAE, 2001). Fig. 5 shows CO_2 and NO_x emissions values for all test fuels. As seen in figure, NO_x emissions with the use of E5 and E10 approximately increased by 1% and 2.2%, respectively. On average of CO_2 emissions with the use of E5 and E10 increased by 1.7% and 3.9%, respectively. Maximum increase

ratios in NO_x emission was calculated, with E5 (1.6%) and E10 (3.6%), respectively, at 2500 rpm of engine speed compared with pure gasoline values.

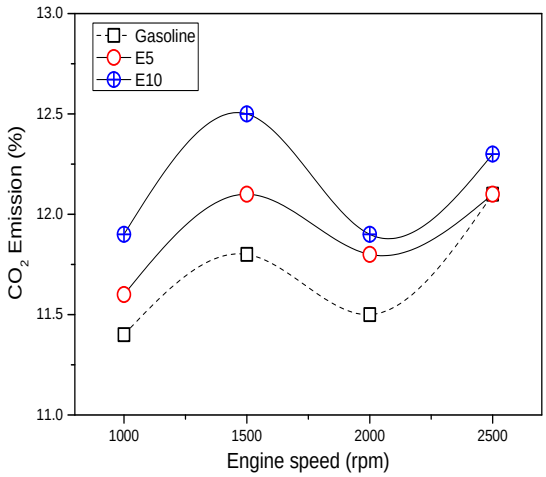

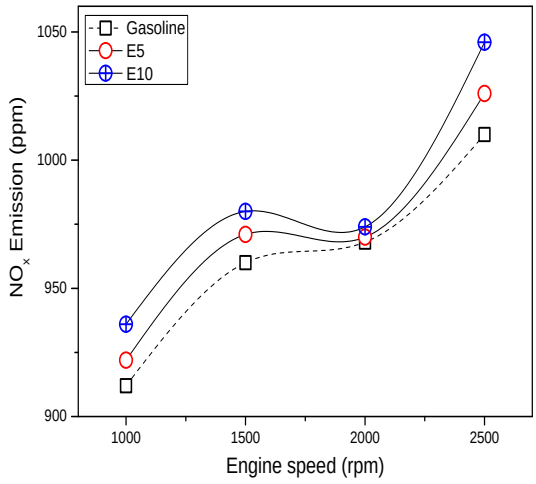

Fig.5. The effect of test fuels on CO_2 and NO_x emissions

4. Conclusion

This paper evaluates the environmental effects of bioethanol-gasoline blends in use a SI engine. The experimental results showed that when the test engine was fueled with bioethanol-gasoline blends, there is an increase in brake fuel consumption (~ 5% with E5 and ~ 7.5% with E10) compared with pure gasoline. With use of the bioethanol-gasoline blends, CO (~ 3% with E5 and ~ 9% with E10), unburned HC emissions (~ 8.5% with E5 and ~ 14.2% with E10) decreased and NO_x (~ 1% with E5 and ~ 2.2% with E10), CO_2 (~ %1.7 with E5 and ~ 3.9% with E10) slightly increased. The best combustion efficiency was obtained with the use of bioethanol-gasoline blends. It can be said that the decreases in unburned HC emission levels with use of the alcohol-gasoline blends led to increase in the combustion efficiency. And also it did not appear a cold start problem when using the fuel mixtures.

References

Abdel-Rahman AA. On the emissions from internal-combustion engines: a review, International Journal of Energy Research 1998, 22(6), 483-513.

Canakci, M., Ozsezen, A. N., Alptekin, E., Eyidogan, M. Impact of alcohol–gasoline fuel blends on the exhaust emission of an SI engine, Renewable Energy 2012, 52, 111-117.

Costa, R.C. and Sodre, J.R. Hydrous ethanol vs. gasoline-ethanol blend: Engine performance and emissions, Fuel 2010, 89, 287–293.

Costagliola, M.A., De Simio, L., Iannaccone, S. and Prati, M.V. Combustion efficiency and engine out emissions of a S.I. engine fueled with alcohol/gasoline blends, Applied Energy 2013, 111, 1162–117.

He, B.Q., Wang, J.X., Hao, J.M., Yan, X.G. and Xiao, J.H. A study on emission characteristics of an EFI engine with ethanol blended gasoline fuels, Atmospheric Environment 2003, 37, 949-957.

Heywood, J.B. Internal combustion engine fundamentals. Singapore, Mc-Graw Hill, 1988, p.82.

Hsieh, W.D., Chen, R.H., Wu, T.L. and Lin, T.H. Engine performance and pollutant emission of an SI engine using ethanol–gasoline blended fuels, Atmospheric Environment 2002, 36(3), 403–410.

Li, L., Liu, Z., Wang, H., Deng, B., Xiao, Z., Wang, Z., Gong, C., Su, Y. Combustion and emissions of ethanol fuel (E100) in a small SI engine, SAE Technical Paper 2003-01-3262, Society of Automotive Engineers, Inc., USA; 2003.

Masum, B.M., Masjuki, H.H., Kalam, M.A., Rizwanul Fattah, I.M., Palash, S.M. and Abedin M.J. Effect of ethanol–gasoline blend on NO_x emission in SI engine, Renewable Sustainable Energy Review 2013, 24, 209-222.

Menrad, H., Haselhorst, M. and Erwig, W. Pre-ignition and knock behavior of alcohol fuels, SAE Paper 1982; No.821210.

Ozsezen, A.N. and Canakci, M. Performance and combustion characteristics of alcohol–gasoline blends at wide-open throttle, Energy 2011, 36(5), 2747–275.

Palmer, F.H. Vehicle performance of gasoline containing oxygenates. MI MechE, 1986, C319/86, 33-46.v

Pischinger, F.F. Alcohol Fuels for Automotive Engines. 11th World Petroleum Congress, RTD 6(3), London, 1983.

Popuri, S.S.S and Bata, R.M. A performance study of iso-butanol-, methanol-, and ethanol- gasoline blends using a single cylinder engine, SAE Paper 1993; No.932953.

Raveendran, K. and Ganesh, A. Heating value of biomass and biomass pyrolysis products, Fuel 1996, 75, 1715-1720.

SAE Handbook, MI Vol.1, SAE Inc.: Warrendale, 2001; 1304-1306.

Stein, R., Anderson, J. and Wallington, T. An Overview of the Effects of Ethanol-Gasoline Blends on SI Engine Performance, Fuel Efficiency, and Emissions, SAE Int. J. Engines 2013, 6(1), 470-487.

Sward, K. The Legend of Henry Ford. 1rd ed. New York: Rinehart; 1948.

Topgül, T., Yücesu, H.S., Cinar, C. and Koca, A. The Effects of ethanol-unleaded gasoline blends and ignition timing on performance and exhaust emissions, Renewable Energy 2006, 31, 2534-2542.

Wu, C.W., Chen, R.H., Pu, J.Y., Lin, T.H. The Influence of air-fuel ratio on engine performance and pollutant emission of an SI engine using ethanol-gasoline-blended fuels, Atmos. Environ. 2004, 38, 7093-7100.

Yanju, W., Shenghua, L., Hongsong, L., Rui, Y., Jie, L. Ying W. Effects of methanol/gasoline blends on a spark ignition engine performance and emissions. Energ Fuel 2008, 22, 1254–1259

Zervas, E., Montagne, X., Lahaye, J. Influence of gasoline formulation on specific pollutant emissions, J. Air & Waste Manage. Assoc. 1999, 49, 1304-1314.

INVESTIGATION OF SMALL WIND TURBINE AIRFOILS FOR KAYSERI WEATHER CONDITIONS

Cevahir TARHAN[1*] and İlker YILMAZ[2]

1. Faculty of Aeronautics and Astronautics, Erciyes University, Kayseri, Turkey; email: ctarhan@erciyes.edu.tr
2. Faculty of Aeronautics and Astronautics, Erciyes University, Kayseri, Turkey; email: iyilmaz@erciyes.edu.tr

*Corresponding author

Abstract

Wind energy has an increased usage in last years. Its importance is because of the renewability and potential for usage with a low budget. In this study we focus on the small wind turbines which can easily usable by public and small operations with a small budget. 14 types of best small wind turbine airfoils (A18, BW3, Clark Y, E387, FX77, NACA 2414, RG 15, S822, S823, S6062, S7012, SD6060, SD7032, SD7062) determined from past studies and examined with Ansys Fluent fluid dynamics program. Their lift and drag coefficients determined for 50000 Reynolds number which is a function of Kayseri's common wind speed and air density. As a result best suited small wind turbine airfoil type is determined for Kayseri usage.

Keywords: Wind Turbine, Airfoil, Lift, Drag

Nomenclature

C_d Drag Coefficient
C_l Lift Coefficient

1. INTRODUCTION

As a result of increasing demand to energy, increasing greenhouse gases and the need for energy independence; most of the developed countries investing in renewable energy area in recent years. One of the most advantageous types of renewable energy is wind energy. Sun's heat produces wind on earth's surface and this wind energy can be used for benefit of mankind by usage of wind turbines. For areas of low wind potential; small, cheap and portable wind turbines are beneficial. Airfoils are used in wind turbines to capture the wind and to rotate the rotor. In this study we performed simulations for 14 types of (A18, BW3, Clark Y, E387, FX77, NACA 2414, RG 15, S822, S823, S6062, S7012, SD6060, SD7032, SD7062) small scale wind turbine airfoils which are commonly used in small wind turbines[1-3]. Simulations performed for 50,000 Reynolds number with Ansys Fluent fluid dynamics program. This Reynolds number choice is because of the air density of 1.036 kg/m^3 and average wind speed of 7 m/s for Kayseri, Turkey, [4]. $(C_l/C_d)_{max}$ and $C_{l\ max}$ parameters are choosed for evaluation process. This is because of the dependency of efficiency to high lift coefficient and low drag coefficient while converting wind power to torque power.

2. PERFORMED SIMULATIONS

At Fig. 1 and Fig. 2, C_l and C_d results for the choosen airfoils after the performed simulations with Ansys Fluent fluid dynamics program are given. As seen on Fig. 1, BW3airfoil has best lift coefficient and the second best one is A18.

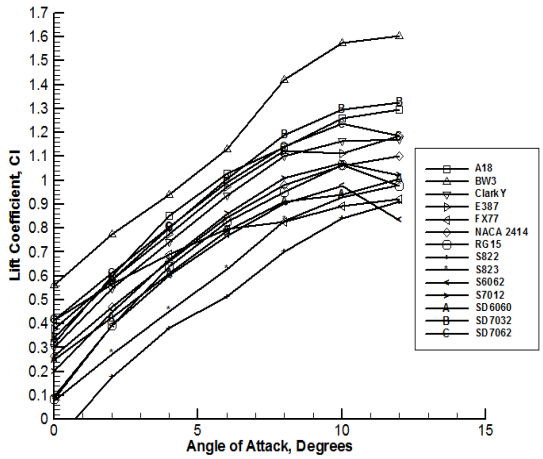

Figure 1. Lift Coefficient Curves for the Airfoils at Re= 50,000

Fig. 2, shows us the drag coefficients of the airfoils and as seen on figure that BW3 has far better drag coefficient results.

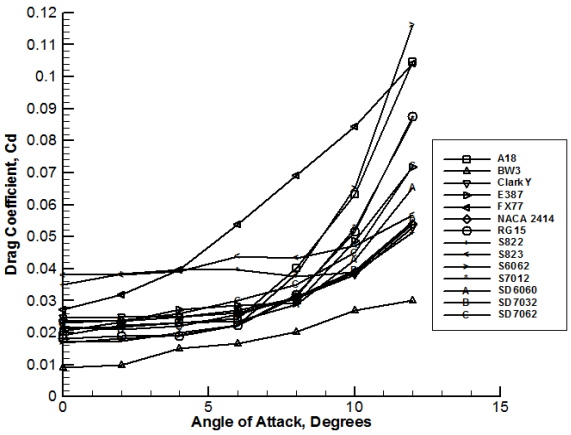

Figure 2. Drag Coefficient Curves for the Airfoils at Re= 50,000

As seen at Fig. 3, lower drag coefficient results of BW3 gives us the best airfoil C_l/C_d for this type.

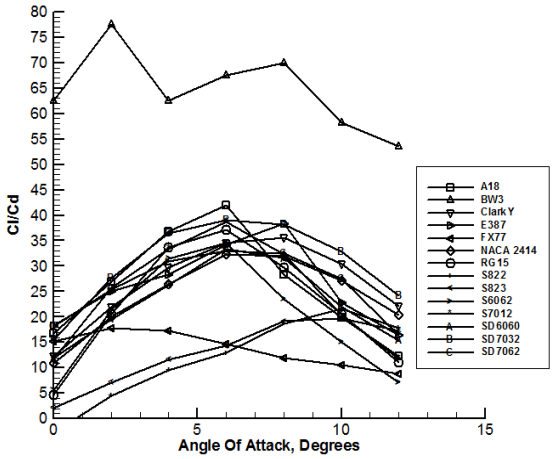

Figure 3. Lift Coefficient / Drag Coefficient Curves for the Airfoils at Re= 50,000

In Table 1, all 14 airfoil's evaluated performance parameters are given. $(C_l/C_d)_{max}$ corresponds to the best value for angle of attacks between 0° to 12° for the airfoils. C_l and C_d are coefficients which are used for the calculation of $(C_l/C_d)_{max}$ ratio.

Table 1. Performance Parameters for the Airfoils Considered

Airfoil	$(C_l/C_d)_{max}$	$C_{l\,max}$	C_l	C_d
A18	42.00	1.29	1.02	0.024
BW3	77.56	1.60	0.77	0.010
Clark Y	35.56	1.17	1.10	0.031
E387	38.42	1.19	1.12	0.029
FX77	17.73	0.92	0.56	0.031
NACA2414	32.29	1.10	0.84	0.026
RG15	37.08	1.06	0.82	0.022
S822	21.70	0.91	0.84	0.039
S823	19.68	0.97	0.93	0.047
S6062	34.59	0.97	0.77	0.022
S7012	38.78	1.07	0.86	0.022
SD6060	33.33	1.01	0.80	0.024
SD7032	39.10	1.32	1.00	0.026
SD7062	33.00	1.23	0.99	0.030

3. CONCLUSION

After the numerical simulations BW3 airfoil is evaluating as the best suited airfoil for small wind turbines in Kayseri weather conditions and for similar areas where the Reynolds Number is near 50,000. BW3 has far better C_l/C_d ratio and high lift coefficient when compared to other choosen small wind turbine airfoils.

Acknowledgements

This study was supported and funded by Erciyes University, Department of Scientific Research Projects, Turkey with a Project ID of FDK-2016-6806.

REFERENCES

[1] N. Karthikeyan, K. Kalidasa, S. Arun Kumar , S. Rajakumar, Review of aerodynamic developments on small horizontal axis wind turbine blade, Renewable and Sustainable Energy Reviews 42 (2015) 801–822.
[2] J.C.C Henriques., F. Marques da Silva, A.I. Estanqueiro, L.M.C. Gato, Design of a new urban wind turbine airfoil using a pressure-load inverse method, Renewable Energy 34 (2009) 2728–2734
[3] J.L. TangIer, D.M. Somers, NREL Airfoil Families for HAWTs, National Renewable Energy Laboratory, 1995.
[4]http://www.eie.gov.tr/YEKrepa/KAYSERI-REPA.pdf**, September 2016.**

3D COLD FOLLOW SIMULATION INSIDE INTAKE MANIFOLD AND CYLINDER OF AN IC ENGINE

Bilge Albayrak ÇEPER*, Melih YILDIZ*, Vedat DEMIRTAS, Hakan Serhad SOYHAN***, Nafiz KAHRAMAN***
*Erciyes University, Faculty of Engineering, Department of Mechanical Engineering, 38039 Kayseri, Turkey
** Afyon Kocatepe University, Faculty of Technology, Dept. of Automotive Engineering, 03200 Afyonkarahisar
*** Sakarya University, Faculty of Engineering, Department of Mechanical Engineering, 54187 Sakarya
*Corresponding author: E-mail: balbayrak@erciyes.edu.tr Tel: +90 352 2076666, Fax: +90 352 4375784

Abstract
This paper presents 3D cold follow simulation inside the intake manifold, valves and cylinders of the engine which has two cylinders with two valves in each, and a compression ratio of 10.7. The purpose of this study is to analyze the change in the cylinders in terms of temperature, pressure and velocity depending on crank angle degree for 300 K and 450 intake temperatures. This is, particularly, important for a controlled auto ignition (CAI) engine which has sensitive to temperature distribution and pressure for combustion development in cylinders. In this study, the engine model based on the real dimension of Lombardini LGW523 engine was structured and then meshed for follow fields. Fluent CFD code which uses finite volume method was used as an analysis tool. 3D Pressure based Implicit unsteady solver was used to solve the basic governing equations (mass, momentum and energy). RNG k-ε turbulence model was used to simulate the turbulence follow in the cylinders. The analyses in this study were carried out for four strokes of the engine using dynamic mesh. As a result, in cylinder temperature, pressure and velocity distribution were obtained with change in crank angle positions and compared for two different intake temperature.

Keywords: Cold flow simulation, Spark Ignition Engine, Intake manifold, Cylinder Pressure

1. INTRODUCTION

An inlet manifold or intake manifold is the part of an engine that supplies the fuel/air mixture (in case of SI engine) or only fresh air (in case of CI engine) to the engine cylinder. The primary function of the intake manifold is to evenly distribute the combustion mixture (or just air in a direct injection engine) to each intake port in the cylinder heads[1]. Improvements in engine efficiency can also be attained by enhanced in-cylinder flow motions using optimized cylinder head, port and valve timing. A well-designed intake manifold and cylinder head will reduce the flow resistance and increases the swirl. Swirl is the rotation of charge about cylinder axis and it is used in SI engines to speed up the combustion[2]. In-cylinder flow field structure in an internal combustion (IC) engine has a major influence on the combustion, emission and performance characteristics. The fluid motion in an internal combustion engine is induced during the induction process and later modified during the compression process. Intake charge enters the combustion chamber through the intake manifold of an IC engine with high velocity. Then the kinetic energy of the fluid resulting in turbulence causes rapid mixing of fuel and air, if the fuel is injected directly into the cylinder. In-cylinder fluid motion governs the flame propagation in spark-ignition engines, and controls the fuel-air mixing and premixed burning in diesel engines. With optimal turbulence, better mixing of fuel and air is possible which leads to effective combustion [3].

Paul and Ganesan [4]studied the effect of helical, spiral, and helical-spiral combination manifold configuration on air motion and turbulence inside the cylinder of a Direct Injection (DI) diesel engine motored at 3000 rpm. Three dimensional model of the manifolds and the cylinder was created and meshed using the pre-processor GAMBIT. The flow characteristics of these engine manifolds were examined under transient conditions using Computational Fluid Dynamics (CFD) code STAR-CD. The predicted CFD results of mean swirl velocity of the engine at different locations inside the combustion chamber at the end of compression stroke were compared with experimental results carried out by other researchers. They concluded that swirl ratio inside the cylinder and turbulent kinetic energy was higher for spiral manifold. Volumetric efficiency for the spiral-helical combined manifold was 10% higher than that of spiral manifold.

Kumar and Nagarajan [5], deals with experimental investigation of swirling flow in the cylinder of a spark ignited engine. The variations in different non-dimensional parameters such as flow coefficient, swirl coefficient and swirl ratio at various valve lifts and throttle opening was studied using a steady flow bench. Their results indicate that a higher swirl coefficient and swirl ratio could be achieved with shrouded valve and twisted tape with penalty on flow coefficient. These experimental results could be utilized to verify the results of modeling using commercial CFD codes and also for increasing the

accuracy of mathematical modeling of combustion process in internal combustion engines.

Karthikeyan et al.[6] indicated from the AVL BOOST software that the sudden increase in pressure waves are observed with initial manifold design. Therefore the initial intake manifold was optimized for uniform flow, by using CFD software. From the CFD results, 76% mass fraction of air was observed for all the three runners at 1800 rpm. Further experimentally air pressure inside the runners were investigated and increased air pressure of 13% shows that flow of air increased inside the runner for the optimized intake manifold design.

The manifold design and temperature distribution in a cylinder is also important for a CAI engine which is alternative combustion mode to conventional SI and CI engines. This is because CAI combustion takes place at many points in a cylinder. During CAI combustion, premixed fuel and air mixture is compressed to a temperature so high (usually 1000 K or more) that auto ignition happens[7]. In case of high ignition temperature, we have to increase the in-cylinder temperature by means of heating intake port, modified compression ratio and using internal exhaust gas recirculation. Therefore, intake temperature value, temperature distribution and mass fractions of mixture directly influence on CAI combustion process. In this study, 3D flow simulation was performed at two different intake temperatures for CAI engine converted from SI engine in order to attain temperature distribution in the flow fields.

2. NUMERICAL ANALYSIS

The specifications of the SI engine analyzed are given in Table 1. A geometric model of the engine including intake manifold, combustion chamber, intake and exhaust ports, intake and exhaust valves, was structured and meshed for computational domains by using GAMBIT. The computational mesh consisted of 2.368.713 cells at TDC and 5.605.462 cells at BDC. Figure 1 shows the computational domain of the three-dimensional geometric model.

Table 1. Engine Specification

Description	Unit	Value
Bore	[mm]	72
Stroke	[mm]	62
Displacement volume	[lt]	0.505
Compression ratio	[-]	10.7
Intake valve diameter	[mm]	32
Exhaust valve diameter	[mm]	27

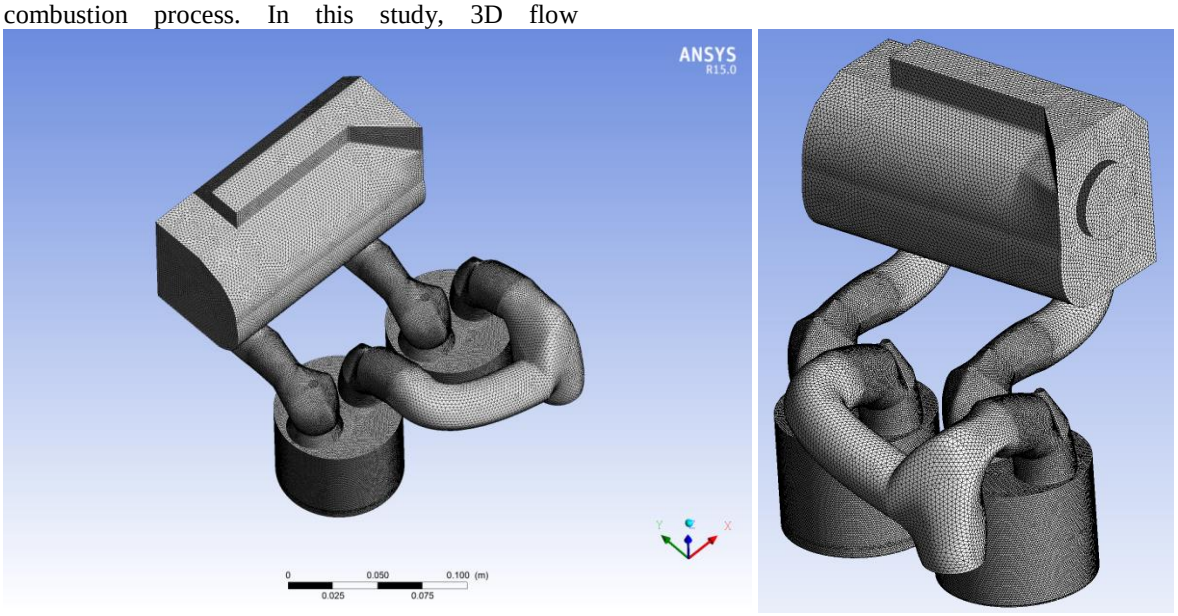

Figure 1. Geometric model.

Model formulation:

The model considered was solved using FLUENT which uses the control-volume-based method to convert the governing equation to algebraic equations. The governing equations of continuity, momentum, energy and the sub-model equations of turbulence, radiation and species transport with finite rate chemistry, auto-ignition and NOx model, which are necessary to simulate the engine cycle were solved in time dependent deforming two-dimensional control volume. The integral form of the conservation equation for ϕ scalar quantity is written for an arbitrary control volume V as follows [8]:

$$\int_V \frac{\partial \rho\phi}{\partial t} dV + \oint \rho\phi\vec{v}.d\vec{A} = \oint \Gamma_\phi \nabla\phi.d\vec{A} + \int_V S_\phi dV \quad (1)$$

where ρ is density, $\vec{v}$ is velocity vector, $\vec{A}$ is surface area vector, Γ_ϕ denotes diffusion coefficient for ϕ and S_ϕ represents source of ϕ per unit volume.

A. Turbulence Model

The RNG k-ε turbulence model was used owing to its degree of accuracy in obtaining the effect of swirling flow. Transport equations for the RNG k-ε are expressed as follows:

$$\frac{\partial}{\partial t}(\rho k) + \frac{\partial}{\partial x_i}(\rho k u_i) = \frac{\partial}{\partial x_j}\left(\alpha_k \mu_{eff} \frac{\partial k}{\partial x_j}\right) + G_k + G_b - \rho\varepsilon - Y_M + S_k \quad (2a)$$

$$\frac{\partial}{\partial t}(\rho\varepsilon) + \frac{\partial}{\partial x_i}(\rho\varepsilon u_i) = \frac{\partial}{\partial x_j}\left(\alpha_\varepsilon \mu_{eff} \frac{\partial \varepsilon}{\partial x_j}\right) + C_{1\varepsilon}\frac{\varepsilon}{k}(G_k + C_{3\varepsilon}G_b) - C_{2\varepsilon}\rho\frac{\varepsilon^2}{k} - R_\varepsilon + S_\varepsilon \quad (2b)$$

In these equations, Gk and Gb denote the generation of turbulence kinetic energy due to mean velocity gradients and buoyancy, respectively. YM is the contribution of fluctuating dilatation in compressible turbulence. αk and αε are the inverse effective Prandtl number for k and ε. Sk and Sε are user-defined source terms. C1ε and C2ε are the model constants derived analytically by the RNG theory.

The total temperature is set to 300 K for case one, and then 450 K for case two, assuming that the engine is naturally aspirated. Three main boundary features were used (i) pressure inlet (ii) pressure outlet and (iii) walls. Turbulence in the related boundaries was specified using Intensity and Hydraulic Diameter. Wall temperatures were also set to 300 K. 3D Semi Implicit unsteady solver was used to solve the basic governing equations (mass, momentum and energy). RNG k-ε turbulence model was used to simulate the turbulence in the engine cylinder. SIMPLE (Semi-Implicit Method for Pressure-Linked Equations) was used as the pressure velocity coupling scheme.

3. RESULTS AND DISCUSSION

The results from the manifold and cylinders modeling and CFD simulation using FLUENT software are shown and discussed. Figure 1 shows the contours of velocity magnitude at different crank angles. As seen in this figure, velocity magnitudes are clearly seen in manifold and cylinder with valve. Piston is in TDC position where the exhaust valve is closed and the inlet valve is open i.e., beginning of intake stroke for first cylinder. Maximum velocity obtained at 540° is 38.54m/s.

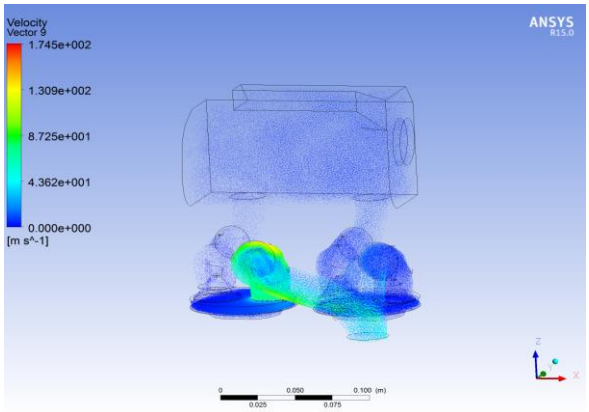

a) 360 CA

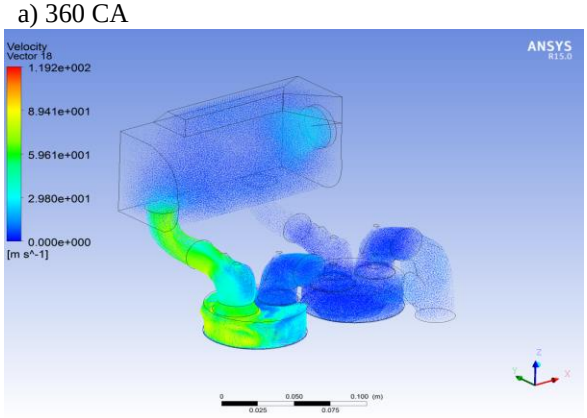

b) 420 CA

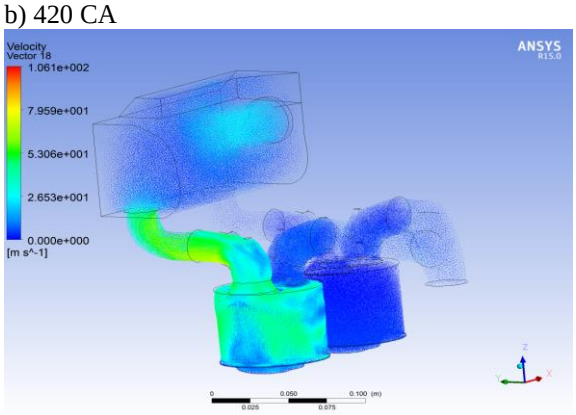

c) 480 CA

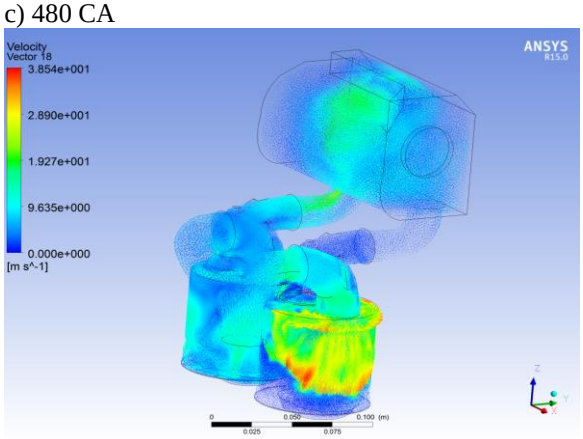

d) 540 CA

Figure 1. Velocity magnitude for different crank angles

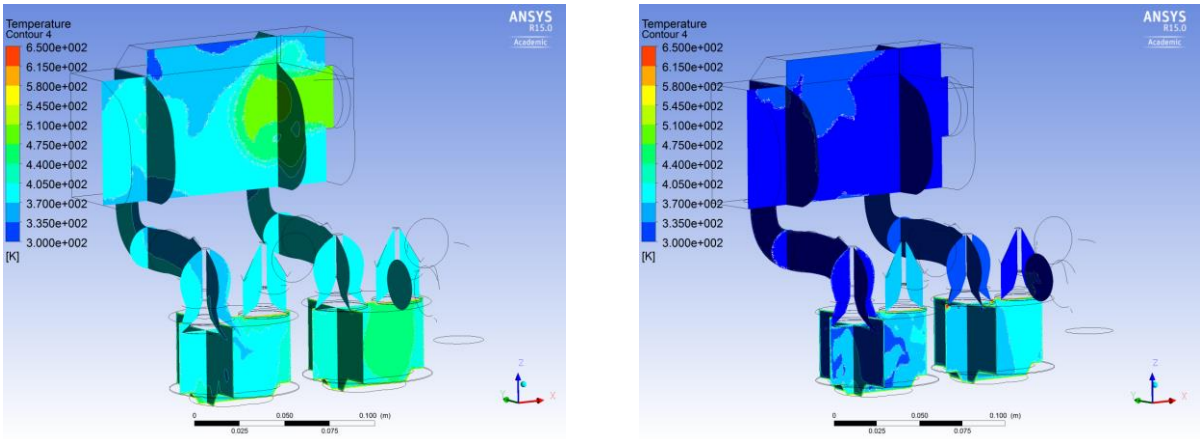

a) 450 K at 450CA b) 300K at 450CA

Figure 2. Temperature distribution for 300 and 450 K at 450 CA

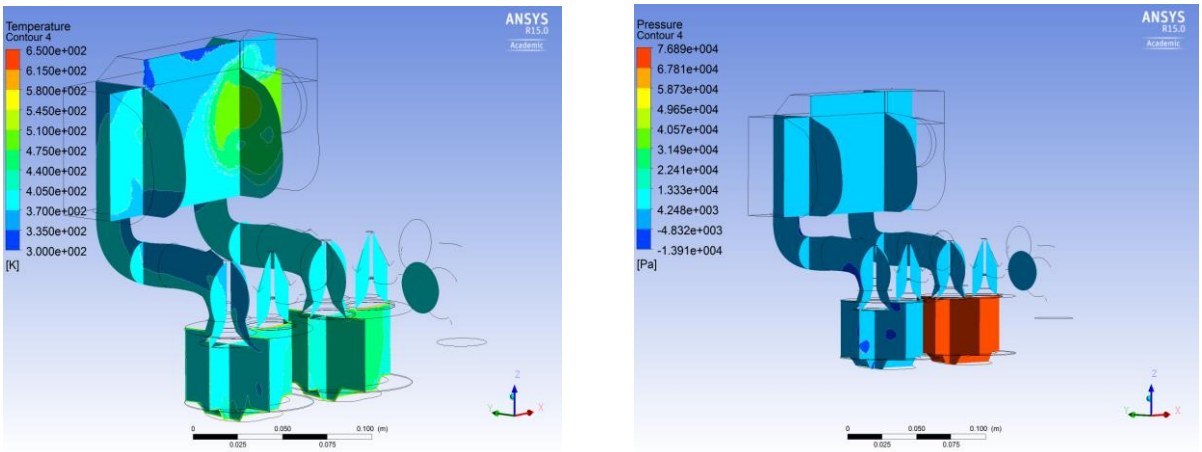

a) 450 K at 450CA b)300K at 450CA

Figure 3. Pressure distribution for 300 and 450 K at 450CA

Figure 4 shows pressure values versus the crank angle for 300 and 450 K intake temperature. With the increasing of intake temperature, pressure values were decrease in both cylinders.

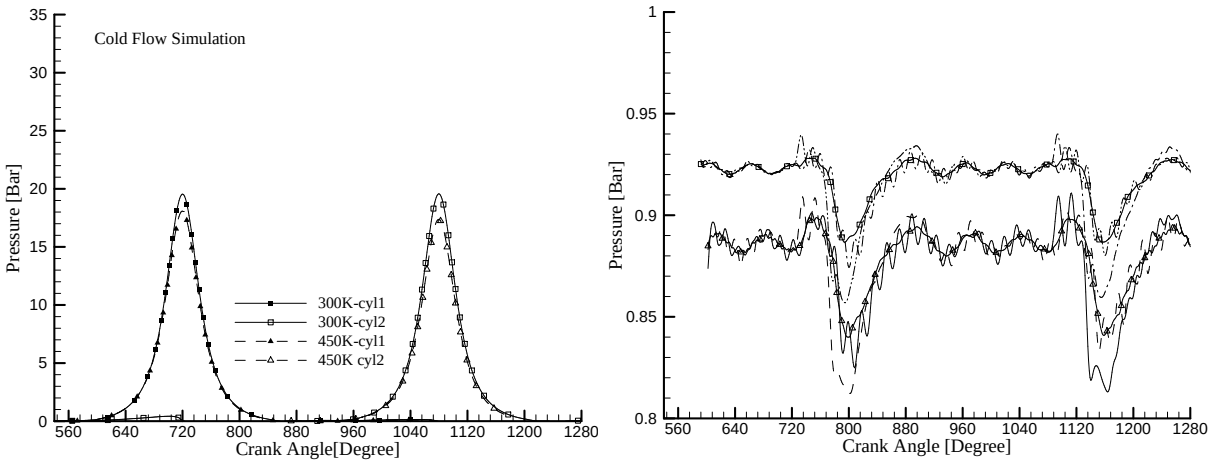

Figure 4. Pressure values versus the crank angle for 300 and 450 K intake temperature.

The initial intake manifold is not able to provide uniform air distribution to all the cylinders for CAI combustion mode(heating intake temperature). This leads to decrease the performance of the engine. Therefore, this manifold is changed different configuration relative with CAI engine mode.

4. CONCLUSIONS

The effect of intake temperature on controlled auto-ignition (CAI) engine considering the two different intake temperature by using the CFD code FLUENT program. RNG k-ε model was used to simulate the turbulence in the engine cylinder. SIMPLE (Semi-Implicit Method for Pressure-Linked Equations) was used as the pressure velocity coupling scheme. All four strokes and their effect on in-cylinder air motion were studied effectively using the numerical approach followed in this paper. CFD can be used as a useful tool to determine the effect of the parameters related to engine on performance.

ACKNOWLEDGMENTS

The authors of this paper would like to acknowledge the financial support provided by TUBITAK Turkey under contract number 113M101.

References

[1] Shah J.V., Patel P.D., Jotava D.J., Effect of Intake Manifold Inclination on Performance and Emission Parameters of 4-Stroke Single Cylinder C.I. Engine: A Technical Review, Int J of Engineering Research & Technology (IJERT), Vol. 3 Issue 1, January - 2014.

[2] Heywood J.B., Internal Combustion Engine Fundamentals. McGraw-Hill, New York, USA, 1988.

[3] Murali Krishna B., Bijucherian A., and Mallikarjuna J. M., Effect of Intake Manifold Inclination on Intake Valve Flow Characteristics of a Single Cylinder Engine using Particle Image Velocimetry, World Academy of Science, Engineering and Technology, 44, 2010.

[4] Paul B., Ganesan V., Flow field development in a direct injection diesel engine with different manifolds, International Journal of Engineering, Science and Technology Vol. 2, No. 1, pp. 80-91, 2010.

[5] Kumar C.R. and Nagarajan G., Investigation of Flow During Intake Stroke of a Single Cylinder Internal Combustion Engine, ARPN Journal of Engineering and Applied Sciences, vol 7 no. 2, 2012.

[6] Karthıkeyan, S., Harıganesh, R., Sathyanadan, M., Krishnan, S., Vadivel, P., Vamsidhar, D., Computational analysis of intake manifold design and experimental investıgatıon on diesel engine for LCV. International Journal of Engineering Science and Technology (IJEST). Vol. 3 No.4, pp- 2359-2367, 2011.

[7] Li J., Zhao H., Ladommatos N., Ma T., Research and Development of Controlled Auto-Ignition (CAI) Combustion in a 4-Stroke Multi-Cylinder Gasoline Engine, SAE Technical Paper 2001-01-3608, 2001.

[8]Fluent 6.3 User's Guide, 2006. Fluent Incorporated, Centerra Resource Park, 10. Cavendish Court, Lebanon, NH 03766,USA.

Sayı 4, Aralık 2016 Volume 4, December 2016

THERMAL PERFORMANCE ANALYSES OF WATER BASED CuO-TiO_2 HYBRID NANOFLUID FLOW IN A HORIZONTAL TUBE

Toygun DAGDEVIR[1*], Veysel OZCEYHAN [1]
[1]Erciyes University, Faculty of Engineering, Department. of Mechanical Engineering,
Kayseri, Turkey, 38039
toygun@erciyes.edu.tr

Abstract
In this study, a CFD modelling of a horizontal straight tube was carried out to investigate the effect of fraction of hybrid water based CuO-TiO_2 nanofluid on thermal performance. In the numerical analysis, in order to ensure fully developed flow, the tested tube was adjusted, and uniform heat flux was applied on outer surface of the test tube. Different turbulence models were examined and *k-ω Shear Stress Transport (SST)* turbulent model was employed to simulate turbulent flow, and analyses were implemented for Reynolds number ranging from 10,000 to 50,000. The flow was simulated as a mixture model, and properties of nanoparticles and water are assumed as not depends on temperature. Thermo-physical properties of nanofluid were calculated from commonly used equations in literature. Nanofluid volume fractions (φ) in water were employed as 5, 4, 3, and 2% in which each concentration has different volume fractions of CuO and TiO_2. As a result, the higher volume concentration of CuO compared to TiO_2, the higher heat transfer coefficient was obtained. However, the highest effective Nusselt number of 1.145 is obtained for volume fraction of CuO and TiO_2 is 0.02 and 0.03, respectively at Reynolds number of 50,000.
***Keywords*:** hybrid nanofluid; convective heat transfer; numerical study

1. Introduction

In studies in recent years, nanofluids have shown higher heat transfer performance compared to conventional heat transfer fluids, such as water, oil and ethylene glycol. The reason of that, thermal conductivity of solid metals is so higher than the fluids. Thanks to that, nanofluids enhance the heat transfer coefficient in comparison with distilled fluids. In the other hand, the other advantage of nanoparticles is of higher surface area per volume than micro-particles. Choi [1] is probably the first researcher about the use of particles in nano dimension. Many researchers experimentally studied on this field and reported that nano-particles in the fluids augment heat transfer performance depends on concentration amount, particle size and Reynolds number at last three decades [2-10].

Many numerical studies were conducted to investigate the effect of nanofluid feature on heat transfer enhancement by researchers, due to saving cost and time in comparison with experimental setups.

Demir et al.[11] investigated numerically forced convection flows of nanofluids consisting of water with Al_2O_3 and TiO_2 nanoparticles in a horizontal tube with constant wall temperature used of a single-phase model.

Dawood et al. [12] numerically investigated the effect of nanoparticles on heat transfer enhancement in an elliptic annulus, unlike circular pipe. Al_2O_3, CuO, SiO_2 and ZnO were employed as nanoparticles and volume fraction and Reynolds number respectively was ranging from 0.5% to 4% and 4,000 to 10,000. Their numerical outcomes showed that the best heat transfer was obtained for gyliserin-SiO_2 mixture that was volume fraction of 4% and Reynolds number of 10,000.

Abdolbaqi et al. [13] investigated the effect of water based CuO, TiO_2 and Al2O3 nanofluid flow through a straight square channel under constant heat flux, numerically. They assumed the nanofluid is a single phase since nanoparticles diameters are so smaller (less than 100 nm). They concluded that Nusselt number of CuO has the highest value than the other nanoparticles.

In this study, water based CuO-TiO_2 hybrid nanofluid flow through a horizontal tube is numerically investigated. Volume fraction of the nanoparticles in water is considered as from 2 to 5%. Constant heat flux of 50 kW/m^2 is applied on the outer surface of the test tube. It is assumed that inner wall of the tube has no-slip boundary condition. The test tube material is aluminium and the flow is under developed turbulent condition, Reynolds number is in the range of from 10,000 to 50,000.

2. CFD Investigation

2.1 Validation of Numerical methodology

CFD (Computational Fluid Dynamics) simulations have been commonly used to predict, solve and analyze the problems which involve fluid flows, heat and momentum transfer, by using equations and algorithms of fluid mechanics. Used conversation equations in CFD program are as follows:

Conservation of mass (continuity) equation [15]*:*

$$\frac{\partial \rho}{\partial t} + \nabla.(\rho u) = 0 \quad (1)$$

Conservation of momentum equation [15]:

$$\frac{\partial}{\partial t}(\rho \vec{v}) + \nabla(\rho \vec{v}\vec{v}) = -\nabla P + \nabla(\bar{\bar{\tau}}) + \rho \vec{g} + \vec{F} \quad (2)$$

Energy equation [15]:

$$\frac{\partial}{\partial t}(\rho E) + \nabla\left(\vec{v}(\rho E + p)\right) = \nabla\left(k_{eff}\nabla T - \sum_j h_j \vec{J}_i + (\bar{\bar{\tau}}_{eff}\cdot\vec{v})\right) + S_h \quad (3)$$

2.2 Computational domain

A 3D model is composed to describe nanofluid flow characteristic in a straight circular tube under constant heat flux of 50 kW/m^2 and velocity inlet (m/s) depends on Reynolds numbers in a turbulent flow regime. The model is selected as 10 mm diameter and an entrance section (L_1) is considered as a 10D to supply fully developed flow at the inlet of the test region, test section (L_2) is considered as 1m and an exit section (L_3) from the test section is selected as 5D to defect the reverse flow. Boundary condition types and dimensions of the computational domain are depicted in Fig 1. Quad grid structure with boundary layer is generated for the test tube as shown in Fig 2. A non-dimensional parameter, y^+ is used to explain whether the grid structure is appropriate. y^+ value of boundary mesh should be $5< y^+<30$ at high Reynolds numbers as stated by Salim and Cheah [14], and the used grid structure has y^+ of 13.74.

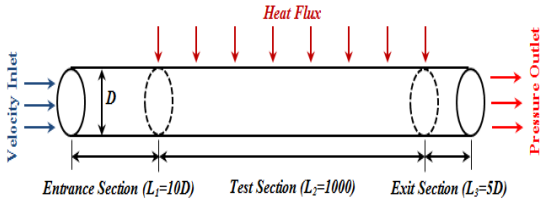

Figure 1. Schematic diagram of the computational domain

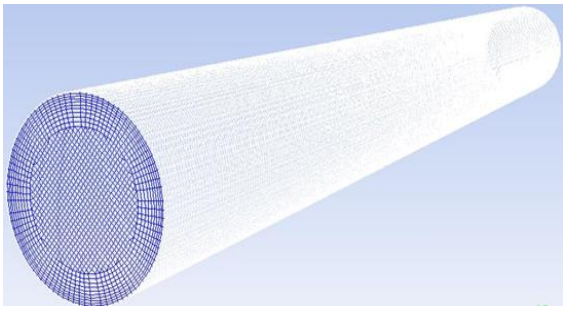

Figure 2. Grid structure of used circular tube

2.3 Validation of the Results

The advantage of CFD simulations is to optimize system variations of models with shorter time and cheaper than experimental setup with ensured validation. In order to ensure accuracy of the numerical methodology, grid independence and turbulence model were tested. *SST k-ω* turbulence model is selected in all considered cases. Detail information about used the turbulence model is available in Fluent Guide [15]. The results were compared with commonly used equations that are Colburn Eq. (4) and Blasius Eq. (5) in terms of Nusselt number (6) and friction factor (8), respectively.

Colburn Equation [16]:

$$Nu = 0.023Re^{0.8}Pr^{0.4} \quad (4)$$

Blasius Equation [17]:

$$f = 0.316Re^{-0.25} \quad (5)$$

$$Nu = \frac{hD}{k} \quad (6)$$

$$h = \frac{q}{T_s - T_b} \quad (7)$$

$$f = \frac{\Delta P}{\frac{1}{2}\rho V^2 \frac{L}{D}} \quad (8)$$

The numerical results are evaluated and compared with these equations (4 and 5) and a study by Rostamani et al. [18] in literature, as in Fig 3.

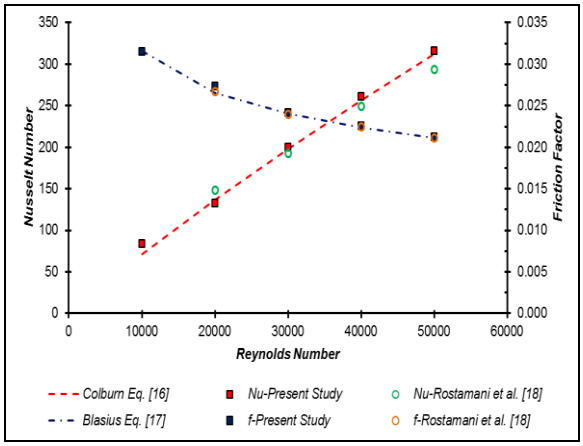

Figure 3. Comparison of distilled water results in terms of both Nusselt Number and friction factor as a function of Reynolds number

In addition to validation of distilled water results, validation of nanofluid results are required for ensuring accuracy of the present study, as well. A single phase model is used for nanofluid flow through the test tube due to saving computational time. Properties of the used materials are given in Table 1. Main aim of using nanofluid is to raise thermal conductivity value and Pr (Prandtl number) as well, and it causes to increase viscous diffusion rate of base fluid.

Table 1. Properties of water and nanoparticles

	Water	CuO	TiO_2
ρ [kg/m^3]	998.2	6510	3980
Cp [j/kgK]	4182	540	690
μ [kg/ms]	1.003x10^{-3}	-	-
k [W/mK]	0.6	18	10.2

Volume fraction of hybrid CuO-TiO_2 nanoparticles into water is totally considered up to 5%. Thermal and physical properties of the nanofluid are calculated with commonly used correlations in

independence temperature. The hybrid nanofluid properties are evaluated likewise as below:

Density of nanofluid:

$$\rho_{nf} = (1-\varphi)\rho_{bf} + \varphi\rho_{np} \quad (9)$$

Density of Hybrid mixture:

$$\rho_{nf,hybrid} = \frac{(\varphi_{CuO})(\rho_{nf-CuO})+(\varphi_{TiO2})(\rho_{nf-TiO2})}{\varphi_t} \quad (10)$$

Specific heat of nanofluid:

$$Cp_{nf} = \frac{(1-\varphi)(\rho_{bf})(Cp_{bf})+(\varphi\rho_{np})(Cp_{np})}{\rho_{nf}} \quad (11)$$

Specific heat of Hybrid mixture:

$$Cp_{nf,hybrid} = \frac{(\varphi_{CuO})(Cp_{nf-CuO})+(\varphi_{TiO2})(Cp_{nf-TiO2})}{\varphi_t} \quad (12)$$

Thermal conductivity:

One of most used formula (Eq. 13) for calculation the thermal conductivity of nanofluid is developed by Hamilton and Crosser [19], in 1962.

$$k_{nf} = k_{bf}\frac{[k_{np}+(n-1)k_{bf}-(n-1)\varphi(k_{bf}-k_{np})]}{[k_{np}+(n-1)k_{bf}+\varphi(k_{bf}-k_{np})]} \quad (13)$$

$$n = 3/\psi \quad (14)$$

where n is the empirical shape factor and ψ is the sphericity, defined as the ratio of the surface area of a sphere to the surface area of the particle (Eq. 14), as stated by Duangthongsuk and Wongwises [20]. The sphericity value assumed as 1. Expressions of k_{nf}, k_{np} and k_{bf} are the thermal conductivity of nanofluid, nanoparticle and base fluid, respectively. Dynamic viscosity of hybrid nanofluid does not need to calculate again due not to including expect of volume fraction (φ) in the formula.

Thermal conductivity of hybrid mixture:

$$k_{nf,hybrid} = \frac{(\varphi_{CuO})(k_{nf-CuO})+(\varphi_{TiO2})(k_{nf-TiO2})}{\varphi_t} \quad (15)$$

Dynamic viscosity:

$$\mu_{nf} = \mu_{bf}(123\varphi_t^2 + 7.3\varphi_t + 1) \quad (16)$$

Result of the nanofluid flow is validated with Rostamani et al. [18] used CuO nanoparticles into water. The validation for water based CuO nanofluid is illustrated in Fig 4.

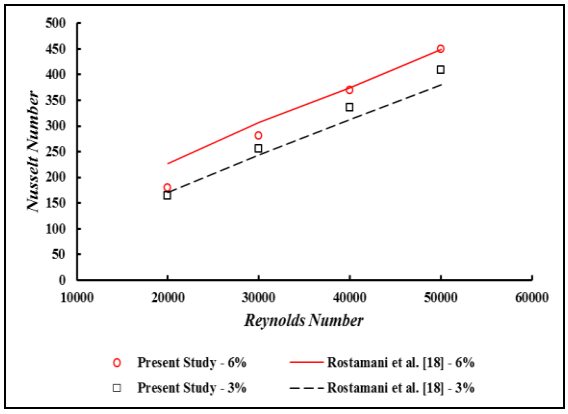

Figure 4. Comparison of CuO nanofluid results in terms of Nusselt number as a function of Reynolds number

3. Results and Discussions

Influence of water based CuO-TiO_2 hybrid nanofluid through a horizontal tube under developed turbulent flow condition and constant heat flux on convective heat transfer and pressure drop was numerically investigated. Variance in individually thermo physical properties for considered volume fraction combinations is given in Table 2.

Table 2. Individually thermo physical properties of used nanofluid

		φ [%]					
		0	***1***	***2***	***3***	***4***	***5***
ρ [kg/m³]	CuO	998.2	1053.3	1108.4	1163.6	1218.7	1273.8
	TiO_2	998.2	1028.0	1057.8	1087.7	1117.5	1147.3
Cp [kj/kgK]	CuO	4182.0	3956.9	3754.2	3570.7	3403.8	3251.3
	TiO_2	4182.0	4046.8	3919.2	3798.7	3684.5	3576.3
k [W/mK]	CuO	0.600	0.616	0.633	0.650	0.668	0.685
	TiO_2	0.600	0.615	0.631	0.647	0.663	0.679
μ [kg/ms]	CuO	0.00100	0.00109	0.00120	0.00133	0.00149	0.00168
	TiO_2	0.00100	0.00109	0.00120	0.00133	0.00149	0.00168
Pr [-]	CuO	6.99	6.99	7.11	7.32	7.61	7.96
	TiO_2	6.99	7.16	7.45	7.83	8.30	8.83

Main purpose of using nanofluid into a fluid is to augment the thermal conductivity property of the fluid. The results show that as the thermal conductivity of the working fluid increases, heat transfer coefficient increases in comparison to distilled water, as illustrated in Fig 5. Furthermore, as can be seen in this figure, when volume fraction of CuO higher than that of TiO_2, more heat transfer coefficient is obtained according to effective thermal conductivity $(k_{eff} = k_{nf}/k_{bf})$.

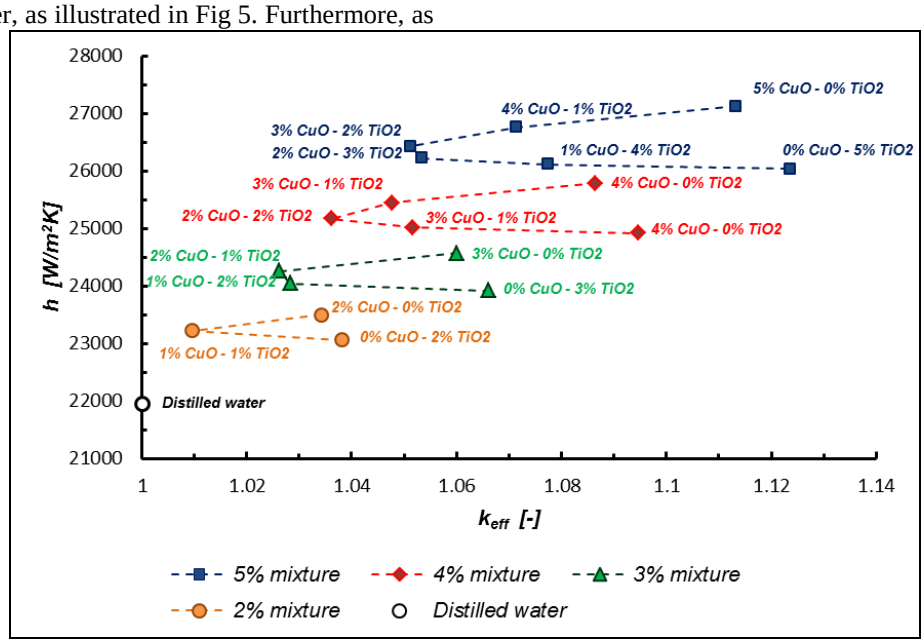

Figure 5. Convective heat transfer coefficient versus effective thermal conductivity for the hybrid nanofluid mixture

In addition to increasing the thermal conductivity of the working fluid, increment in Prandtl number of working fluid has another effect on enhancement heat transfer of the system. Nusselt number is non-dimensional parameter to determine thermal performance for a flow field through a smooth tube which dominantly depends on Prandtl and Reynolds number. In this scope, the results for effective Nusselt number $(Nu_{eff} = Nu_{nf}/Nu_{bf})$ at constant Reynolds number of 50,000 revealed that TiO_2 has more positive effect on Nusselt number than CuO, since Prandtl number of TiO_2 is greater than that of CuO. Moreover, when volume fraction of both of them is approximately equal to each other, the highest effective Nusselt number is obtained, as can be seen in Fig 6.

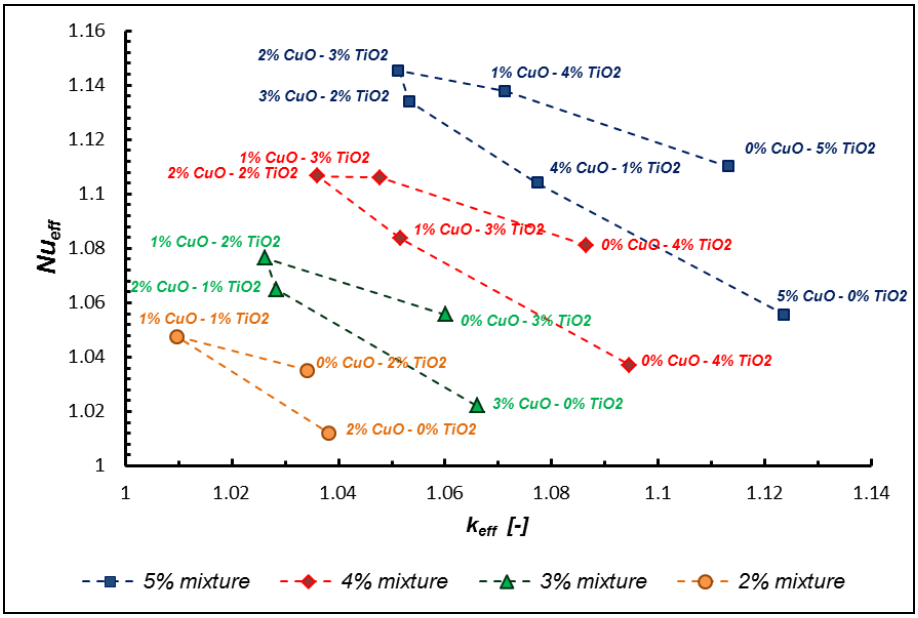

Figure 6. Distribution of average Nusselt number with respect to effective thermal conductivity for the hybrid nanofluid mixture for Reynolds number of 50,000

Hydraulic performance is another parameter to determine a heating system through a tube. Pressure drop results from the present study are given in Fig 7. Supplementing nanoparticles to distilled water increases dynamic viscosity of the distilled water. Thus, pressure drop increases for the all considered nanofluid flow. In the other hand as Reynolds number increases, pressure drop increases. CuO has causes a further increase pressure drop in comparison to TiO_2, as can be seen in Fig 7. The main reason of this result is that, intermolecular bonds are more strength and viscos forces adjacent the walls are more powerful, since CuO especially has more density than TiO_2.

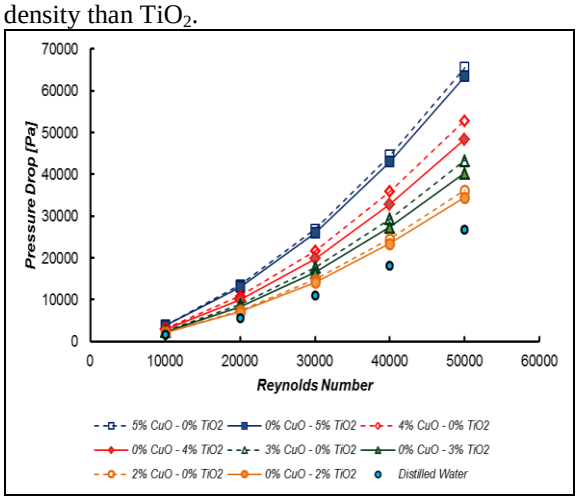

Figure 7. Volume fraction of used nanofluid mixture effect on pressure drop as a function of Reynolds number

4. CONCLUSION

In this study, effect of hybrid nanofluid mixture (CuO-TiO_2) on heat transfer and pressure drop is numerically investigated by using mixture phase model. Results showed that convective heat transfer enhances for all considered volume fraction of the hybrid CuO-TiO_2 nanofluid with increasing Reynolds number. Major reason of the heat transfer enhancement is that thermal conductivity of the nanofluid is so greater than distilled water. In the hybrid nanofluid mixture, the highest effective Nusselt number is obtained for which volume fraction of CuO and TiO_2 is close to each other. In the other hand, hydraulic performance of hybrid nanofluid flow is examined. Adding nanoparticle, especially CuO increases the pressure drop in comparison with distilled water. The main findings can be summarized as below:

- ✓ The mixture model that is used to simulate nanofluid flow shows good agreement with literature on heat transfer and pressure drop.
- ✓ Increasing of effective thermal conductivity causes to increase convective heat transfer coefficient. Furthermore, using CuO instead of TiO_2 shows better performance on increasing convective heat transfer coefficient.
- ✓ The average Nusselt number increases for all nanofluid mixture with increasing effective thermal conductivity in comparison with distilled water. With this conclusion, using hybrid nanofluid can be beneficial even if volume fraction is less than single nanofluid.
- ✓ The highest Nusselt number is obtained for 2% CuO – 3% TiO_2 for Reynolds number of 50,000.
- ✓ Pressure drop increases in all considered volume fraction as Reynolds number increases. In other hand, the more pressure drop increases, the more CuO nanoparticle is added rather than TiO_2. The main reason of this conclusion is that density magnitude of CuO particles is higher than TiO_2, and it causes to occur more viscous forces adjacent the wall.

NOMENCLATURE

C_p	[J/kg K]	specific heat capacity of air
D	[m]	inner diameter of the tube
f	[-]	friction factor
h	[W/m^{2}K]	convective heat transfer coefficient
k	[W/mK]	thermal conductivity
L	[m]	length of the test tube
n	[-]	empirical shape factor
Nu	[-]	Nusselt number
ΔP	[Pa]	pressure drop
Pr	[-]	Prandtl number
Re	[-]	Reynolds number
q	[W/m^2]	heat flux
T	[K]	steady state temperature
V	[m/s]	mean fluid velocity
y^+	[-]	dimensionless wall distance

Greek letters

ρ	[kg/m$^{3]}$	fluid density
φ	[-]	volume fraction
μ	[kg/ms]	dynamic viscosity
ψ	[-]	sphericity

Subscripts

b	bulk
bf	base fluid
eff	effective
nf	nanofluid
np	nanoparticle
s	surface
t	total

REFERENCES

[1] U.S. Choi, Enhancing thermal conductivity of luids with nanoparticles, ASME FED 231 (1995) 99-103.

[2] S. Eimsa-ard, P. Promvonge, Numerical study on heat transfer of turbulent channel flow over periodic grooves, International Communications in Heat and Mass Transfer 35 (2008) 844-852.

[3] A. Azari, M. Lalbasi, M. Derakhshandeh and M. Rahimi, An experimental study on Nanofluids convective heat transfer through a straight tube under constant heat flux, Fluid Dynamics and Transport Phenomena 21 (2013) 1082-1088.
[4] S. Z. Heris, S. Gh. Etemad and M. N. Esfahany, Experimental investigation of oxide nanofluids laminar flow convective heat transfer, International Communications in Heat and Mass Transfer 33 (2006) 529-535.
[5] S. Suresh, K. P. Venkitaraj, P. Selvakumar and M. Chandrasekar, Effect of Al_2O_3-Cu/water hybrid nanofluid in heat transfer, Experimental Thermal and Fluid Science. 38 (2012) 54-60.
[6] M. M. Heyhat, F. Kowsary, A. M. Rashidi, S. A. V. Esfehani, A. Amrollahi, Experimental investigation of turbulent flow and convective heat transfer characteristics of alumina water nanofluids in fully developed flow regime, International Communications in Heat and Mass Transfer 39 (2012) 1272-1278.
[7] D. Wen and Y. Ding, Experimental investigation into convective heat transfer of nanofluids at the entrance region under laminar flow conditions, International Communications in Heat and Mass Transfer 47 (2004) 5181-5188.
[8] B. Sahin, G. G. Gültekin, E. Manay, S. Karagoz, Experimental investigation of heat transfer and pressure drop characteristics of Al2O3-water nanofluid, Experimental Thermal and Fluid Science 50 (2013) 21-28.
[9] M. H. Esfe, S. Saedodin, M. Mahmoodi, Experimantal studies on the convective heat transfer performance and thermo physical properties of MgO-water nanofluid under turbulent flow, Experimental Thermal and Fluid Science 52 (2014) 68-78.
[10] V. Trisaksri, S. Wongwises, Critical review of heat transfer characteristics of nanofluids, Renewable and Sustainable Energy Reviews 11 (2007) 512-523.
[11] H. Demir, A. S. Dalkilic, N. A. Kürekci, W. Duangthongsuk, S. Wongwises, Numerical investigation on the single phase forced convection heat transfer characteristics of TiO_2 nanofluids in a double-tube counter flow heat exchanger, International Communications in Heat and Mass Transfer 38 (2011) 218-228
[12] H. K. Dawood, H. A. Mohammed, N. A. C. Sidik, K. M. Munisamy, Numerical investigation on heat transfer and friction factor characteristics of laminar and turbulent flow in an elliptic annulus utilizing nanofluid, International Communications in Heat and Mass Transfer 66 (2015) 148-157.
[13] Abdolbaqi M. Kh., Azwadi C.S.N., Mamat R., Heat transfer augmentation in the straight channel by using nanofluids, Case Studies in Thermal Engineering. 3 (2014) 59-67.
[14] S. M. Salim and S. C. Cheah, Wall y+ strategy for dealing with wall-bounded turbulent flows, Proceedings of the International Multiconference of Engineers and Computer Scientists Vol II, (2009).
[15] Fluent v.6.3 User Guide, Fluent Corporation, Lebanon, New Hampshire, 2006.
[16] J.R. Welty, G.L. Rorrer, and D.G. Foster, Fundamentals of Momentum, Heat and Mass Transfer, Sixth Edition, Wiley, New Jersey, 2014
[17] F.M. White, Viscous Fluid Flow, 2nd Edition McGraw Hill, New York, 1991
[18] M. Rostamani, S. F. Hosseinizadeh, M. Gorji, J. M. Khodadadi, Numerical study of turbulent forced convection flow of nanofluids in a long horizontal duct considering variable properties, International Communications in Heat and Mass Transfer 37 (2010) 1426-1431.
[19] R.L. Hamilton, O.K. Crosser, “Thermal conductivity of heterogeneous two component system”, Industrial and Engineering Chemistry Fundamentals, vol. 1, pp. 187-191, 1962.
[20] W. Duangthongsuk and S. Wongwises, "An Experimental Study on the Heat Transfer Performance And Pressure Drop of Tio2-Water Nanofluids Flowing Under a Turbulent Flow Regime," Int. Journal of Heat and Mass Transfer, vol. 53, pp. 334-344, October, 2010

KETENCİK ETİL ESTERİNİN TURBO ŞARJLI BİR MOTORDA YAKIT OLARAK KULLANIMINDA MOTORUN EGZOZ EMİSYONLARINA ETKİSİNİN ARAŞTIRILMASI

Hasan AKAY*, Hasan AYDOĞAN**

*S.Ü. Fen Bilimleri Enstitüsü, Otomotiv Mühendisliği ABD, Konya

**S.Ü. Teknoloji Fakültesi, Makine Mühendisliği Bölümü, Kampüs, Selçuklu, Konya

ÖZET

Metil alkol kullanımı ile üretilen biyodizel çalışmaları, etil alkol kullanımı ile üretilen biyodizel çalışmalarına oranla daha ağırlıklı olmuştur. Bu çalışmada farklı olarak ham ketencik yağından etanol kullanımı ile elde edilen ketencik etil esterinin belirli oranlarda diesel yakıtı ile karıştırılarak egzoz emisyon değerlerinin belirlenmesi amaçlanmıştır. Yapılan çalışmalar 4 silindirli 1900 cc Turboşarj beslemeli common rail yakıt sistemine sahip olan bir diesel motor ile gerçekleştirilmiştir.. Elde edilen veriler istatistiksel olarak incelenmiştir ve 3 tekrar yapılarak sonuçların ortalamaları alınmıştır. Sonuçlar incelendiğinde minimum CO emisyon miktarı 3500 devirde 0,01 %vol olarak Ketencik Etil Esteri yakıtında, minimum NO_x emisyon miktarı 1000 devirde 427,5 ppm vol olarak diesel yakıtında, minimum HC emisyon miktarı 2000 ve 3500 devirde 9 ppm vol olarak Ketencik Etil Esteri yakıtında, minimum duman koyuluğu değeri 4000 devirde 0,01/m olarak Ketencik Etil Esteri yakıtında ölçülmüştür.

Anahtar Kelimeler: Etil ester, Ketencik biyodizeli, Motor emisyonu.

EFFECT ON EXHAUST EMMISSIONS OF ENGINE WITH TURBOCHARGED ON USE AS FUEL OF CAMELINA SATIVA ETHYL ESTER

ABSTRACT

Methyl alcohol use work produced biodiesel, biodiesel compared to the work generated by the use of ethyl alcohol was obtained. In this study, different camelina sativa crude oil from the specific ratio of the resulting ethyl ester to the use of ethanol was aimed to determine the exhaust emissions mixed with diesel fuel. The studies were performed with a 4-cylinder diesel engine with turbocharger, a 1900 cc common rail fuel system. The data are averaged and the results were analyzed statistically and 3 performed again. Results in the camelina sativa Ethyl Ester Fuel minimum CO emissions as 0.01% volume at 3,500 rpm compared, the minimum NOx emissions at 427.5 ppm volume in diesel fuel at 1000 rpm, the minimum HC emissions in 2000 and 3500 rpm 9 ppm volume as pro- cedure Ethyl Ester of fuel minimum smoke values of the 4000 revolutions 0.01 / m is measured in camelina sativa Ethyl Ester fuel.

Keywords: Ethyl ester, Camelina sativa biodiesel, Engine emission.

1.GİRİŞ

Petrolün sonlu bir kaynak olmasından ziyade; oluşumundaki döngünün uzun yıllar sürmesi, petrol payındaki seviyelerin ilerleyen zamanlarda düşeceğini göstermektedir. Petrol payındaki seviyenin düşmesi, petrolün kullanım alanlarını kısıtlayacak ve bu durum ülkeler için her anlamda ciddi sıkıntılar doğuracaktır. Ayrıca petrolün çevreye vermiş olduğu zararlar günümüze kadar bütün kesimler tarafından söylenmekte ve bilinmektedir. Bu durumlar taşıt yakıtlarında büyük kullanım alanına sahip olan petrolün yerine, biyoyakıtların kullanılmasını uzun yıllardır gündemde tutmuştur. 1980'lerde, alternatif yakıt olabilecek bitkisel yağların yüksek viskozite sorununun yağların metil alkolle reaksiyonuyla metil esterlerine, biyodizele, dönüştürülerek giderildiği görülmüştür. Böylece biyodizel ismi telaffuz edilir olmuştur [1]. Biodizel ismi ilk olarak 1992 yılında Amerika Ulusal Soy Diesel Geliştirme Kuruluşu tarafından telaffuz edilmiştir. Kimyasal olarak yenilenebilir yağ kaynağından türetilen uzun zincirli yağlı asitlerin mono alkol esterleri olarak tanımlanır [2-4].

Biyodizel, yağlı tohum bitkilerinden elde edilen yağların bir katalizör eşliğinde kısa zincirli bir alkol (metil veya etil alkol) ile reaksiyonu sonucunda oluşan ve yakıt olarak kullanılan bir üründür [5]. Biyodizel, diesel motorlarda en fazla kullanım alanı bulan ve üzerinde sürekli çalışma yapılan bazı özelliklerinin dizel yakıtına yaklaştırılmaya çalışıldığı bir biyoyakıt çeşididir. Biyodizelin motorda yağlamayı geliştirmesi, biyolojik olarak bozunabilir olması, zehirleyici etkisinin düşük olması, düşük emisyon profili ve yenilebilir olması

gibi avantajlarından dolayı biyodizele olan ilgi artmıştır [6]. Konvansiyonel dizel motorlarında biyodizel direk olarak kullanılabileceği gibi dizel yakıtı ile karıştırılarak ve çok küçük değişiklikler veya değişiklik gerektirmeden kullanılabilir [7]. Bununla birlikte, biyodizelin yağlayıcı özelliğinden dolayı motorun önemli parçalarında aşınmalarda azalmaktadır [8]. Yapılan çalışmalara göre; bitkisel yağlar motorine belirli oranlarda katıldığında ya da direkt olarak uzun süreli kullanılmaları durumunda motor elemanlarında aşınma ve karbon birikintisine sebep olurken motor performansında fazla etkili olmadıkları buna karşın özgül yakıt tüketimlerinin arttığı fakat kirletici egzoz emisyonlarında iyileşmelerin olduğu belirtilmiştir [9-11]. Biyodizel kullanımı ile yanmamış hidrokarbon (HC), karbon monoksit (CO) ve partikül madde (PM) emisyonlarında azalmalar sağlanmaktadır. Bu azalmalara karşın, NOx emisyonlarında artış olduğu, azalma veya değişimin olmadığını bildiren çalışmalar mevcuttur [12-13].

Biyodizel üretiminde birçok yöntem olmasına rağmen ucuz maliyeti nedeniyle sodyum hidroksit veya potasyum hidroksit gibi bazik katalizör kullanarak alkol ve yağı esterleştirme yöntemi (transesterifikasyon) tercih edilmektedir [5]. Biyodizel üretiminde alkol olarak etanol ya da metanol kullanılmaktadır. Metil ester ifadesi metanol ve bitkisel yağlardan elde edilen biyodizel anlamına gelir. Etil Ester ifadesi de etanol ve bitkisel yağlardan elde edilen biyodizel anlamına gelmektedir. Günümüze kadar metanol kullanılarak yapılan biyodizel çalışmaları daha ağırlıklı olmuştur. Yapılan bu çalışmada etanol kullanımı ile ketencik ham yağından Ketencik Etil Esteri üretilmiştir. Diesel yakıtı, ketencik etil esteri ve diesel yakıtı-ketencik etil esteri karışımı yakıtların motor egzoz emisyonlarına olan etkileri araştırılmıştır. Bu çalışmada Fiat 1.9 Multijet Diesel motoru, motor dinamometresi, egzoz emisyon değerlerinin ölçülmesinde ise Bosh BEA 350 model egzoz emisyon cihazı kullanılmıştır.

2. MATERYAL VE YÖNTEM

Çalışmada motor denemeleri 1.9 Doblo Multijet motorunda yapılmıştır. Tablo 1'de deney motorunun teknik özellikleri verilmiştir. Deney esnasında egzoz gazlarının ölçümü için Bosch BEA 350 model emisyon cihazı kullanılmıştır. Yapılan çalışmada yakıt testlerinin güvenilir olması için deneyler tekrarlı olarak yapılmış ve elde edilen sonuçlar diesel yakıtı ile mukayese edilmiştir. Ketencik biyodizelinin elde edilmesinde ise alkol olarak etanol kullanılmıştır. Ham ketencik yağından ketencik etil esteri üretilmiştir. Elde edilen biyodizel, hidrolik dinamometreye bağlı olan Multijet, 4 silindirli 1900 cc, Fiat Doblo motoru ile test edilmiş, emisyon ölçümleri Bosch BEA 350 model egzoz emisyon ölçüm cihazı ile yapılmıştır. Elde edilen biyodizel yakıtının viskozite, yoğunluk değerleri yoğunluk ölçüm cihazı ve viskozite ölçüm cihazı ile yapılmıştır. Yapılan testler 3 tekrarlı olarak yapılmış ve değerlerin ortalaması alınmıştır. Deneylerde %100 Dizel (B0), hacimsel olarak %80 Dieel + %20 Ketencik Etil Esteri (B20) ve 100 Ketencik Etil Esteri (B100) kullanılmıştır. Testler 1000 devir/dak'dan başlanarak 500 devir/dak aralıklar ile 4000 rpm e kadar kademeli olarak yapılmıştır. Her bir aralıkta CO emisyonu, NO_x emisyonu, HC miktarı ve duman koyuluğu değerleri ölçülmüştür. Çalışmada kullanılan deney düzeneği şekil 1'de verilmiştir.

Tablo 1. Test motorunun teknik özellikleri

Motor Özellikleri	1.9 Multijet
Silindir adedi ve yerleşimi	4, tek sıra, önde enlemesine
Silindir hacmi (cc)	1910
Sıkıştırma oranı	18,5:1
Maksimum güç hp-d/d	105 - 4000
Maksimum tork Nm(kgm) - d/d	200 - 1750
Yakıt	Motorin
Yakıt besleme	Elektronik kontrollü common rail tipi multijet direkt enjeksiyon, turbo ve intercooler
Ateşleme	Sıkışmalı
Çap × Strok (mm)	82 × 90,4

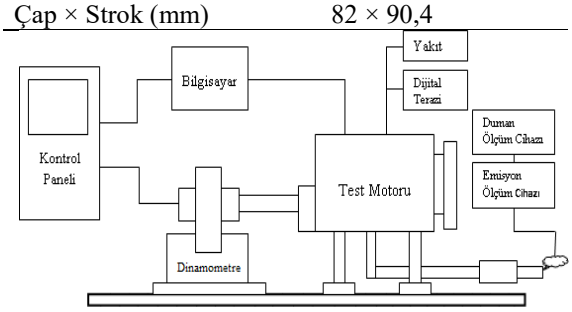

Şekil 1. Deney Test Düzeneği

3. ARAŞTIRMA SONUÇLARI VE TARTIŞMA

Yapılan çalışmada test sonuçları CO emisyonu, NO_x emisyonu , HC miktarı ve duman koyuluğu değerleri bakımından değerlendirilmiş ve diesel yakıtı ile karşılaştırılmıştır. Bu değerler grafiksel olarak incelenmiş ve açıklanmıştır. Şekil 2'de diesel yakıtı, %80 Diesel + %20 KEE yakıt karışımı ve KEE'nin motor devir sayısına bağlı olarak CO emisyon değişimleri %vol olarak gösterilmiştir.

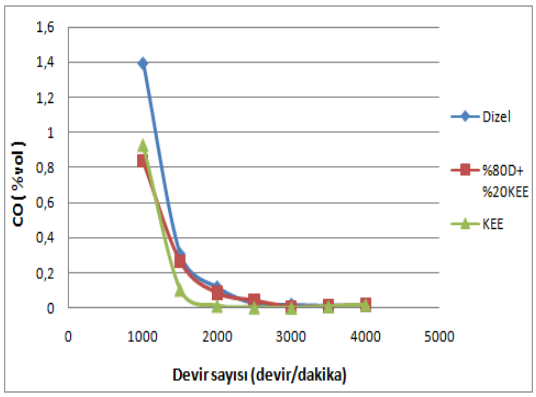

Şekil 2. Yakıt türlerinin CO emisyon değeri bakımından karşılaştırılması

Grafiğe bakıldığında en yüksek CO emisyon değerinin disel yakıtı kullanımında elde edildiği görülmüştür. Diesel yakıtı ile 1000 devir de % 1,397 CO emisyon değeri elde edilirken, aynı devirde %80 Dizel + %20 KEE yakıt karışımı % 0,837, KEE yakıtının % 0,938 CO emisyon değerine ulaştığı görülmüştür. Bu değerlere bakıldığında diesel yakıtına ilave edilen KEE oranı arttıkça CO emisyonları de belli oranda düşüş göstermiştir. CO emisyonlarında meydana gelen bu düşüşler; ketencik etil esterindeki oksijen miktarının fazla olmasına bağlanabilir.

Şekil 3' de diesel yakıtı, %80 Diesel + %20 KEE yakıt karışımı ve ketencik etil esterinin (KEE) motor devir sayısına bağlı olarak CO_2 emisyon değişimleri % olarak gösterilmiştir.

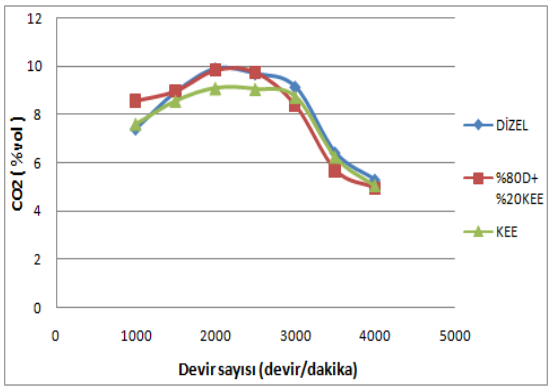

Şekil 3. Yakıt türlerinin CO_2 emisyon değeri bakımından karşılaştırılması

Egzoz gazlarındaki CO_2 emisyonundaki değişimler incelendiğinde en yüksek CO_2 emisyon değerine dizel yakıtında ulaşıldığı tespit edilmiştir. dizel yakıtı kullanıldığında 2000 devirde % 9,9 CO_2 emisyon değeri elde edilmiştir. Yine aynı devirde %80 Diesel + %20 KEE yakıt karışımında % 9,84, KEE yakıtında ise %vol 9,1 CO_2 emisyon değerleri elde edilmiştir. CO_2 emisyonundaki bu azalma; ketencik yağından biyodizel üretimi sırasında ketencik yağının fermantasyonunda karbon bağlarını parçalamak için etanol kullanılmasına bağlanabilir. Tepkimede kullanılan etanol, ketencik etil esteri biyodizelinin yanma hızını artırarak yanmanın iyileşmesini sağladığı düşünülmektedir.

Şekil 4' de diesel yakıtı, %80 Diesel + %20 KEE yakıt karışımı ve ketencik etil esterinin (KEE) motor devir sayısına bağlı olarak HC emisyon değişimleri ppm olarak gösterilmiştir.

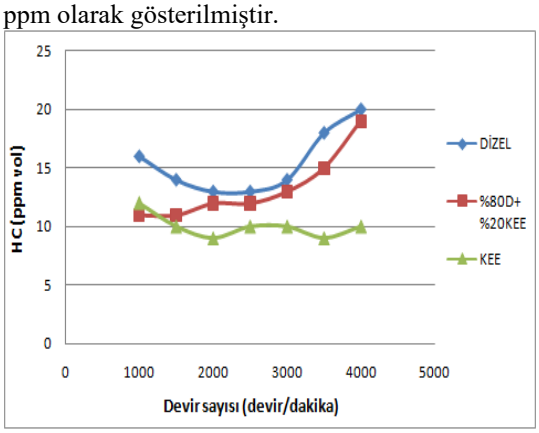

Şekil 4. Yakıt türlerinin HC emisyon değeri bakımından karşılaştırılması

Şekildeki yakıt eğrilerinden de görüleceği gibi en yüksek HC emisyon değeri diesel yakıtı kullanıldığında elde edilmiştir. Diesel yakıtı ile 4000 devirde 20 ppm vol HC emisyon değeri elde edilirken, aynı devirde %80 Dizel + %20 KEE yakıt karışımında 19 ppm vol, KEE yakıtında ise 10 ppm vol HC emisyon değeri elde edilmiştir. Bu değerler incelendiği zaman KEE oranı arttıkça HC emisyonları da belli oranlarda düşüş göstermiştir. Bu durum ketencik yağının kimyasal yapısındaki oksijen miktarının fazla olmasına bağlanabilir. Oksijen miktarının fazlalığı HC emisyonlarındaki karbon miktarını düşürerek zararlı egzoz emisyonlarını azaltmaktadır.

Şekil 5'de diesel yakıtı, %80 Diesel + %20 KEE yakıt karışımı ve KEE'nin motor devir sayısına bağlı olarak NO_x emisyon değişimleri ppm olarak gösterilmiştir.

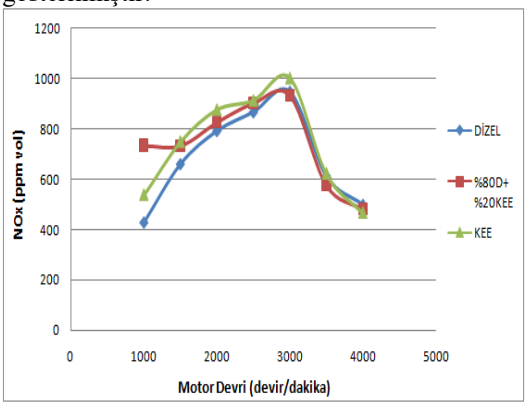

Şekil 5. Yakıt türlerinin NO_x emisyon değeri bakımından karşılaştırılması

Şekildeki yakıt eğrilerinden görüldüğü üzere tüm yakıt türleri için en yüksek NO_x değerleri KEE yakıtı kullanıldığında elde edilmiştir. KEE yakıtı ile 3000 devirde 1005 ppm vol NO_x emisyon değeri elde edilirken, aynı devirde %80 Diesel + %20 KEE yakıt karışımı 931ppm, diesel yakıtında ise 949,5 ppm vol NO_x emisyon değeri elde edilmiştir. Bu değerlerden de anlaşılacağı gibi KEE oranı arttıkça NO_X emisyon değerlerinde belli oranlarda artışlar meydana gelmektedir. Meydana gelen bu artışlar; karışımın oksijen miktarının diesel yakıtına göre yüksek olmasına bağlanabilir.

Şekil 6'da diesel yakıtı, %80 Diesel + %20 KEE yakıt karışımı ve KEE motor devir sayısına bağlı olarak duman koyuluğunun (k faktör) pusluluk/ m olarak değişim grafiği verilmiştir. Şekilden de açıkça görüleceği gibi tüm yakıt türleri için motor devir sayısı arttıkça duman koyuluğu değerlerinde belli oranda azalma görülmüştür. Tüm yakıt türleri için en düşük duman koyuluğu değerleri 4000 devirde gerçekleşmiştir. 4000 devirde diesel yakıtı 0,05/m, %80 Diesel + %20 KEE yakıt karışımı 0.05/m, KEE yakıtında ise 0,01/m duman koyuluğu değeri elde edilmiştir. Grafikten de görüldüğü gibi düşük devirlerde %80 Dizel + %20 KEE yakıt karışımının duman koyuluğu değerleri, dizel yakıtının duman koyuluğu değerlerine göre artışlar göstermiştir. Duman koyuluğunda meydana gelen bu artışlar; KEE ile oluşturulan karışımın diesel yakıtına göre viskozitesinin yüksek, setan sayısının düşük olması ile bağıntılı olarak tam yanmanın gerçekleşmemesinden dolayı is meydana getirmesine bağlanabilir.

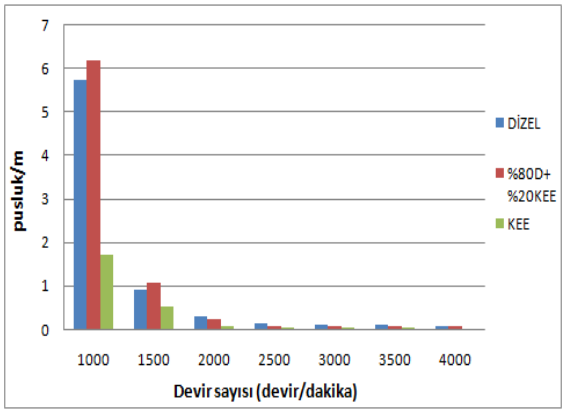

Şekil 6. Yakıt türlerinin pusluluk değerleri bakımından karşılaştırılması

4. SONUÇLAR

CO Emisyon Değerleri

- En yüksek CO emisyon değerinin dizel yakıtında elde edildiği görülmüştür.
- Diesel yakıtı ile 1000 devir de %vol 1,397 CO emisyon değeri elde edilmiştir.
- Emisyon değerleri bütün devirler için incelendiğinde genel olarak; %80 Diesel + %20 KEE yakıt karışımı ve ketencik etil esteri (KEE) yakıtının emisyon değerleri, dizel yakıtının emisyon değerinden düşük çıkmıştır.
- Bu düşüşlerin temel nedeni; ketencik etil esterindeki O_2 miktarının dizel yakıtına göre fazla olmasından kaynaklanmaktadır.

CO_2 Emisyon Değerleri

- En yüksek CO_2 emisyon değerine dizel yakıtında ulaşıldığı tespit edilmiştir.
- Diesel yakıtı kullanıldığında 2000 devirde %vol 9,9 CO_2 emisyon değeri elde edilmiştir.
- Emisyon değerleri bütün devirler için incelendiğinde genel olarak; %80 Dizel + %20 KEE yakıt karışımı ve KEE yakıtının emisyon değerleri, dizel yakıtının emisyon değerinden düşük çıkmıştır.
- Bunun temel nedeni; ketencik yağından biyodizel üretimi sırasında ketencik yağının fermantasyonunda karbon bağlarını parçalamak için etanol kullanılmıştır. Tepkimede kullanılan etanol, ketencik etil esteri biyodizelinin yanma hızını artırarak yanmanın iyileşmesini sağlamıştır.

HC Emisyonu

- En yüksek HC emisyon değeri diesel yakıtı kullanıldığında elde edilmiştir.
- Diesel yakıtı ile 4000 devirde 20 ppm vol HC emisyon değeri elde edilmiştir.
- Emisyon değerleri bütün devirler için incelendiğinde genel olarak; %80 Diesel + %20 KEE yakıt karışımı ve KEE yakıtının emisyon değerleri, diesel yakıtının emisyon değerinden düşük çıkmıştır. Emisyon değerleri yakıtlardaki KEE oranının artmasına bağlı olarak belli oranda düşmüştür.
- Ketencik yağının kimyasal yapısındaki oksijen miktarının fazla olması HC emisyonlarındaki azalmanın en önemli etkenidir.

NO_x Emisyonu

- En yüksek NO_x değerleri KEE yakıtı kullanıldığında elde edilmiştir.
- KEE yakıtı ile 3000 devirde 1005 ppm vol NO_x emisyon değeri elde edilmiştir.
- Emisyon değerleri bütün değerler için incelendiğinde genel olarak; %80 Diesel + %20 KEE yakıt karışımı ve KEE yakıtının emisyon değerleri, diesel yakıtının emisyon değerinden yüksek çıkmıştır.
- Meydana gelen bu artışların sebebi, karışımın oksijen miktarının diesel yakıtına göre yüksek olması ile açıklanabilir.

Duman Koyuluğu

- Tüm yakıt türleri için motor devir sayısı arttıkça duman koyuluğu değerlerinde belli oranda azalma görülmüştür.
- Tüm yakıt türleri için en düşük duman koyuluğu değerleri 4000 devirde gerçekleşmiştir.
- Düşük devirlerde %80 Diesel + %20 KEE yakıt karışımının duman koyuluğu değerleri, dizel yakıtının duman koyuluğu değerlerine göre artışlar göstermiştir.
- Bu durumun temel sebebi; KEE ile oluşturulan karışımın diesel yakıtına göre viskozitesinin yüksek, setan sayısının düşük olması ile bağıntılı olarak tam yanmanın gerçekleşmemesinden dolayı is meydana getirmesi olarak açıklanabilir.

5. SONUÇLAR

Elde edilen sonuçlara göre farklı yakıt ve yakıt karışımlarının özellikle diesel motorlarda kullanılabilmesi için;

- Isıl değeri dizel yakıtına yakın olan yakıtlar seçilmeli ve yakıt karışımları da diesel yakıtının ısıl değerine yakın olmalıdır.
- Yanmanın tam olabilmesi için parlama noktası uygun yakıt türleri seçilmelidir.
- Motor denemelerinin daha sağlıklı yapılabilmesi için mutlaka yakıtın yanında deney motorunun da kalibrasyonu, bakımı ve özellikle yakıt sistemi ile ilgili ayarların en azından fabrika ayarlarına yakın olması gerekmektedir.
- Yapılan testlerde özellikle yakıt filtresi, yakıt pompası, diesel araçlar için enjeksiyon memeleri, hava filtresi temizlenmeli ve bakımı yapılmalıdır.
- Biyodizel çalışmalarında özellikle NO_x emisyonunu azaltmaya yönelik ek çalışmalar yapılmalıdır.
- Üretim maliyetini yükselten bir girdi olarak esterleşme reaksiyonunda etil alkolün (etanolün) yerel kaynaklarla üretilmesi için çalışmalar yapılmalı ve maliyeti düşürülmelidir.
- Bitkisel yağların viskozitelerini düşürmek, ısıl değerlerini artırmak için alternatif katkı maddeleri üzerinde çalışmalar yapılmalıdır.

TEŞEKKÜR

Bu çalışma Türkiye Bilimsel ve Teknolojik Araştırma Kurumu (TÜBİTAK) tarafından, 114M838 nolu proje ile ve Selçuk Üniversitesi Bilimsel Araştırma Projeleri Koordinatörlüğü tarafından 15201111nolu proje ile desteklenmiştir. Yazarlar TÜBİTAK'a ve Selçuk Üniversitesi Bilimsel Araştırma Projeleri Koordinatörlüğüne teşekkür ederler.

KAYNAKLAR

1. Kafadar, B. A.,(2010). "**Yağlardan Biyodizel Eldesine Etki Eden Faktörlerin Araştırılması**", Doktora Tezi, Dicle Üniversitesi Fen Bilimleri Enstitüsü, Diyarbakır, 3-5.
2. Connemann, J. ve Fischer, J., (2000). "**International Congress and Expo Lipids Fats and Oils**", Biodiesel World 2000, Sf. 4, Wurzburg, Almanya, 8-10.
3. Adhvaryu, A., Sharma, Y. K., Singh, I. D., (1999). "**Studies on the Oxidative Behavior of Base Oils and Their Chromatographic Fractions**", Fuel, 78:1293-1302.
4. Koç, Ö., (2010). "**Dizel Motorlarda Biyodizel Kullanımının Motora Etkilerinin Dizel Yakıtı ile Deneysel Karşılaştırmalı Olarak İncelenmesi**", Yüksek Lisans Tezi, Dumlupınar Üniversitesi Fen Bilimleri Enstitüsü, Sakarya, 1-5.
5. Kafadar, B.A., (2010). "**Yağlardan Biyodizel Eldesine Etki Eden Faktörlerin Araştırılması**", Doktora Tezi, Dicle Üniversitesi Fen Bilimleri Enstitüsü, Diyarbakır, 1-18.
6. Wyatt, V.T., ve diğ. , (2005). "**Fuel Properties and Nitrogen Oxide Emission Levels of Biodiesel Produced from Animal Fats**", Journal of the American Oil Chemists' Society (JAOCS), Vol.82, No.8, 585-591.
7. Jung, H., ve diğ., (2006). "**Characteristics of SME Biodiesel-Fueled Diesel Particle Emissions and the Kinetics of Oxidation**", Environ. Sci. Technol, 40, 4949-4955.
8. Agarwal, A.K., (2007). "**Biofuels (Alcohols and Biodiesel) Applications as Fuels for Internal Combustion Engines**", Progress in Energy and Combustion Science, 33(3), 233-271.
9. Ergeneman, M., Arslan, H., Mutlu, M., (1998). "**Taşıt Egzozundan Kaynaklanan Kirleticiler**", Birsen Yayınevi, İstanbul.
10. Borat, O., Balcı, M., Sürmen, A., (1992). "**İçten Yanmalı Motorlar**", Cilt 1, T.E.V. Yayını, Ankara.
11. Karabaş, H., (2009). "**Tütün Tohumu Yağı Metil Esterinin Dizel Motorlarında Yakıt Olarak Kullanılma İmkanlarının Araştırılması**", Doktora Tezi, Sakarya Üniversitesi Fen Bilimleri Enstitüsü, Sakarya, 1-6.
12. Özdemir, M., (2011). "**Bir Dizel Motorda Biyodizel ve Etanol Kullanımının Motor Performansına ve Emisyonlara Etkisinin Araştırılması**", 65-71, 79-86.
13. Özsezen, A.N., Çanakçı, M., Sayın, C., (2008). "**Effects of Biodiesel from Used Frying Palm Oil on the Exhaust Emissions of an Indirect Injection (IDI) Diesel Engine**", Energy & Fuels, 22, 2796–280.

KETENCİK BİYODİZELİNİN ÜRETİMİ VE COMMON RAİL ENJEKSİYON SİSTEMLİ BİR MOTORUN EMİSYONLARINA ETKİSİ

Rahman ŞİMŞEK*, Hasan AYDOĞAN**

** Selçuk Üniversitesi, Teknoloji Fakültesi, Makine Mühendisliği Bölümü, Kampüs, Selçuklu, KONYA

ÖZET

Dünyadaki enerji talebinin her yıl artması ve petrol kökenli yakıt rezervlerinin tükeniyor olması alternatif enerji arayışlarının önemini ortaya koymaktadır. Alternatif enerji kaynaklarının yenilenebilir, çevreci ve ülkemiz topraklarından temin edilebilir olması, enerjisinin %70'ini ithal eden bizim gibi ülkeler için çok önem arz etmektedir. Diesel motorlarda kullanılabilen alternatif yakıtların en önemlisi biyodizeldir. Çevreci ve ekonomik olması nedeniyle biyodizel üretimi önemlidir.

Bu çalışmada, ham ketencik yağından biyodizel üretilmiştir. Daha sonra Eurodiesel yakıtı (B0), B20, B50 ve B100 yakıt karışımları hazırlanmıştır. Bu karışımlar common rail yakıt enjeksiyon sistemine bağlı bir diesel motorda yakıt olarak kullanılmıştır. Yapılan deneysel çalışmalar sonucunda Ketencik biyodizelinin yapısındaki oksijen bütün koşullarda yanma verimine katkı sağlayarak CO, HC ve pusluluk değerlerinin azalmasında ve CO_2 ile NO_x artışlarında etkili olmuştur.

Anahtar kelimeler: Ketencik biyodizeli, diesel yakıtı-biyodizel karışımları, motor emisyonları.

THE PRODUCTION OF BIODIESEL CAMELINA SATIVA BIODIESEL AND EFFECT OF THE ON THE EMISSION OF AN ENGINE WITH A COMMON RAIL INJECTION SYSTEM

ABSTRACT

World energy demand increasing every year and is running out of petroleum-based fuel reserves reveals the importance of the quest for alternative energy. Renewable alternative energy sources, environmentally friendly and can be obtained from the territory of our country, which imports 70% of energy is of great importance for countries like ours. The most important of alternative fuel, biodiesel can be used in diesel engines. Biodiesel production due to environmental and economic benefits is important.

In this study, biodiesel is produced from crude oil camelina sativa. Then Eurodiesel fuel (B0), B20, B50 and B100 fuel mixture has been prepared. This mixture is used as a fuel in a diesel engine with common rail fuel injection system. The experimental study carried out by contributing to oxygen combustion efficiency in all conditions in the construction of the biodiesel camelina sativa as a result of CO, HC is decreased and CO_2, NOx and haziness value is increased.

Keywords: Camelina sativa biodiesel, diesel fuel-biodiesel blends, engine emissions.

1. GİRİŞ

Son yıllarda gerek enerji kaynakları konusunda yaşanan sorun ve sıkıntılar, gerekse bu kaynakların kullanımı neticesinde meydana gelen çevresel tehditler, kaynak kullanımı doğrultusunda yeni arayışlara yönelimi doğurmuş, alternatif kaynak arayışlarını gündeme getirmiştir [1]. Doğada her yıl 150 milyar ton biyokütle üretilmekte, bunun ancak %10'u ticari olarak kullanılmaktadır. Enerji arzının güvence altına alınması ve küresel ısınma ile mücadele açısından önem kazanan biyoyakıtlar tüm dünyanın ilgi odağı olmuş ve tedbirler geliştirilmeye başlanmıştır [2].

Enerji üretiminde mümkün olduğunca yerel kaynakların kullanılması, çevrenin korunmasına dikkat edilmesi, verimliliğin arttırılması, kaynak çeşitliliği ve sürekliliğinin sağlanması da önem kazanmaktadır [3]. İlk olarak 1893 yılında Rudolf Diesel'in icat ettiği diesel motorda yakıt olarak Afrika kökenli yer fıstığı yağını kullanmasına rağmen, günümüze kadar enerji içeriği daha yüksek olan fosil kökenli yakıtlar, diesel motorlarda daha yaygın olarak kullanıla gelmiştir. Oksijenli yakıtların egzoz emisyonlarını azaltmadaki başarısı ve artan çevre bilinci biyodizel olarak adlandırılan yağ asitlerinin diesel motorlarında kullanımını 1980'li yılların başında tekrar gündeme getirmiştir. Özellikle Bitkisel yağlar bazı kritik zamanlarda (1930-1940, 1973 petrol krizi gibi) sadece acil durumlar için diesel motorlarda kullanılmıştır. Fakat bitkisel yağların diesel yakıtına kıyasla viskozitelerinin ve moleküler ağırlığının daha yüksek olması, zayıf yakıt atomizasyonuna; içeriğinde gliserin bulundurması, silindir içerisinde tortulara, yapışkan maddelere, karbon birikimine neden olmaktadır. Bu durum, bitkisel yağ kullanılan motorlarda ciddi problemler

oluşturmuştur. Bitkisel, hayvansal veya atık bitkisel yağların diesel motorunda herhangi bir değişiklik yapılmadan kullanılabilmesi için diesel yakıtına yakın özelliklere sahip bir yakıta dönüştürülmesi gerekmektedir [4].

Biyodizel gelişiminde en önemli ikinci aşama Brüksel Üniversitesi'nde gerçekleşmiştir. Günümüzde yaygın bir şekilde bitkisel yağlardan transesterifikasyon yöntemiyle elde edilen ve biyodizel olarak adlandırılan yakıt için ilk patent Belçikalı bilim adamı G. Chavanne tarafından alınmıştır. G. Chavanne 1937 yılında almış olduğu "Bitkisel Yağların Yakıt Olarak Kullanımındaki Dönüşüm İşlemi Patenti" ile biyodizelin iyi bir alternatif enerji kaynağı olabileceğini ispatlamıştır. Ancak, o dönem itibarıyla petrol ürünlerinin daha düşük maliyetli olmaları ve kullanımlarının yaygınlaşması biyodizelin gelişmesini olumsuz yönde etkilemiştir. Bu nedenlerden dolayı, 1980'li yılların sonuna kadar biyodizel üretiminde kayda değer bir ilerleme gerçekleşmemiştir [5].

Petrol kaynaklı diesel yakıtına alternatif olarak ortaya çıkan biyodizelin üzerinde önemle durulduğu bilinmektedir. Biyodizel saf olarak veya petrolden elde edilen motorinle karıştırılarak da kullanılabilmektedir. Biyodizel ismi ilk olarak 1992 yılında Amerika Ulusal Soy Diesel Geliştirme kuruluşu tarafından telaffuz edilmiştir. Kimyasal olarak yenilenebilir yağ kaynağından türetilen, uzun zincirli yağlı asitlerin mono alkol esterleri olarak tanımlanır. Yani biyolojik kaynaklardan elde edilen, ester tabanlı bir tür oksijenli yakıttır. Genel olarak, biyodizel yüksek kaliteli bitkisel yağlardan üretilmektedir. Avrupa'da biyodizel ham maddesi olarak kanola yağı, Amerika'da ise soya yağı yaygın olarak kullanılmaktadır. Türkiye'de ayçiçeği ve pamuk yağı üretilen yağların başında gelmektedir. Yüksek kaliteli rafine bitkisel yağların biyodizel hammaddesi olarak kullanılması, biyodizeli motorinden daha pahalı hale getirmektedir. Fiyat dengesi sağlayabilmek için, daha düşük maliyetli hammaddeler tercih edilmelidir [6-7].

Yazlık ve tek yıllık bir yağ bitkisi olan Ketencik (Camelina sativa (L.) Crantz) bitkisi yazlık olmakla birlikte sert kışlara dayanıklı tipleri de olan bir kültür bitkisidir. Ketencik bitkisinin 1940'lı yılların başına kadar Doğu Avrupa ve Rusya'da yaygın bir şekilde üretiminin yapıldığı ve daha sonraki yıllarda da yerini kanolaya bıraktığı belirtilmektedir. Bitki diğer yağ bitkilerine kıyasla çok daha yetersiz durumlardaki toprak ve iklim koşullarında daha yüksek verim verme özelliğine sahiptir. Ayrıca vejetasyon süresinin kısa olması ve birçok hastalık ve zararlılara karşı bitkinin üretmiş olduğu belirli fotokimyasal maddeler nedeniyle doğal dayanıklılığa sahip olması nedeniyle son zamanlarda Almanya ve Kanada başta olmak üzere dikkatleri üzerine çekmiş ve bitkiyle ilgili agronomik ve ıslah çalışmaları yoğun bir şekilde yürütüldüğü Almanya gibi ülkelerde erusik asit oranı sıfır olan çeşitler geliştirilmiş durumdadır [8].

Bu çalışmada ketencik biyodizelinin common rail yakıt enjeksiyon sistemli bir dizel motorda yakıt olarak kullanımının motor emisyonlara etkisini diesel yakıtı ile karşılaştırarak incelenmiştir.

2. MATERYAL VE YÖNTEM

Çalışmada ilk önce ketencik yağından transesterifikasyon yöntemi ile biyodizel üretilmiştir. Biyodizel elde etmek için ham yağ 55°C'ye kadar ısıtılmıştır. Daha sonra yağın hacimsel olarak %20'si kadar metanol (CH_3OH) ve 1 litre yağa 3.5 g/litre oranında sodyum hidroksit (NaOH) katalizörü kullanılarak reaksiyon gerçekleştirilmiştir. Reaksiyonda ilk olarak metanol ile NaOH katalizörü 80 ^{o}C'de 60 dakika karıştırılarak metoksit çözeltisi hazırlanmış ve reaktörde ketencik yağına ilave edilerek en az 2 saat dinlendirilmiştir. Reaktör tabanına çöken gliserol alttan alınarak karışımdan ayrıştırılmıştır. Reaktörde kalan ham biyodizelin soğuması ve içerisinde kalan gliserolün çökelmesi için 1 gün beklenerek tabanda biriken gliserol tekrar alınmıştır. 50ºC sıcaklıktaki ham biyodizel ve saf su hacimsel olarak bire bir oranında karıştırılıp yıkanmıştır ve suyun çökmesi için 12 saat dinlendirilmiştir. Yıkama işleminin sonucunda biyodizel içerisindeki reaksiyona girmeyen yağ asitleri, alkol, Na^+ iyonları, katalizör madde ve ayrıştırma esnasında yapıda olabilecek gliserol uzaklaştırılmıştır. Reaktörde dibe çöken su boşaltıldıktan sonra kurutma işlemine geçilerek biyodizelin yapısında kalan su 100ºC'de ısıtılarak en az 2 saat boyunca karıştırılmış ve suyun buharlaşması ile saf biyodizel elde edilmiştir. Transesterifikasyon yöntemiyle üretilen ketencik biyodizeli ile Eurodiesel yakıtından B20 ve B50 karışımları hazırlanmıştır. Testlerde, yakıt olarak Eurodiesel yakıtı (B0), B20 (hacimce %20 biyodizel-%80 Eurodiesel yakıtı), B50 ve B100 yakıtları kullanılmıştır.

Çalışmada motor denemeleri 1.9 Doblo Multijet motorunda yapılmıştır. Tablo 1'de deney motorunun teknik özellikleri verilmiştir. Deney esnasında egzoz gazlarının ölçümü için Bosch BEA 350 model emisyon cihazı kullanılmıştır.

Tablo 1. Test motorunun teknik özellikleri

Motor Özellikleri	**1.9 Multijet**
Silindir adedi ve yerleşimi	4, tek sıra, önde enlemesine
Silindir hacmi (cc)	1910
Sıkıştırma oranı	18,5:1
Maksimum güç hp-d/d	105 - 4000
Maksimum tork Nm(kgm) - d/d	200 - 1750
Yakıt	Motorin
Yakıt besleme	Elektronik kontrollü common rail tipi multijet direkt enjeksiyon, turbo ve intercooler
Ateşleme	Sıkışmalı
Çap × Strok (mm)	82 × 90,4

Motor önce hidrolik bir dinamometreye bağlanmıştır. Dinamometreyle motor yüklenerek emisyon değerleri 1000, 1500, 2000, 2500, 3000, 3500 ve 4000 d/d, tam gaz konumunda ölçülmüştür. Çalışmada kullanılan deney düzeneği şekil 1'de görülmektedir.

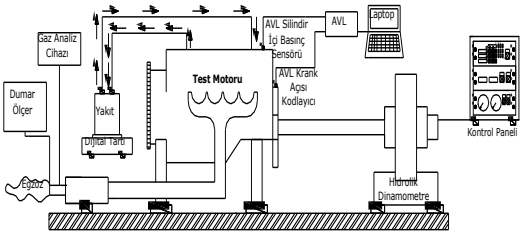

Şekil 1. Çalışmada kullanılan deney düzeneği

Motor yüklemesi hidrolik dinamometre ile yapılmıştır. Test motoru 90ºC çalışma sıcaklığına geldikten sonra her bir test yakıtı ile emisyon değerleri ölçümü yapılarak kaydedilmiş. Deneyler farklı zamanlarda 3 defa tekrarlanmış ve ölçülen değerlerin ortalamaları alınmıştır. Ölçümler tam yükte ve 1000-1500-2000-2500-3000-3500 ve 4000 d/d aralıklarında yapılmış olup testler sırasında egzoz gazı sıcaklıkları ve emisyonları ölçülmüştür. Her yakıt değişiminde motorun yakıt hattı, yakıt filtresi boşaltılmıştır.

Ketencik yağı ile diesel yakıtının bazı özelliklerinin karşılaştırılması tablo 2'de verilmiştir. Ketencik biyodizelinin özellikleri ise tablo 3'de verilmiştir.

Tablo 2. Ham ketencik yağı ve diesel yakıt özelliklerinin karşılaştırılması [8]

Özellikler	Ketencik yağı	Diesel yakıtı
Yoğunluk 15°C (kg/m^3)	918	838
Kinematik viskozite 40°C (mm^2/s)	24	2,92
Parlama noktası (°C)	> 220	102
Alt ısıl değeri (MJ/kg)	38	42,3
Kül (% kütle)	0,0025	0,01
Kükürt (mg/kg)	13,85	9
Su içeriği (mg/kg)	710	43,8
Asit değeri (mg KOH/g)	1,39	-
İyot sayısı (g.I_2/100g)	151,5	-

Tablo 3. Ketencik biyodizelinin yakıt özellikleri [8]

Yakıt Özellikleri	EN 14214: 2012	Ketencik biyodizel	Test metodu
Yoğunluk (15°C kg/m$^{3)}$	860–900	885–888	EN ISO 12185
Kinematik viskozite (40°C mm^2/s)	3.5–5	4.53–5.45	EN ISO 3104
Soğukta filtre tıkanma noktası (CFPP) °C	-	-3	EN 116
Bulutlanma noktası °C	-	3	EN 23015
Metil ester içeriği (wt%)	96.5	97.5	EN 14103
Alevlenme noktası (°C)	101	202	EN ISO 3679
Kükürt içeriği (mg/kg)	10	0.59	EN ISO 20846
Karbon kalıntısı (wt.%)	0.30	0.019	EN ISO 10370
Su içeriği (mg/kg)	500	120	EN ISO 12937
Bakır korozyon testi (3h, 50°C)	1	1A	EN ISO 2160
Oksidasyon kararlılığı (110°C) h	8	1.3-2.2	EN 14112
Asit değeri (mgKOH/g)	0.50	0.36	EN 14214
İyot sayısı max. (g.I_2/g)	120	154	EN 14111

3. DENEY SONUÇLARI VE TARTIŞMA

CO eksik yanmanın bir ürünüdür. Deney sonucu elde edilen CO değerleri şekil 2'de verilmiştir. 2500 devir/dak'daki CO değerleri sırasıyla B0 için 0,19, B20 için 0,13, B50 için 0,11 ve B100 için 0,085 olarak gerçekleşmiştir. B100 yakıtı eurodiesel yakıtına göre %55 oranında daha az CO üretmektedir. B100 bu oranla büyük bir avantaj sağlamaktadır. Bu durumun nedeni yakıtın oksijen içerikli olmasından dolayı yanma veriminin yüksek oluşudur. Devir artışına bağlı olarak CO miktarları azalmıştır.

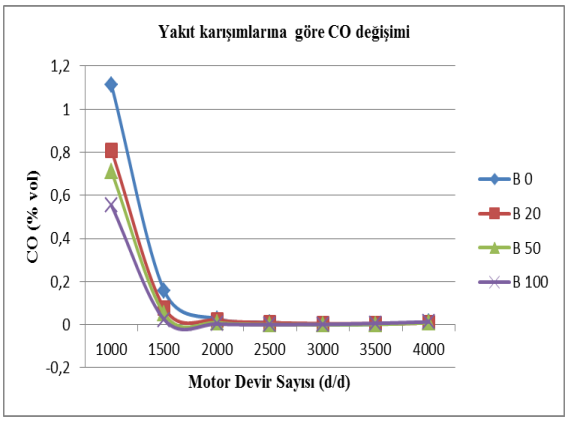

Şekil 2. CO değişimleri

Deney sonucu elde edilen CO_2 değerleri şekil 3'de verilmiştir. 2500 devir/dak'daki CO_2 değerleri sırasıyla B0 için 6.79, B20 için 8,24, B50 için 8,16 ve B100 için 8,05 olarak gerçekleşmiştir. B100 yakıtı eurodiesel yakıtına göre yaklaşık %18,5 oranında daha fazla CO_2 üretmektedir. Bu durumun nedeni yakıtın oksijen içerikli olmasından dolayı yanma veriminin yüksek oluşudur.

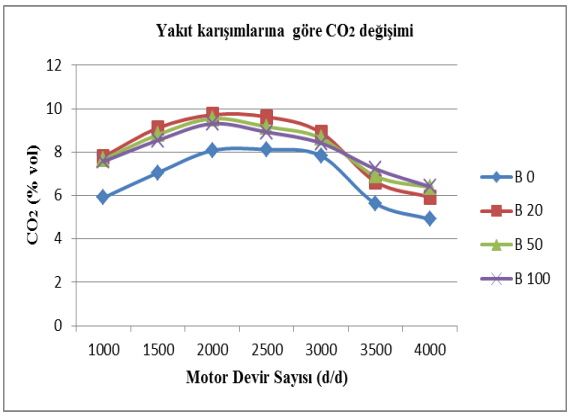

Şekil 3. Yakıtların CO_2 değişimleri

HC yanmamış yakıtı ifade eder. Deney sonucu elde edilen HC değerleri şekil 4'de verilmiştir. 2500 devir/dak'daki HC değerleri sırasıyla B0 için 12,3, B20 için 11,43, B50 için 7,86 ve B100 için 8 olarak gerçekleşmiştir. B100 yakıtı eurodiesel yakıtına göre yaklaşık %35 oranında daha az HC üretmektedir. Bu durumun nedeni yakıtın oksijen içerikli olmasından dolayı yanma veriminin yüksek oluşudur.

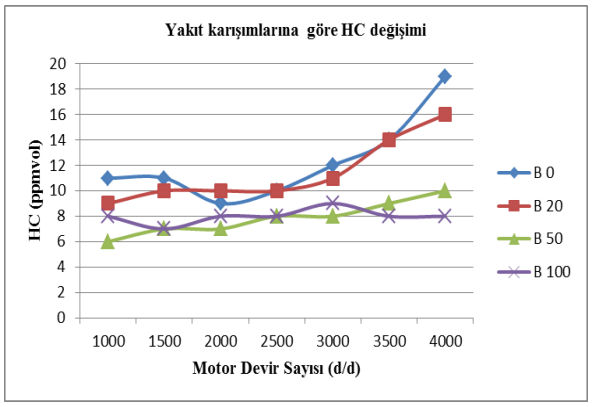

Şekil 4. Yakıtların HC değişimleri

Deney sonucu elde edilen NO_x değerleri şekil 5'de verilmiştir. 2500 devir/dak'daki NO_x değerleri B0 için 676,86, B20 için 834,14, B50 için 860,43 ve B100 için 888,86 olarak gerçekleşmiştir. B100 yakıtı eurodiesel yakıtına göre yaklaşık %31.32 oranında daha fazla NO üretmektedir. Bu durumun nedeni biyodizelin oksijen içerikli olmasından dolayı yanma veriminin yüksekliği; silindir içi yanma sonu sıcaklığının 1600°C fazla oluşu ve azot ile oksijenin daha fazla miktarda kimyasal reaksiyona katılmasıdır.

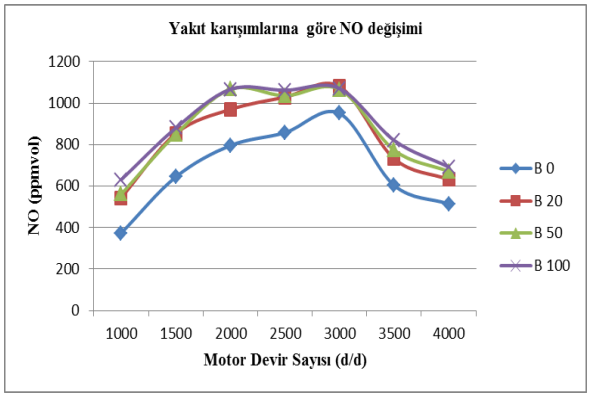

Şekil 5. Yakıtların NO değişimleri

Diesel motorlarda egzoz emisyonlarından bir diğeri pusluluk değerleridir. Deney sonucu elde edilen pusluluk değerleri şekil 6'da verilmiştir. 2500 devir/dak'daki pusluluk değerleri B0 için 0,66, B20 için 0,56, B50 için 0,30 ve B100 için 0,13 olarak gerçekleşmiştir. B100 yakıtına göre eurodiesel yakıtı 5 kat daha pusludur. Bu durumun yanma verimi ile ilişkili olduğu söylenebilir.

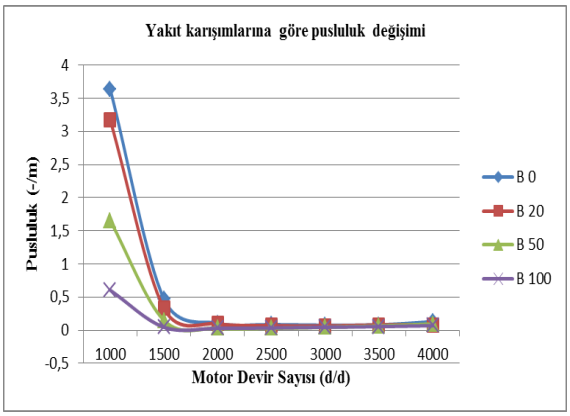

Şekil 6. Pusluluk değerleri

Bu grafik egzoz gazıyla havaya transfer olan ısı enerjisi değişimini göstermektedir. Deney sonucu ölçülen egzoz sıcaklıkları şekil 7'de verilmiştir. Yakıtların sahip oldukları alt ısıl değerleri ile egzoz gazı sıcaklıkları doğru orantılıdır. Grafik incelendiğinde en az egzoz gazı sıcaklığının B100 ile sağlandığı görülür. En yüksek sıcaklık değerleri de B0 yakıtında ölçülmüştür.

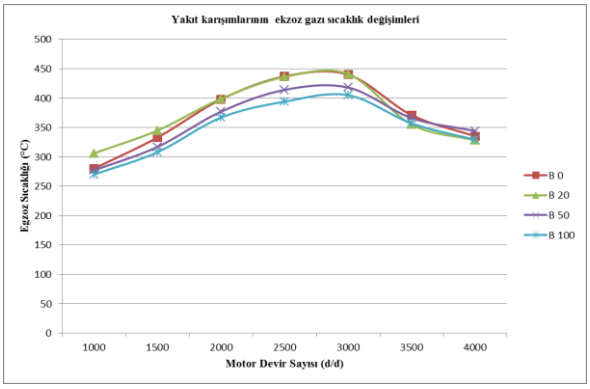

Şekil 7. Egzoz sıcaklık değişimleri

5. SONUÇLAR

Bu çalışmada ketencik biyodizeli ve karışımlarının common rail yakıt enjeksiyon sistemine sahip bir diesel motorunda yakıt olarak kullanımında emisyon değerleri karşılaştırılmıştır. Yapılan deneysel çalışmalar sonucunda Ketencik biyodizelinin yapısındaki oksijen bütün koşullarda yanma verimine katkı sağlayarak CO, HC ve pusluluk değerlerinin azalmış, CO_2 ile NO_x değerleri artmıştır. Yapılan bu çalışma sonucunda ketencik biyodizelinin common rail yakıt enjeksiyon sistemli bir motırda herhangi bir değişiklik yapılmadan kullanılabileceği görülmüştür.

TEŞEKKÜR

Bu çalışma Türkiye Bilimsel ve Teknolojik Araştırma Kurumu (TÜBİTAK) tarafından, 114M838 nolu proje ile desteklenmiştir. Yazarlar TÜBİTAK'a teşekkür ederler.

KAYNAKLAR

1. Dinçbaş, A., 2007, Biyodizel kullanımının dizel motoru üzerindeki etkilerinin uzun süreli testlerle ve motorinle karşılaştırmalı olarak araştırılması, Yüksek Lisans Tezi, Ege Üniversitesi Fen Bilimleri Enstitüsü, İzmir, 1.
2. Anonim, 2012a, Türkiye, Alternatif Enerji ve Biyodizel Üreticileri Birliği,
3. Haşimoğlu, C., 2005, Düşük ısı kayıplı bir dizel motorunda biyodizel kullanımının performans ve emisyon parametrelerine etkisi, Doktora Tezi, Sakarya Üniversitesi, Fen Bilimleri Enstitüsü, Sakarya, 1.
4. Özsezen, A.N. ve Çanakçı, M., 2009, Biyodizel ve karışımlarının kullanıldığı bir dizel motorda performans ve emisyon analizi, Pamukkale Üniversitesi Mühendislik Bilimleri Dergisi, 15 (2): 173-180.
5. Hatunoğlu, E. E., 2010, Biyoyakıt politikalarının tarım sektörüne etkileri, DPT - Uzmanlık Tezleri, Ankara, 14-26, http://tarim.kalkinma.gov.tr/wp-content/uploads/2014/11/EmrahHatunoglu-Tez.pdf [Ziyaret Tarihi: 20 Mayıs 2015].
6. Alptekin, E. ve Çanakçı, M., 2011, Hayvansal kökenli yağlardan biyodizel üretimi, VI. Yeni ve Yenilenebilir Enerji Kaynakları Sempozyumu (YEKS, 2011), Kayseri, 1-9.
7. Şahin, S., 2013, Keten yağı biyodizelinin ve motorinle karışımlarının motor performansına ve egzoz emisyonlarına etkisinin araştırılması, Yüksek Lisans Tezi, Selçuk Üniversitesi, Fen Bilimleri Enstitüsü, Konya, 2-46.
8. Özçelik, A.E., Aydoğan, H., Acaroğlu, M., 2015, Determining the performance, emission and combustion properties of camelina biodiesel blends, Elsevier, Selçuk Üniversitesi, Energy Conversion and Management 96 (2015) 47–57.

Sayı 4, Aralık 2016 Volume 4, December 2016

TERMOELEKTRİK SİSTEMLİ YEMEK TAŞIMA MODÜLÜ TASARIMI VE ANALİZİ

Murat HACI*, Zafer KAHRAMAN*
*Öztiryakiler Ar-Ge ve Teknoloji Merkezi, Büyükçekmece/İSTANBUL

ÖZET
Bu çalışmada iki bölmede, farklı sıcaklıklarda yiyecek ve içecek taşıyabilen, eş zamanlı ısıtma ve soğutma sağlayabilen endüstriyel mutfaklara yönelik mobil yemek taşıma modülü, Ar-Ge sistematiğine dayanan çalışmalarla üniversite-sanayi işbirliği ile geliştirilmiştir. Soğutucu bölmede termoelektrik modül (peltier), ısıtıcı bölmede ise boru rezistans kullanılmıştır. Tasarlanan kabinin istenilen sıcaklığa en uygun termoelektrik/rezistans gücünde ve termoelektrik sistem konumun ulaşmasını sağlamak için Hesaplamalı Akışkanlar Dinamiği (HAD) analizleri yapılmıştır.

Anahtar kelimeler: Isıtma, Soğutma, Termoelektrik sistem (Peltier), Termal analiz, Yemek taşıma modülü

1. GİRİŞ

Yiyecek taşıma kapları, yemekleri dış ortamdan izole edip soğumasını veya ısınmasını önlemek için tasarlanır. Genellikle plastik bir kabin içinin izolasyon maddesi ile kaplanmış şekilde üretilirler. Isıtma veya soğutma üniteleri bulunmadığından uzun süreli muhafazalara uygun değildir.

Endüstriyel mutfaklar için yemek taşıma modülleri (banket arabası), yiyecek ve içeceklerin uygun ortam koşullarında servis edilmeden önce belirli periyotlarda muhafazasının sağlanması için mutfak sektöründe yaygın olarak kullanılmaktadır. Yemek taşıma modüllerinin ülkemizde yalnızca sıcak veya soğuk koşullarda istenilen yiyecek ve içeceklerin saklayacak şekilde üretimleri bulunmaktadır. Fakat hem soğuk hem de sıcak olacak şekilde tek bir sistem üzerinde toplanmış yemek taşıma modüllerinin ülkemizde yerli imalatı bulunmamaktadır.

Termoelektrik soğutma sistemleri mekanik hareketli parçalarının olmaması, hafif ağırlıklı ve akışkan sıvı içermemesinden dolayı tercih edilmektedirler. Termoelektrik sistemlerin soğutucu gazları kullanan sistemlere kıyasla daha ekolojik olduğu ve bu sistem kompresör içermediğinden daha sessiz ve montaj kolaylığı sağlayacak şekilde kullanabileceği vurgulanmıştır. [1-10].

Ancak bu projede tasarlanan yemek taşıma kabininde soğuk taraf termoelektrik sistemle soğuk tutulmakta, sıcak taraf ise boru rezistans ile sıcak tutulmaktadır. Kabinin iç ve dış yüzeyi paslanmaz çelik (AISI 304) olup ara katman yalıtım malzemesi olarak poliüretan kullanılmıştır. Bu çalışmanın en büyük özelliği sıcak ve soğuk bölme arasında bulunan batarya ile enerji ihtiyacı karşılanarak uzun sürekli yiyecek muhafaza etmektir. Ayrıca soğutucu bölmede termoelektrik sistem kullanılması ile kompresör ve akışkan gaz kullanımının neden olacağı çevresel kaygılarında önüne geçilmesi sağlanmıştır. Termoelektrik sistem, sessiz çalışması ve ağırlık bakımından da avantajlar sağlamaktadır. Benzer çalışmalar halen devam etmekte olup farklı sektörlerde kullanım alanları bulmuştur.

2. TERMOELEKTRİK MODÜLLER VE ÖZELLİKLERİ

Termoelektrik sistem, elektrik enerjisi ile ısı enerjisinin birbirleri arasındaki dönüşüm sağlayan bir sistemdir. Termoelektrik olay Joule yasası, Peltier etkisi, Seebeck etkisi ve Thomson etkisi ile izah edilebilir. Bir termoelektrik modül N ve P tipi yarıiletkenlerden oluşan termoelement malzemelerden oluşmaktadır. Bu termoelement sistem elektriksel olarak seri, termal olarak paralel bağlanarak değişik amaçlar için değişik kapasitelerde termoelektrik modüller elde edilmesi sağlanır. İki ucuna doğru akım verildiğinde N ve P tipindeki elemanlar elektronları bir uçtan diğerine doğru iterler ve bir yüzde ısınma diğer yüzde soğutma meydana getirirler. Böylece termoelektrik modül bir ısı pompası gibi çalışır (Şekil 1). Ayrıca termoelektrik modülün iki yüzeyi arasında sıcaklık farkı oluşturulsa termoelektrik modül bir DC akım kaynağı gibi davranarak elektrik üretir [11].

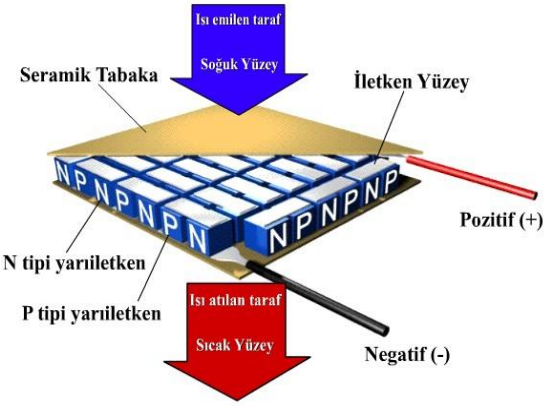

Şekil 1: Termoelektrik modül [11].

Şekil 2'de görüldüğü üzere projektör, kol saati, jeneratör, ısıtıcı gibi temel alanlar olmakla birlikte uzayda uydu sistemlerinin üzerinde de kullanım alanları bulunmaktadır. Farklı malzeme (p ve n tipi yarı iletken malzemeleri) içeriklerine göre sıcaklık uygulamaları farklılıklar göstermektedir [12].

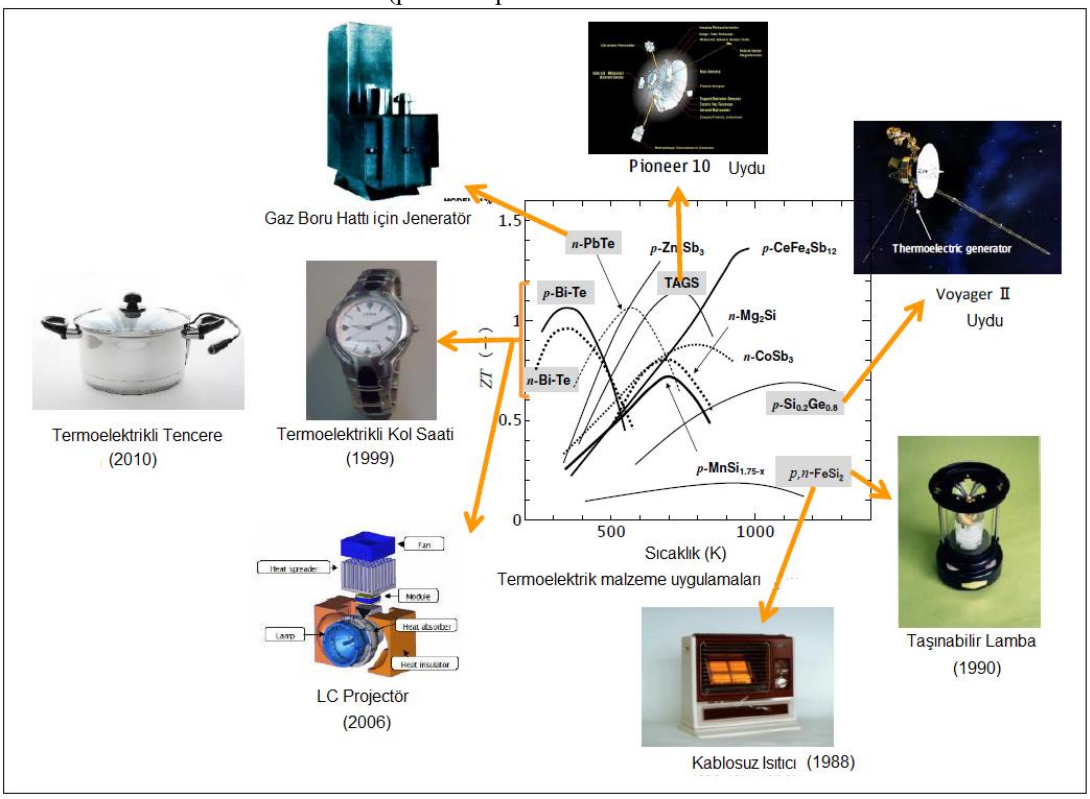

Şekil 2: Termoelektrik sistemlerinin çeşitli kullanım alanları [12].

3. YEMEK TAŞIMA MODÜLÜ TASARIMI VE ÖZELLİKLERİ

Modülün soğutucu tarafı için 200 W'lık TE-127-1.4-1.5 termoelektrik modülü kullanılmıştır. Sıcak taraf için ise 400 W'lık boru tipi rezistans kullanılmıştır. Ulaşmak istenen sıcaklık soğuk taraf için +10°C, sıcak taraf için ise +65°C'dir. Kabinin dış boyutları 1100*910*810 mm'dir. Dış ve iç yüzeyler paslanmaz çelik ve iki yüzey arasında kalan kısım ise poliüretan izolasyon malzemesi olacak şekilde tasarlanmıştır (Şekil 3).

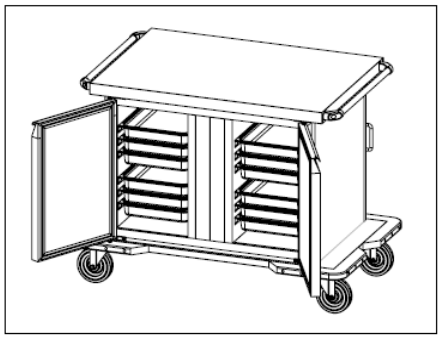

Şekil 3: Termoelektrik sistemli yemek taşıma modülü tasarımı.

4. YÖNTEM

Soğuk tarafta +10°C sınır şartını sağlamak için en uygun termoelektrik sistem gücünü ve en uygun sıcaklık dağılımını bulmak için en uygun termoelektrik sistem konumu araştırılmıştır. Analizlerde 50W termoelektrik sistem gücü ile başlayıp termoelektrik sistem gücünü 25W arttırarak 325W'a kadar analizler yapılmıştır.

Termoelektrik sistem konumu için üst cidar çizgisinden başlayıp 50 mm öteleyerek alt cidara kadar ötelenip analizler yapılmıştır. Sıcak taraf için ise +65°C'ye ulaşmak için rezistans gücü 50W'tan 50W arttırarak 600W'a kadar analizler yapılmıştır.

5. SONUÇLAR

Yapılan analizler sonucunda soğutucu bölmede +10°C sıcaklık için en uygun termoelektrik sistem gücünün 200 W ve sıcaklık dağılımının düzenli olması için en uygun termoelektrik sistem konumunun üst kapak noktasından 100 mm aşağıda olduğu bulduk. Isıtıcı tarafında +65°C'ye ulaşması

için en uygun rezistans gücünün 400 W olduğu bulunmuştur.
Tablo 1'de soğutucu bölmenin termoelektrik sistem gücü ve konumu değişken olan analiz sonuçları verilmiştir. Isıtıcı bölmede rezistans gücü değişken olan analiz sonuçları Tablo 2'de verilmiştir.

Tablo 1: Soğutucu bölmenin termoelektrik sistem gücü ve konumu değişken olan analiz sonuçları.

SOĞUK TARAF İÇİN TERMOELEKTRİK SİSTEM GÜCÜ DEĞİŞKEN OLAN ANALİZ SONUÇLARI												
Peltier Gücü(W)	50	75	100	125	150	175	200	225	250	275	300	325
Ortalama Sıcaklık(K)	295,19	292,35	291,28	287,97	287,6	284,89	282,97	281,79	281	278,95	277,625	275,86

SOĞUK TARAF İÇİN TERMOELEKTRİK SİSTEM KONUMU DEĞİŞKEN OLAN ANALİZ SONUÇLARI											
Konum(mm)	0	50	100	150	200	250	300	350	400	450	500
Ortalama Sıcaklık(K)	291,81	285,99	277,79	278,87	278,9	281,51	286,37	289,53	280,65	279,52	278,74

Tablo 2: Isıtıcı bölmede rezistans gücü değişken olan analiz sonuçları.

SICAK TARAF İÇİN REZİSTANS GÜCÜ DEĞİŞKEN OLAN ANALİZ SONUÇLARI												
Rezistans gücü (W)	50	100	150	200	250	300	350	400	450	500	550	600
Ortalama Sıcaklık(K)	307,79	313,24	319,33	324,08	328,25	330,36	337,19	339,89	342,0	348,71	355,89	362,44

Termoelektrik sistemli yemek taşıma modülü prototipine yönelik ısıtıcı ve soğutucu bölmelerde yapılan analiz sonuçları Şekil 4-6'da verilmiştir.

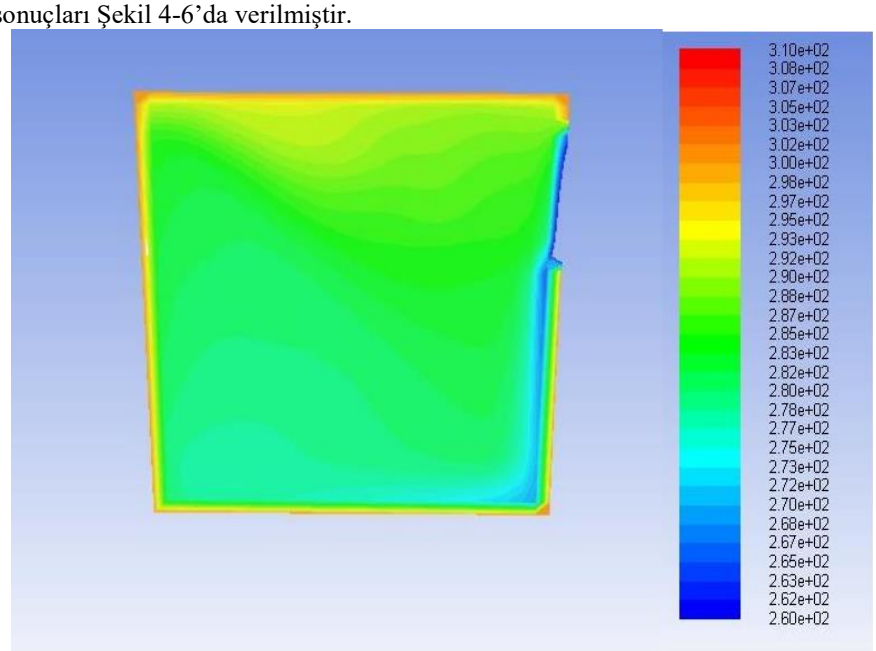

Şekil 4: 200W Termoelektrik sistem gücü için analiz sonuçları.

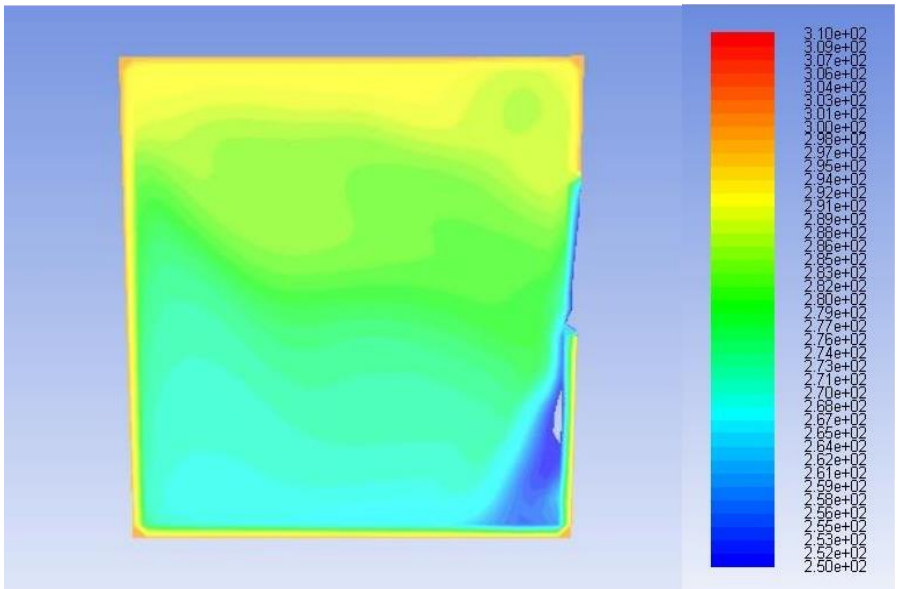

Şekil 5: Termoelektrik sistem konumu 100 mm ötelenmiş analiz sonuçları.

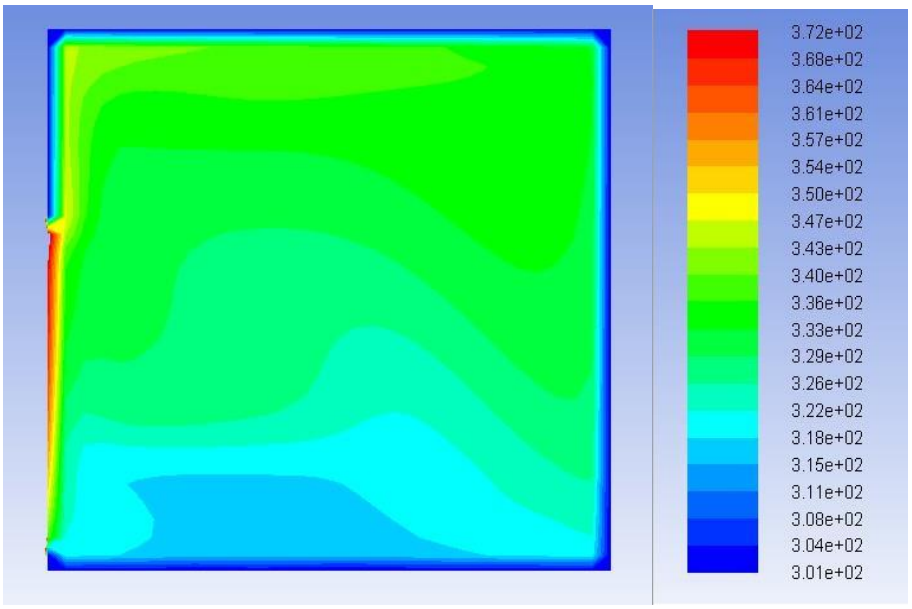

Şekil 6: 400W rezistans gücü için analiz sonuçları

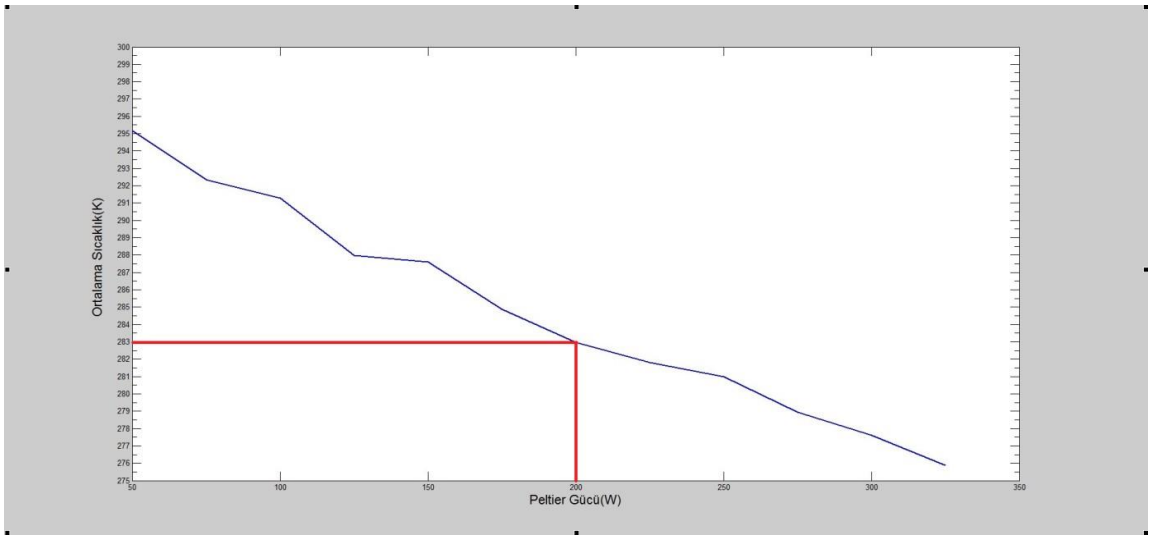

Şekil 7: Termoelektrik sistem gücü değişken olarak yapılan analiz sonuçları.

Yapılan analizler sonucunda termoelektrik sistem gücünün değişken olduğu durumlarda yukarıdaki grafikteki sonuçlar elde edilmiştir. En fazla termoelektrik sistem gücünde 276K sıcaklığa kadar inilmiştir. İstenilen değer (+4°C) için en ideal termoelektrik sistem gücü ise 200 W olduğu belirlenmiştir (Şekil 7).

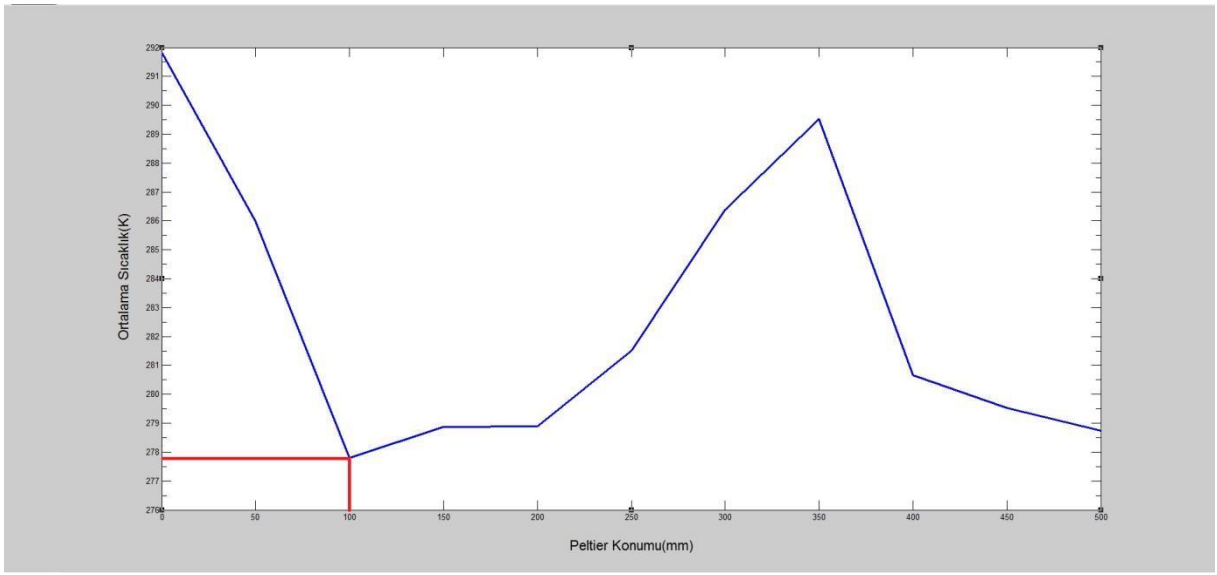

Şekil 8: Termoelektrik sistem konumunun değişken olduğu durumda analiz sonuçları.

Sıcaklık dağılımını ve sabit termoelektrik gücünde en ideal termoelektrik modül konumunu bulmak için yapılan analizler sonucu Şekil 8'de verilmiştir. Termoelektrik sistem kapak üst çizgisinden aşağıya doğru ötelendikçe ortalama sıcaklık azalmaktadır. Fakat 100 mm ötelemeden sonra ortalama sıcaklık tekrar yükseltmektedir. Bunun sebebi ise kabin içindeki havanın türbülansıdır.

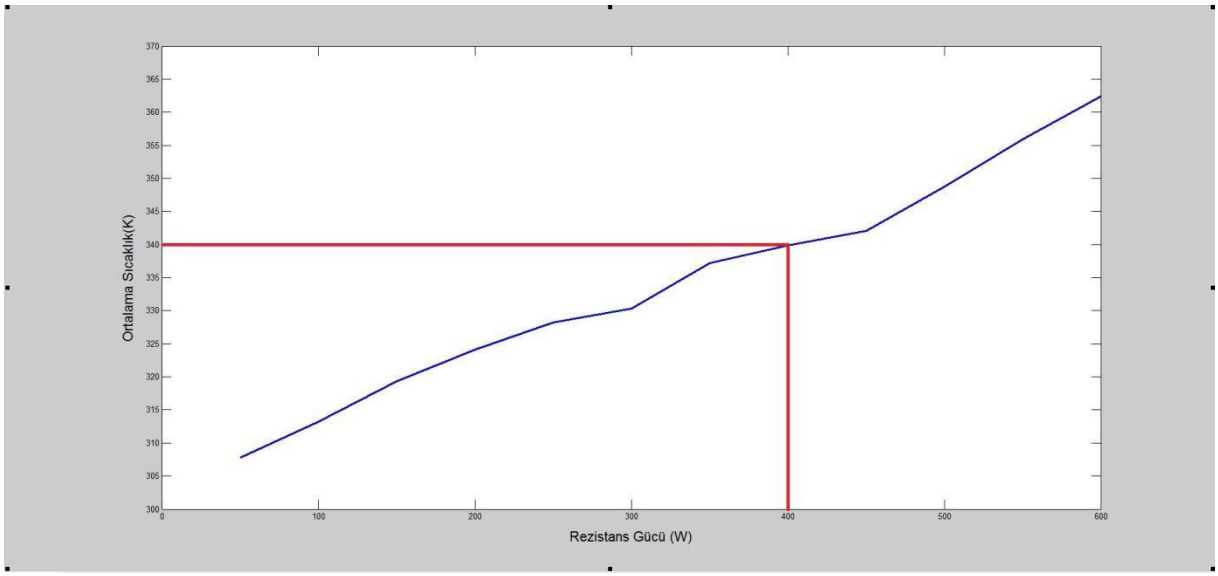

Şekil 9: Rezistans gücünün değişken olduğu durumda analiz sonuçları.

Sıcak tarafta +65°C ye ulaşmak için en uygun rezistans gücünü bulmak için yapılan analizlerin sonuçları Şekil 9'da verilmiştir. Rezistans gücü arttırıldıkça kabin içi ortalama sıcaklığı artmaktadır.

İstenen sıcaklık değeri için en uygun rezistans gücü 400 W olarak belirlenmiştir.
Ülkemizde ilk kez endüstriyel mutfak alanında yerli olarak hem ısıtma hem de soğutmayı eş zamanlı

sağlayan yemek taşıma modülünün mobil prototipi elde edilmiştir.

6. TEŞEKKÜRLER

Bu çalışma, 1501 TÜBİTAK-TEYDEB Sanayi Araştırma Teknoloji Geliştirme ve Yenilik Projeleri Destekleme Programı'nda "Eş Zamanlı Isıtma ve Soğutma Sağlayan Yenilikçi Endüstriyel Banket Arabası Tasarımı ve Prototip İmalatı" başlıklı ve 3150505 numaralı proje kapsamında yürütülmüştür. Bu proje çalışmasının yürütülmesi konusunda desteklerinden dolayı TÜBİTAK Ulaştırma, Savunma, Enerji ve Tekstil Teknolojileri Grubu'na (USETEG) teşekkür ederiz.

KAYNAKLAR

1. A review of thermoelectric cooling: Materials, modeling and applications, Applied Thermal Engineering, Volume 66, Issues 1–2, May 2014, Pages 15-24, Dongliang Zhao, Gang Tan.
2. Computational model for refrigerators based on Peltier effect application, Applied Thermal Engineering, Volume 25, Issues 17–18, December 2005, Pages 3149-3162, D. Astrain, J.G. Vián, J. Albizua.
3. **Experimental evaluation of prototype thermoelectric domestic-refrigerators,** Applied Energy, Volume 83, Issue 2, February 2006, Pages 133-152, Gao Min, D.M. Rowe.
4. **A review of thermoelectrics research – Recent developments and potentials for sustainable and renewable energy applications,** Renewable and Sustainable Energy Reviews, Volume 32, April 2014, Pages 486-503, X.F. Zheng, C.X. Liu, Y.Y. Yan, Q. Wang.
5. **Thermoelectrics: a review of present and potential applications,** Applied Thermal Engineering, Volume 23, Issue 8, June 2003, Pages 913-935, S.B Riffat, Xiaoli Ma.
6. Characterization of a thermoelectric cooler based thermal management system under different operating conditions, Applied Thermal Engineering, Volume 50, Issue 1, 10 January 2013, Pages 652-659, M.K. Russel, D. Ewing, C.Y. Ching.
7. Methodology on sizing and selecting thermoelectric cooler from different TEC manufacturers in cooling system design, Energy Conversion and Management, Volume 49, Issue 6, June 2008, Pages 1715-1723, F.L. Tan, S.C. Fok.
8. Thermodynamic comparison of Peltier, Stirling, and vapor compression portable coolers, Applied Energy, Volume 91, Issue 1, March 2012, Pages 51-58, Christian J.L. Hermes, Jader R. Barbosa Jr.
9. **Geometric effect on cooling power and performance of an integrated thermoelectric gen ration-cooling system,** Energy Conversion and Management, Volume 87, November 2014, Pages 566-575, Wei-Hsin Chen, Chien-Chang Wang, Chen-I Hung.

10. Thermoelectric generators: Linking material properties and systems engineering for waste heat recovery applications, Sustainable Materials and Technologies, Volumes 1–2, December 2014, Pages 26-35, Saniya LeBlanc.
11. **Study and Fabrication of Thermoelectric Air Cooling and Heating System**, International Journal of Engineering Inventions, Volume 4, Issue 2, 2014, Pages 20-30, N. B. Totala1, V. P. Desai, Rahul K. N. Singh, Debarshi Gangopadhyay, Mohd. Salman Mohd. Yaqub, Nikhil Sharad Jane.
12. **The State of the Art on Thermoelectric Devices in Japan, Materials Today: Proceedings**, Volume 2, Issue 2, 2015, Pages 877-885, Yoshikazu Shinohara.

TAŞIYICI-YÜKLEYİCİ BİR İŞ MAKİNESİ İÇİN DİFRANSİYEL DİŞLİ KUTUSU TASARIMI

Tuncay KAZAR[1], Cihan ASAL[2], Hakan Serhad SOYHAN[3,4], Vedat DEMIRTAS[5]
[1]HEMA Research and Development Center, İstanbul, Turkey; email: tuncaykazan@hattat.com.tr
[2]HEMA Research and Development Center, İstanbul, Turkey; email: cihanasal@hattat.com.tr
[3]Department of Mechanical Engineering, Sakarya University, Sakarya, Turkey; email: hsoyhan@sakarya.edu.tr
[4]TEAM-SAN Co., Sakarya, Turkey
[5]Institute of Natural Sciences, Sakarya University, Sakarya, Turkey; email: vedaddemirtas@gmail.com

Özet
Tekerleklere ne kadar tork uygulanabileceğini belirleyen iki faktör vardır. Bunlar, donanım ve çekiş gücüdür. Kuru yolda çekiş gücü yüksektir. Tekerleklere uygulanan tork miktarı, motor ve vites tarafından sınırlanır. Buzda sürüş gibi düşük çekiş gücü durumlarında, tork miktarı tekerleğin bu koşullarda kaymasına sebep olmayacak en büyük miktarla sınırlanır. Taşıt daha fazla tork üretebilmesine rağmen, bu torku yere aktarmak için yeterli çekiş gücüne ihtiyaç vardır. Maksimum tork miktarı, tekerleklerin bulunduğu koşullarda kaymasına sebep olmayacak en büyük miktarla sınırlanır. Bu problemlerin çözümü için sınırlı kaymalı diferansiyel (LSD) ve kilitli diferansiyel sistemleri geliştirilmiştir. Bu çalışmada, Taşıyıcı-yükleyici (Backhoe Loader) bir iş makinesi için LSD sistemi ve multidisk diferansiyel kilitleme sistemi tasarlanıp incelenmiştir.

Anahtar Kelimeler: Diferansiyel, Dişli kutusu, LSD, Çok diskli diferansiyel kilitleme sistemi

DESIGN OF A DIFFERENTIAL GEAR BOX FOR THE BACKHOE LOADERS

Abstract
There are two factors that determine how much torque can be applied to the wheels. These are hardware and traction. Traction is high on dry road. The amount of torque applied to the wheels is limited by the motor and the transmission. In the low-traction situations such as driving on ice, the amount of torque is limited by the largest amount which will not cause slipping of the wheel under these conditions. Although the vehicle can generate more torque, adequate traction is needed to transfer this torque to the ground. The maximum amount of torque is limited by the largest amount which will not cause the wheels to slip. Limited slip differential (LSD) and locked differential systems have been developed to solve these problems. In this study, LSD and multidisc differential locking system were designed and investigated for Backhoe Loader.

Keywords: Differential, Gear box, LSD and Multidisc differential locking system.

1. GİRİŞ

Yanal sapma kontrol sistemleri günümüzde otomotiv endüstrisinde sık kullanılır hale gelmiştir. Üretim aşamasında olan bu sistemlerin büyük kısmı, her bir tekerlekteki farklı fren müdahaleleriyle araç dengesini koruyacak yanal sapma momentlerini geliştiren elektronik denge kontrol sistemleridir. Güvenlik açısından bu yöntemler oldukça etkindir ve özel araçlarda standart olarak kullanılmaktadır. Ancak, yanal sapma kontrol sistemlerinin gelecek nesli için özel araç üreticilerinin odak noktası sadece güvenliği arttırmak değil, sürüş keyfini de sağlamaktır. Frene dayalı sistemler ani ivme kaybı ve araç hızında azalmaya neden olduğundan sürüş keyfi açısından elverişli değildir [1-4].

Fren bazlı sistemlerin olumsuzluklarını barındırmadan, dengede artış ve araç kontrolünü sağlayan alternatif sistemler üzerinde düşünülmektedir. Sürüş esnasındaki tork dağıtımını bir aks vasıtasıyla sağlayan aktif diferansiyeller buna bir örnek oluşturmaktadır. Bu aygıtlar, geleneksel anlamda arazi araçları veya yüksek performanslı araçlar için çekiş gücünü arttırıcı aygıtlar olarak düşünülmüş ve bu alandaki özellikleri araştırılmıştır. Fren bazlı sistemlere oranla, araç kontrolü ve dengesinde çok daha önemli gelişmeler oluşturma potansiyelleri vardır [4-7].

Literatürde birçok sınırlı kayma yapabilen diferansiyel sistemi (LSD) örneği bulunmaktadır [7-9]. LSD 'nin ayırıcı özelliği, torku her zaman daha yavaş olan tekerleğe aktarmasıdır. Bu yüzden genel amaç, LSD 'nin negatif özelliklerini elimine ederek, pozitif özelliklerini geliştiren bir sistem üretmektir. Aktif diferansiyellerdeki gelişim ise tork aktarımının hem büyüklüğünün hem de yönünün kontrol edilmesini olası kılar. Bu gelişim, sonuçta ortaya çıkan yanal sapma momentinin yönünün kontrol edilmesini sağlar ve kontrollü tork transferi sağlayan aktif yanal sapma kontrol momentinin gelişimine yol

açar. Bu tarz sistemlerin yetenekleri ile ilgili detaylar henüz yeterli değildir [4,5,10].

Motordan aktarma organları vasıtasıyla iletilen güç, tahrik tekerleklerinin her ikisini de döndürebilir. Tekerleklerin dönebilmesi için bu gücün dağıtımı gereklidir. Gücü tekerlekten tekerleğe aktaran ve dönüşlerdeki hareket farklılığını sağlayan düzeneğe diferansiyel dişli kutusu adı verilir [5,10-11]. Diferansiyel araçların performansına, yol tutuşuna ve bazı özel durumlara göre tasarlanır. İhtiyaçlar için farklı diferansiyel çeşitleri kullanılmaktadır. Prensipte tümünün işlevi aynıdır. Bu çalışmada, sınırlı kayma yapabilen diferansiyeller (LSD) üzerine araştırmalar yapılmıştır [4,12].

2. DİFERANSİYEL DİŞLİ KUTUSU

2.1 Diferansiyel Dişli Kutusunun Yapısı ve Çalışma Prensibi

Hızla gelişen Otomotiv Endüstrisinin temel ihtiyaçlarından biri olan diferansiyel dişli kutusu sistemleri, tekerlekli araçlarda kullanılan aktarma sistemlerden birini oluşturmaktadır. Motor tarafından üretilen gücün; aracı tahrik edilebilmesi için, tahrik türüne göre önden, arkadan ya da dört tekerden tahrik sistemlerine bağlı olarak tahrik tekerlerine kadar iletilmesi gerekmektedir. Bunun için aktarma organları kullanılmaktadır [12-15]. Diferansiyelin amacı, kardan mili torkunu akslara ve taşıtın tahrik tekerlerine iletmektir. Şekil 1'de diferansiyel dişli parçaları görülmektedir.

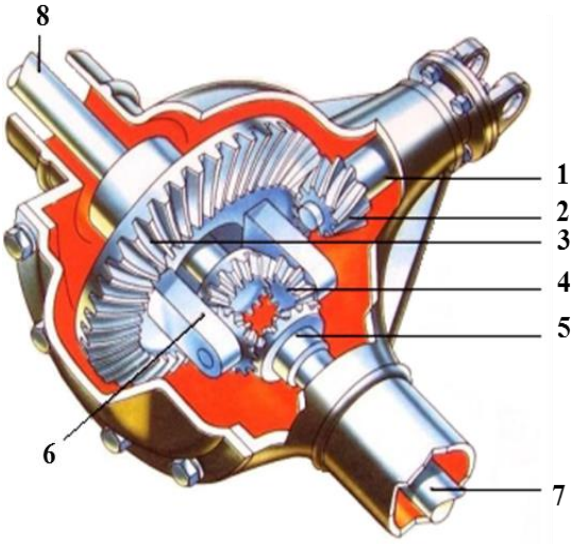

1. Pinyon mili
2. Pinyon dişlisi
3. Ayna dişlisi
4. İstavroz dişlisi
5. Aks dişlisi
6. Dişli gurubu yataklanması
7. Sağ teker aksı
8. Sol teker aksı

Şekil 1. Diferansiyel dişli kutusunun parçaları [12]

Kardan mili tarafından aktarılan krank mili dönme devri, gücün pinyon dişliden ayna dişliye aktarılması esnasında azaltılır. Buna karşın aktarılan tork değeri yükselir ve şanzımanın hareket yönü 90 derece değiştirilir [12-15]. Şekil 2'de gösterildiği gibi iki istavroz dişli ve iki aks dişli, ayna dişli ile beraber diferansiyel gövdesi içinde bulunurlar.

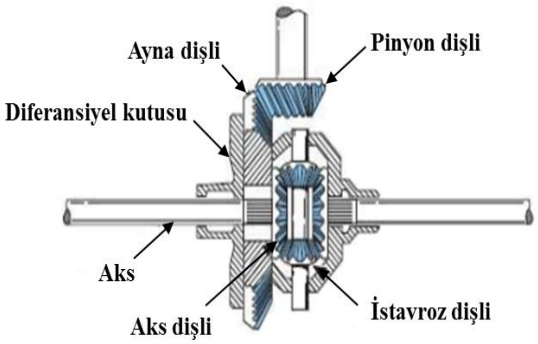

Şekil 2. Diferansiyel dişlilerin adlandırılması [12]

Diferansiyel gövdesi döndüğü zaman, istavroz dişli mili yardımıyla diferansiyel gövdesine tutturulmuş istavroz dişlileri aks dişlilerini tahrik etmek suretiyle dönme hareketi yapar. Aks dişlileri arka aks millerine freze ile bağlı olduğundan tekerleklere gücü aktarırlar [12-15].

2.1.1 Diferansiyelin değişik şartlar altında çalışması

Düz ileri hareket durumu

Düzgün bir yolda araç öne doğru hareket ederken iki tekerleğinin dönme direnci hemen hemen aynıdır. Bu yüzden, aks dişlilerinin ikisi de istavroz dişlileri ile eşit miktarda hareket eder ve bütün parçalar tek bir grup halinde hareket ederler. Her iki arka aks milinin de dirençleri aynı olduğundan istavroz dişlileri dönmezler ancak ayna dişli, diferansiyel gövdesi ve istavroz dişli ile birlikte tek bir grup halinde dönerler Bu durumda, istavroz dişlileri sadece sağ ve sol aks dişlileri birleştirme fonksiyonunu gerçekleştirir [12-15]. Sonuçta, Şekil 3'te görüldüğü gibi istavroz dişlilerinin dönüşü ile birlikte tek bir grup halinde dönen iki aks dişlisi, tekerleklerinin aynı devirde dönmelerine neden olurlar.

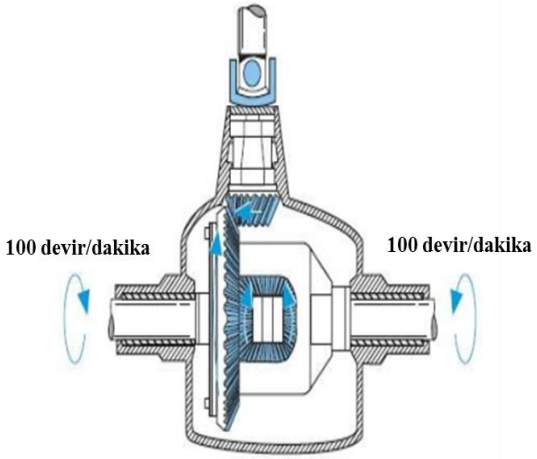

Şekil 3. Düz ileri hareket durumu [12]

Viraj alma durumu
Araç viraja girdiği zaman, iç tarafta kalan tekerlek dıştakine nazaran daha az yol kat eder. Sol taraftaki aks dişlisine bir direnç tatbik edildiği için, istavroz dişlilerin her biri arka aksın etrafında dönerken aynı zamanda kendi milleri etrafında da dönerler [12-15]. Sonuçta sağ taraftaki aks dişlisinin Şekil 4'te görüldüğü gibi devri artar. Bir başka değişle, istavroz dişlileri, istavroz dişli mili etrafında döndüğünden, istavroz dişlileri bir taraftan aks dişlisinin hızını azaltırken diğer taraftaki aks dişlisinin hızını ise o kadar arttırırlar. İstavroz dişlilerinin devir ortalaması ayna dişlinin devrine eşittir.

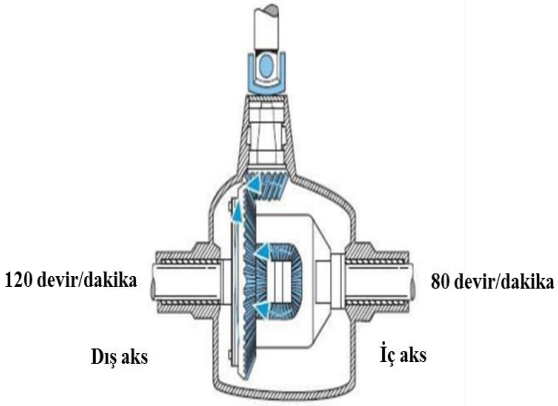

Şekil 4. Viraj alma esnasında diferansiyelden akslara iletilen hızlar [12]

Tek tekerleğin kaygan yüzeyde olması durumu
Eğer tekerleklerden biri çamura girerse, gaz pedalına basıldığında patinaj yapmaya başlar. Bunun nedeni çamurlu yüzeyin düşük sürtünme direncidir. Böyle bir durumda tekerliğin çamurdan çıkarmak çok zordur çünkü ayna dişlinin iki katı hızında dönen çamurdaki tekerlek hareket etme yerine tek başına patinaja devam eder [12-15]. Şekil 5'te devir adetleri görülmektedir.

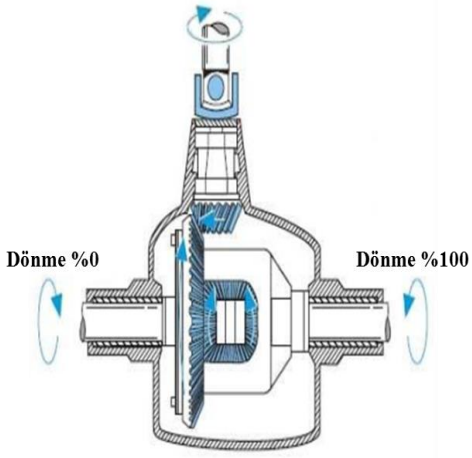

Şekil 5. Tekerleğin tek tarafta dönme durumu [12]

3. DİFERANSİYEL KULLANIMDAYKEN SAĞ VE SOL TEKERLEKLER ARASINDA TORK TRANSFERİ

Klasik bir diferansiyel, sağ ve sol tekerleklerin bir sürüş ekseninde farklı hızlarda dönmelerine izin verir. Bu aracın dönüşü için gereklidir. Klasik bir diferansiyel açık diferansiyel olarak da adlandırılır. Açık diferansiyelin gelişmişi kilitli diferansiyeldir. Kilitli bir diferansiyelle, sürücü sağ ve sol tekerlekleri bir anahtar ile kilitleyerek birlikte çalıştırabilir. İki tekerlekten biri kayan bir yüzey üzerindeyse, diğer tekerlek hala yeterli tork alabilir ve doğrusal çekme kuvvetini sağlayabilir. Böylece kilitli bir diferansiyel, kayan yüzeylerde daha iyi çekiş gücü sağlar ve sürücü tarafından gerektiği zaman kullanılabilir [4-5,10-11].

Diferansiyelin başka bir çeşidi sınırlı kaymalı diferansiyeldir (LSD). Sınırlı kaymalı diferansiyelde, bir kavrama sağ ve sol tekerlekleri kilitler. Anca başlangıçta, bazı kaymalara izin verir. Taşıtın dönüşü sırasında iç ve dış tekerleklerin farklı hızlarda kaymalarına izin verir. Sağ ve sol tekerleğe tork nakletme oranına kesin olarak diferansiyelin tipi tarafından karar verilir. Bir açık diferansiyel, torku tekerleklere daima eşit dağıtır. Kilitli bir diferansiyelde her iki tekerleğin hızı eşittir ve sistemin bir araya gelmesi ile her iki tekerlekten toplam tork alınır. Sınırlı kaymalı diferansiyelde daha yavaş tekerleğe daha fazla tork transfer olabilir. Daha yavaş tekerlek için bu tork artışının eşit olması için LSD içinde kavrama kullanımı gereklidir [4-5,10-11].

3.1 Diferansiyel ve Çekiş Gücü

Tekerleklere ne kadar tork uygulanabileceğini belirleyen iki faktör vardır. Bunlar, donanım ve çekiş gücüdür. Kuru yolda çekiş gücü yüksektir. Tekerleklere uygulanan tork miktarı, motor ve vites tarafından sınırlanır. Buzda sürüş gibi düşük çekiş gücü durumlarında, tork miktarı tekerleğin bu koşullarda kaymasına sebep olmayacak en büyük

miktarla sınırlanır. Taşıt daha fazla tork üretebilmesine rağmen, bu torku yere aktarmak için yeterli çekiş gücüne ihtiyaç vardır [4-5,10-11].

Tekerlekler kaymaya başladıktan sonra taşıtın hızlandırılmaya çalışılması sadece tekerleklerin daha hızlı kaymasına yani patinaj yapmasına neden olur. Maksimum tork miktarı, tekerleklerin bulunduğu koşullarda kaymasına sebep olmayacak en büyük miktarla sınırlanır. Eğer iyi çekiş gücü durumundaki tekerlekler, buzlu ve kaygan zemin gibi düşük çekiş gücü durumunda seyreden tekerleğe uygulanabilecek şekilde çok küçük miktar tork alırsa, taşıt hareket etmekte zorlanır. Eğer ön tekerleklerden ve arka tekerleklerden birinin yerle teması kesilirse, tekerlekler havada dönecek ve hareket iletimi kesilecektir. Bu problemlerin çözümü için LSD (sınırlı kaymalı diferansiyel) ve kilitli diferansiyel sistemleri geliştirilmiştir. Bu çalışmada, sınırlı kayma yapabilen diferansiyeller üzerine araştırmalar yapılmıştır [4-5,10-11].

4. LSD (SINIRLI KAYMALI DİFERANSİYELLER)

Bu sistem, herhangi bir sürüş durumu için en iyi çekişi sağlayacak motor torkunu transfer etmeye çalışır. Modern sınırlı kaymalı diferansiyeller, gücü kayma başlamadan hemen önce iyi durumdaki tekerleğe transfer yeteneğine sahiptir. Ancak, her iki tekerlek kaygan zeminde ise, sistem etkisiz hale gelmektedir. Elektronik olmayan bu sistem, genellikle yeni çekiş kontrol sistemleri kadar iyi görev yapamamaktadır. Bu tür diferansiyeller birkaç çeşit olmakla beraber prensipleri bakımından birbirinin benzeridirler [4-5,7].
Temel olarak, torka duyarlı ve hıza duyarlı olmak üzere iki tip LSD sistemi vardır. Hıza duyarlı LSD ’nin ‘Viskoz Kavrama’ isminde yalnızca bir türü vardır. Fakat, torka duyarlı LSD ’lerin pek çok çeşidi mevcuttur. Bunlardan, en yaygını ‘Kavramalı tip LSD ’dir. Bu tip LSD, bir açık diferansiyeldeki bütün elemanlara sahiptir. Bu tip LSD ile, bir tekerlek buzda, diğeri kuru yolda seyrederken buzdaki tekerlek zemine fazla tork aktaramamasına rağmen, diğer tekerlek hareketi için ihtiyacı olan torku almaya devam edecektir. Buzdaki tekerleğe aktarılan tork, kavramayı yenmek için harcanan tork miktarına eşittir. Araç, gücünü verimli şekilde kullanabilmektedir [4, 8-9].

Tekerleklerden biri çamur, buz gibi zorlayıcı bir şarta maruz kalıp, patinaj yaptığında, diğer tekerleğe gelen moment azalır. Bu olumsuzluk, Sınırlı kaydırmalı Diferansiyel ile giderilir (Şekil 6). Bu gibi durumlarda oluşan iki tekerlek arasındaki devir farkı istavroz dişlilerinin bir biri üzerinde yuvarlanmasına neden olur ve yük altında kalan bu dişlilerin oluşturduğu yandaki resimden de görüleceği üzere istavroz aks dişlisine gelen F kuvvetinin eksenel kuvveti (Fa), yine aynı dişli üzerine sıralanmış sürtünme diskleri gösterilmektedir (Şekil 7). Aracın tekerleği patinaja başladığında bu dişli üzerindeki artan moment neticesinde artan Fa kuvveti, sürtünme disklerini sıkıştırır ve diskler müsaade ettiği sürece tekerleğin patinaj hareketine engel olur.

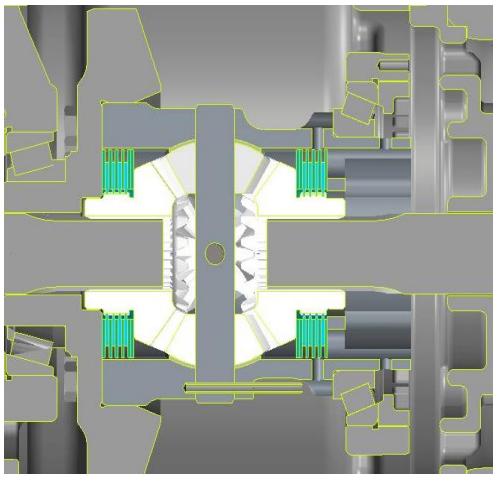

Şekil 6. Taşıyıcı-yükleyici (Backhoe Loader) için tasarlanan Sınırlı Kaydırmalı Diferansiyel (LSD)

Sürtünme diskleri genelde %20 ile %45 arasında bir momente kadar kilitleme yaptıklarında verimli olmaktadır. Daha büyük orandaki kilitlemeler için dişli kuvveti yetmediğinden disk sürtünen yüzey sayısı arttırılmalı ancak bu durumda da sürtünme lineerlikten uzaklaşacağı için verimli olmamaktadır. Daha yüksek bir moment değerinde diskler izafi kayma hareketi yapar.

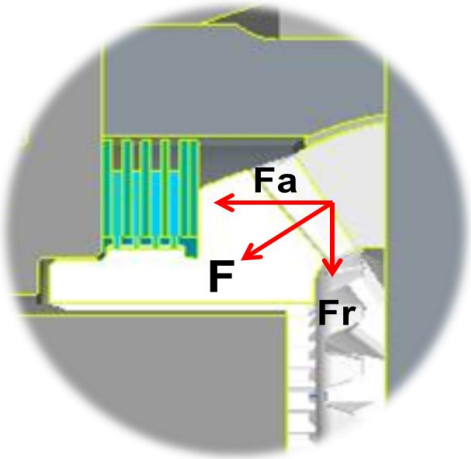

Şekil 7. İstavroz dişliden aks dişlisine nüfuz eden kuvvetler

5. MULTİDİSK DİFERANSİYEL KİLİTLEME SİSTEMİ

Şekil 8’de Diferansiyel kilitlemeyi İstavroz dişlilerden gelen Fa kuvveti yerine, sisteme akuple edilmiş basınçlı akışkan ile hareketi sağlanan bir piston yapacaktır. Tekerlek patinaj eğilimi

gösterdiğinde, kullanıcı sistemi devreye sokabilecek bu sayede piston devreye girip, Multidiskleri sıkıştırdığında sistem %100 e kadar kilitleme sağlayacaktır.

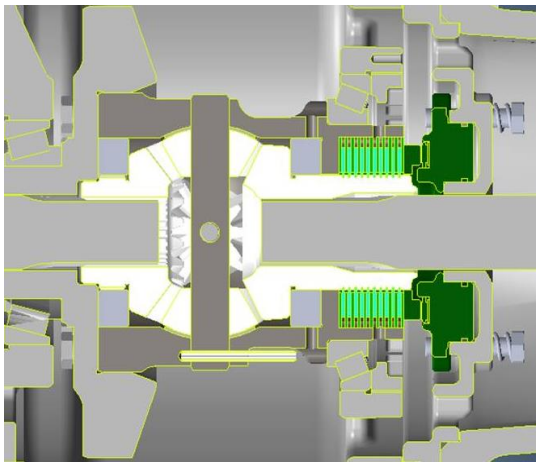

Şekil 8. Taşıyıcı-yükleyici (Backhoe Loader) için tasarlanan Multidisk diferansiyel kilitleme sistemi

Multidiskler ile iletilen moment; Sürtünen yüzey sayısı, kavrama malzemesinin sürtünme katsayısı pistona uygulanan basınç vb. etkilerin düzenlenerek, zor koşullarda aracın tekerlek başına gelen maksimum tork miktarını geçmeyecektir. Eğer sürtünme kuvveti ve buna bağlı olarak tork, belirlenen maksimum tork miktarı değerinin üzerine çıktığında, Multidiskler kaymaya başlayacaktır. Bu kayma sayesinde izin verilen maksimum torka göre hesaplanmış olan aktarma organları korunmuş olur.

6. SONUÇ

İyi bir sürüş kabiliyeti ve yakıt tüketimi açısından diferansiyeller, araçların performansına, yol tutuşuna ve bazı özel durumlara göre tasarlanmalıdırlar. Çok çeşitli ihtiyaçlar için farklı diferansiyel türleri mevcuttur. Bu çalışmada, Taşıyıcı-yükleyici (Backhoe Loader) bir iş makinesi için LSD (Sınırlı Kaymalı Diferansiyel) ve Multidiskli diferansiyel kilitleme sisteminin tasarımı yapılmıştır. Elde edilen sonuçlara göre LSD ve Multidisk diferansiyel kilitleme sisteminin oldukça başarılı olduğu tespit edilmiştir.

KAYNAKLAR

1. Hancock M.J., Williams R.A., Fina E. and Best M.C. 2007. “Yaw Motion Control Via Active Differentials”, Transactions of the Institute of Measurement and Control UK, 29 (2), 137 – 157.
2. Rajamani, R. 2006. Vehicle Dynamics and Control, Springer, USA.
3. Kıencke, U., Nıelsen L. 2005. Automative Control Systems, 2nd ed., Springer, XVIII, 512 p. 345 illus.
4. Bahçekapılı, O. 2008. “Kilitli Diferansiyeller ve Yanal Sapma Kontrolüne Etkileri”, Yüksek Lisans Tezi, Yıldız Teknik Üniversitesi, Fen Bilimleri Enstitüsü, İstanbul.
5. Hancock M.J., Williams R.A., Gordon T J. and Best M.C. 2005. “A Comparison of Braking and Differential Control of Road Vehicle Yaw-Sideslip Dynamics”, Proc. IMechE. Vol. 219 Part D: I. Automobile Engineering, UK.
6. Gillespie, T. D. 1992. Fundamentals of Vehicle Dynamics, Society of Automotive Engineers, Inc., Warrendale, PA, ISBN 1-56091-199-9.
7. Ishikaqa, Y., Teraoka, M., Ishikawa, O., Kamibayashi, H., Izawa, T., Rohregger, W., and Yuhashi, Y. 1994. “Development of Hybrid l.s.d.—Development of Speed and Torque Sensing”, l.s.d. JSAE Autumn Convention, Japan, Proceedings 944 1994-10 (257–260), pp. 5–11.
8. Boos, M. and Koepf, P. 1992. “Electronically Controlled Limited Slip Differentials and 4-Wheel Drive Transfer Gear Boxes for Cars”, 3rd International Conference on Innovation and Reliability, Firenze, Italy, SAE paper 92A071, p. 819–821.
9. Huchtkoetter, H. and Klein, H. 1996. “The Effect of Various Limited Slip Differentials in Front Wheel Drive Vehicles on Handling and Traction”, SAE International Congress and Exposition, Detroit, Michigan, SAE paper 960717, p. 133–134.
10. Çavdar, A. ve Demir, A. 2006. “Taşıtlardaki Dört Tekerden Tahrik (Awd - Fwd) ve Kontrol Sistemlerinin İncelenmesi”, Makine Teknolojileri Elektronik Dergisi (MTED), 3 (1), 45-50.
11. Leske, A. and Schaffler, R. 1994. ZF Getriebe, Druckerei, Friedrichhshafen.
12. Arslan, M. 2011. “Bilgisayar Destekli Diferansiyel Dişli Kutusu Tasarımı, Modelleme ve Animasyonu”, Yüksek Lisans Tezi, Fırat Üniversitesi, Fen Bilimleri Enstitüsü, Elazığ.
13. Andreev, A.F., Kabanau, V. and Vantsevich, V. 2010. Driveline Systems of Ground Vehicles: Theory and Design, CRSC Press, Taylor and Francis group, LLC.
14. Heinz., H. 1999. “Vehicle and Engine Technology”, Second Edition, The Bath Press, Bath.
15. Heinz, H. 2002. Advanced Vehicle Technology, Second Edition, Elsevier, Great Britain.